DYNAMICS OF PLASMA DISKS AROUND COMPACT OBJECTS

by

BHASKARAN P.

A THESIS

SUBMITTED FOR THE DEGREE OF

DOCTOR OF PHILOSOPHY

OF THE

GUJARAT UNIVERSITY

OCTOBER 1989

PHYSICAL RESEARCH LABORATORY

AHMEDABAD 380 009

INDIA

Certificate

I hereby declare that the work presented in this thesis is original and has not formed the basis of the award of any degree or diploma by any University or Institution.

Bhaskaran P.
Author

Certified by:

A.R. Prasanna
(Professor-in-Charge)

Place : Ahmedabad

Date : 16th October, 1989

Acknowledgement

I am extremely grateful to Prof. A.R. Prasanna for his expert guidance and constant encouragement throughout the course of this work.

I acknowledge the help of all the members of theory group for all their help and encouragement at various stages of my work. I would like to specially thank Prof. A.C. Das and my colleague Sushanta for many fruitful discussions that I had with them.

I have benefitted a lot from my colleagues and friends within and outside this laboratory. My heartfelt thanks to all of them.

I sincerely thank Mr. V.T. Viswanathan for the neat and efficient typing of the thesis. My thanks are also due to Mr. S.C. Bhavsar for drafting and Mr. D.R. Ranpura for photography work.

I also thank the staff of Library and Computer Centre for their kind cooperation.

CONTENTS

Abstract

One of the outstanding problems in theoretical astrophysics for the last two decades has been the energetics of high energy astrophysical objects like Quasars and X-ray sources. However, the consensus of the scientific community on the basic issue of the energy producing mechanism has been on the mechanism of accretion of matter by compact objects.

Any gravitating body attracts matter from its surroundings, and if the matter being attracted has angular momentum with respect to the body,it forms a disk around it. Such gaseous disks around astronomical objects,known as accretion disks, while spiralling down, convert the gravitational energy of the object into radiation in a very effective way.

The material will fall onto the object only if it looses its angular momentum. Presence of viscosity,while trying to equalize the differential velocity present in the disk, helps in transferring the angular momentum to the outer regions of the disk. This process generates high temperature and the material in the disk will generally be in plasma state. In the general studies of accretion disks very little has been said about the role of magnetic fields and that of general relativity.It has been shown (Prasanna 1980), in the earlier studies of charged particle trajectories in electromagnetic fields on curved space time

that the presence of magnetic fields help in giving rise to stable orbits for particles closer to r=3m,whereas in the absence of magnetic fields the particle orbits lie beyond r=6m. Thus bringing the particle closer would increase the gravitational potential energy and help in getting out more energy. Also when the particles are in the range $3m<r<6m$,the effects of general relativity on their dynamics would not be negligible (in fact the pure Newtonian description is inadequate) and thus it would become relevant to study the dynamics of disks in the presence of electromagnetic fields on curved spacetime.

In this thesis we have taken up this problem in a carefully devised formalism and then solved the possible equilibrium configurations for several special cases of velocity distributions and further shown explicitly the inter-dependence of certain physical parameters like outer density, seed magnetic field, and continuous pressure distribution in the disk configurations around very compact objects.

The dynamical equations for a magnetofluid in a curved background is obtained from the conservation laws in the given background alongwith the Maxwell's equations for electromagnetic fields.We consider the background metric as the linearized Kerr metric, which corresponds to the geometry around a slowly rotating ($a/m < 0.5$) compact object. The dynamical equations are obtained from the conservation laws $T^{ij}_{;j} = 0$

and the Maxwell's equations from

$$F^{ik}{}_{;k} = -J^i \; ; \qquad F[ij,k] = 0$$

with the current four vector J^i defined through the generalized Ohm's law

$$J^i = \varepsilon u^i + \sigma F^i{}_k u^k \, ,$$

ε being the charge density and σ the electrical conductivity.

We have obtained the dynamical equations in terms of the spatial 3 velocity V^α defined as $u^\alpha = V^\alpha u^t$ and further, using the appropriate local Lorentz frames, considered the following different cases with only the coefficient of bulk viscosity nonzero, and obtained the equilibrium configurations for these cases and studied the behaviour of different properties of the disk.

Before considering the dynamics of plasma disks, the motion of a radiating charged particle moving around a compact object was studied. As the particle radiates it looses energy and should slowly spiral into the object. It was found that the timescale in which this effect becomes appreciable is much larger compared to the orbital period and hence it would be possible to have an equilibrium disk configuration of charged particles around a compact object. So in the study of plasma disks, it is not necessary to consider the effects due to radiation reaction, atleast in the first approximation.

After developing the formalism for studying the dynamics of plasma disks around compact objects, we first consider the equilibrium configuration of an axially

symmetric stationary fluid disk with only the azimuthal velocity component V^{ϕ} non-zero around a non-rotating compact object. For an uncharged fluid with infinite conductivity and a magnetic field which is dipolar at infinity, we get analytical solutions for azimuthal velocity and magnetic and electric field components.The pressure profiles corresponding to different angular momentum parameter and radial dependance of velocity for a disk of incompressible fluid (ρ = const) confined to the equatorial plane ($\theta = \pi/2$) of the object were obtained by numerically integrating the equation of motion.It was found that it is possible to get equilibrium configuration of disk structure only with velocity distributions which decrease for increasing r. Also,the inclusion of magnetic fields allows the possibility of the inner edge of the disk extending to regions much closer to the event horizon, unlike in the absence of magnetic fields, where in Schwarzschild background the inner edge has to be beyond r = 6m. Further,using the general expression as given by Page and Thorne (1974),but adapted to Schwarzschild geometry by Luminet (1974) and Hanawa (1989),we obtain the radiation flux from the disk corresponding to different velocity distributions. It was found that variation from the Keplerian velocity distribution does not have much effect on the flux distribution.

Next we consider the equilibrium configuration of an axially symmetric stationary disk with finite electrical conductivity with nonzero radial and azimuthal components of

velocity. With the toroidal component of magnetic field B_ϕ taken as zero and the electromagnetic field satisfying Ohm's law, we get analytical solutions for the components of velocity, electric and magnetic fields and further get an expression for accretion rate.

Pressure and density profiles were obtained for different values of magnetic field strength, conductivity and angular momentum for given values of density at the outer edge, to investigate the effects of these parameters on the equilibrium configurations of the disk. It was found that for a given value of density at the outer edge, there is a critical value for the magnetic field strength, above which no equilibrium configuration is possible. Similarly the conductivity has to be higher than a critical value for equilibrium configuration. Also we have obtained the dependence of different parameters, on the disk structure and the allowed range of their values.

Finally, we consider the equilibrium configuration of a fluid disk of infinite conductivity around a slowly rotating compact object. With the toroidal component of magnetic field taken as zero, and assuming the azimuthal velocity to be a modified Keplerian velocity by including the effects of frame dragging, we obtain analytical solutions for magnetic and electric field components. Further we obtain pressure profiles for $\theta = \pi/2$ plane of the central object for the cases of (a) disk of incompressible fluid, and (b) disk with an equation of state given by $P = C_1 \rho^{\gamma} - B^2/8\pi$ by numerically integrating the

momentum equation.

It has been found that it is possible to get equilibrium configuration of disks around slowly rotating compact objects, wherein the influence of co- and counter-rotation with respect to the central object bears a definite contribution which is particularly significant in the inner regions. One also finds that, the magnetic field structure is influenced by the frame dragging, again as evidenced by the difference in co- and counter-rotating disks.

CHAPTER I

INTRODUCTION

One of the outstanding problems in theoretical astrophysics for the last two decades has been the energetics of high energy astronomical objects like quasars, active galactic nuclei and X-ray sources.The efficiency of conventional energy generation mechanism in astrophysics, viz., nuclear burning,is not capable of explaining the large amounts of radiation ($L \backsim 10^{12}$ $L_{\odot}$) coming from a small region of the sky ($r \backsim 1$ pc) in quasars and active galactic nuclei, and the large power ($L \backsim 10^{36}$ erg/s) emitted predominantly in X-rays observed in X-ray sources.Now it is

widely accepted that the source of energy is gravitational, the mechanism by which energy is released being accretion of matter by compact objects.

Any gravitating body attracts matter from its surroundings. If the matter being attracted has angular momentum with respect to the body, it cannot fall directly onto it, but starts orbiting the body at a fixed distance determined by its angular momentum, and the mass of the gravitating body. This leads to the formation of disks of matter rotating around the object and are known as accretion disks. Matter without angular momentum falls directly onto the object and is known as spherical accretion. The efficiency of energy generation is small in spherical accretion as compared to disk accretion.

For a body of mass M and radius R, the gravitational potential energy released by accretion of mass m onto its surface is given by $\Delta E_{ac} = \frac{GMm}{R}$ where G is the gravitational constant. For a neutron star with $M = 1\ M_\odot$ and $R \sim 10$ Km, we get $\Delta E_{ac} \sim 10^{20}$ erg/accreted gm, whereas while Hydrogen is converted into Helium in nuclear burning, $\Delta E_{ac} = 0.007\ mc^2 \sim 6 \times 10^{18}$ erg/gm only. However, it is evident from the expression for ΔE_{ac} that, the efficiency of energy release depends on the ratio (GM/R) i.e., the gravitational potential of the object. Thus for accretion onto black holes and neutron stars with $M = 1\ M_\odot$ and $R \sim 3$ km and 10 km respectively, acceretion of matter is a more efficient energy generation mechanism than nuclear burning. For a solar mass white dwarf with $R \sim 10^4$ km, even though

nuclear burning is more efficient, there are stages in the life of a white dwarf when accretion becomes the predominant energy source.

If all the kinetic energy of the infalling matter is converted into radiation at the surface of the object, the resultant luminosity is given by $L_{acc} = \frac{GM\dot{M}}{R}$, where $\dot{M}$ is the rate at which matter is being accreted. However, in practice, energy may not be released at this rate and one can introduce a parameter η such that $L_{acc} = 2\eta \frac{GM\dot{M}}{R} = \eta \dot{M} c^2$ where $R = 2GM/c^2$, is the Schwarzschild radius of the object, and η is the efficiency at which the rest mass is converted into radiation. Nuclear burning has an efficiency $\eta = 0.007$ and to account for the enrgy production in quasars it is necessary to process 250 $M_\odot$ yr^{-1} to produce the observed luminosity of $\sim 10^{47}$ erg s^{-1} which varies by an order of 2, on time scales of weeks or even less than that. If on the other hand, accretion with efficiency of energy production ~ 0.1 is the process which generates the energy, it is enough to have an accretion rate of 20 $M_\odot$ yr^{-1} to produce the above luminosity.

For a radiation of frequency ν in the continuum spectrum, a temperature T_{rad} can be associated through the relation $T_{rad} = \frac{h\nu}{K}$ where K is Boltzman's constant. For an object of radius R radiating as a black body with a luminosity L_{acc}, a black body temperature can be defind as $T_b = L_{acc}/(4\pi R^2 \sigma)^{1/4}$, where σ is the Stefan-Boltzman constant. If all the potential energy is converted into thermal energy, yet another temperature T_{th}, can be

associated with this system, defined through $T_{th} = \frac{GMm_p}{3kR}$ where m_p is mass of proton. If the accreting matter is in thermal equilibrium we get $T_{rad} \backsim T_b$. If all the accretion energy is converted directly into radiaton we have $T_{rad} \backsim T_{th}$. In general the temperature will lie between these two extremes and hence one can write $T_b < T_{rad} < T_{th}$. Now, if we make an estimate of what can be the temperatures attainable in accretion process, we see that, for a solar mass neutron star $T_{th} \backsim 5.5 \times 10^{11}$ K which corresponds to a thermal energy, $KT_{th} \backsim 50$ MeV. Similarly, for a luminosity of $L_{acc} \backsim 10^{38}$ ergs^{-1}, the blackbody temperature is $T_b \backsim 10^7$ K i.e. $KT_b \backsim 1$ KeV. This shows that accretion onto a solar mass neutron star can produce photons with energies in the range 1 KeV $\leq h\nu \leq$ 50 MeV, which corresponds to X-ray enegies. In the same way, it can be shown that accretion onto a solar mass white dwarf produces photons with energy 6 eV $\leq h\nu \leq$ 100 KeV which corresponds to ultraviolet and soft X-rays.

Matter in accretion flow is expected to be in plasma state due to the high temperature generated. The flow of charged particles creates magnetic fields, which in turn can affect the flow as well as the radiation mechanism. If a seed magnetic field was present in the accreted matter, it can be amplified to large values near the inner regions of the disk. So a realistic study of accretion flow should take into account the effects of magnetic field in the dynamics of accretion flow. It has been shown in the study of single particle dynamics around black holes that, it is possible to have stable orbits very near to the object, which is not

possible in a pure Schwarzschild background, where one cannot have stable orbits for particles below the last stable orbit ($\gtrsim$ 4m) (Prasanna and Varma,1977). Znajek (1977) has shown the possibility of having stable orbits very near to the black hole,when magnetic field is present. The fact that,one can have a disk very close to the compact object, is important, because it allows the extraction of more energy. As the gravitational field near the compact object will be very intense, it becomes necessary to consider the effects of general relativity. So a better understanding of accretion process is possible only by a self-consistent study of plasma processes in curved space time with the associated electromagnetic fields.A fluid approach is necessary if collective effects are important, whereas study of particle dynamics can give a good understanding of the phenomenon if the densities involved are sufficiently low. A brief description of the study of single particle dynamics as well as fluid dynamics is presented in this chapter.

1.1. Particle Dynamics

To obtain the particle trajectories in a general curved spacetime, with an associated electromagnetic field,first, the metric potentials and the electromagnetic field tensor F_{ij} should be obtained by solving the Einstein-Maxwell equations and then solve the covariant Lorentz force equation in this background.Kerr-Newman metric represents

the unique solution of Einstein-Maxwell equation corresponding to the geometry outside a blackhole of mass M, charge Q and angular momentum per unit mass a = JM/c.This solution reduces to Kerr metric for Q = 0, the Reissner-Nordstrom metric for a=0 and to Schwarzschild metric for a=0,Q=0.Carter (1973) has obtained the complete set of first integrals of motion in Kerr-Newman geometry. Ruffini (1973) studied the dynamics of charged particle in Kerr-Newman and Reissner-Nordstrom geometry. However, in astrophysical situations, as one does not expect to have an object with net charge on it,electromagnetic fields can be produced only by the presence of external currents.If the electromagnetic field energy is much less than the rest mass energy of the compact object,the Maxwell's equations can be solved in the given spacetime geometry around the object to obtain the structure of electromagnetic fields there. Ginzburg and Ozernoi (1965),Petterson (1974),Bicak and Dvorak (1977) have obtained such solutions for Schwarzschild geometry and Chitre and Vishveshwara (1975), Petterson (1975) and King et al (1975) have found solution for Kerr geometry.

Dynamics of charged particle in curved spacetime with superimposed electromagnetic fields have been extensively studied by Prasanna and Varma (1977) for Schwarzschild background, Prasanna and Vishveshwara (1978),Chakraborty and Prasanna (1981) for Kerr background.An extensive treatment of charged particle dynamics in curved spacetime with electromagnetic fields is given in Prasanna (1980).One

important result of these studies is that in presence of magnetic fields it is possible to have bound state orbits for charged particles very close to the event horizon, unlike the case of pure Schwarzschild background where it is not possible to have stable orbits for $r < 6m$.

An accelerated charged particle radiates energy. A radiating charged particle experiences a force which is proportional to the time rate of change of its acceleration and is known as radiaton reaction.In Chapter II we give an account of the study that we have done to undrstand the effect of radiation reaction on the motion of charged particle.

1.2. Disk Dynamics

Importance of accretion of matter by gravitating objects was realized long back in connection with solar system studies. Hoyle and Lyttleton (1939) have obtained an expression for the rate at which mass is accreted by a star like Sun moving through cold interstellar gas.In 1952,Bondi considered the case of infall of matter to a self gravitating body, obtained analytical solutions for the fluid flow and evaluated the accretion rate.

Following the discovery of objects like X-ray sources and quasars, there was a renewal of the study of accretion mechanism. The observed large luminosities in quasars and the large power emitted, predominantly in X-rays in the X-ray sources demanded a different energy generation

mechanism which is more efficient than the conventional nuclear burning.As discussed earlier,accretion of matter by compact objects can convert the rest mass into radiation with far more efficiency than nuclear burning. Models proposed for quasars, have massive compact objects at the centre of galaxies accreting matter from the surroundings producing large amount of luminosity.

Even before the detection of X-ray sources,Hayakawa and Matsuoka (1964) had suggested that close binary stars may be detectable as X-ray sources, because of the mass accretion (gas from the companion impinging upon the primary) yielding high temperature plasma which can emit thermal X-rays. In a similar vein, Novikov and Zeldovich (1966) and Shklovsky (1967), Prendergast and Burbridge (1968) had proposed that accretion onto neutron stars and black holes in binaries could produce X-rays emitted as a consequence of the liberation of gravitational binding energy released by the infalling matter.The discovery in 1971 of the sources Cen X-3 and Her X-1 by the UHURU satellite, exhibiting eclipses and periodic Doppler variations of the pulsation period was really the beginning of a new era in astronomy.In the following years lots of new X-ray sources were discovered and correspondingly many theoretical models were proposed. Paczynski (1978) discussing the evolution of binary X-ray systems,expressed a belief that the majority of strong galactic X-ray sources are interacting close binaries with the optical component being O or B type giants nearly filling their Roche Lobe

and the X-ray emitter being a neutron star (Cen X-4,Vela X-1, SMC X-1) or possibly a black hole like Cyg X-1 and Cir X-1. Further it was argued that the type II sources which have a very high ratio of X-ray to optical luminosity could very well be compact objects like neutron stars or black holes surrounded by massive (thick) accretion disk.

Whether it is high mass X-ray binary or the low mass one, the main mechanism of X-ray emission is attributed as due to accretion with mass transfer through stellar wind (spherical accretion) for the high mass ones and through Roche Lobe filling (disk accretion) for the low mass ones. In the former case, the orbiting primary comes in as an obstacle in the wind stream of the companion which has expanded and a bow shaped shock forms around the primary and the gas stream accreates onto the primary in a spherically symmetric fall.On the other hand,in the latter case, wherein the secondary fills its Roche Lobe and then the expanding gas from its corona moves through the inner Lagrange point L_1 onto the orbiting primary (pulled in by the intense gravity of the primary).As this directed flow will have significant angular momentum,the infall will no longer be radial but form a disk around the compact primary with the matter in the disk being balanced by the centrifugal and gravitational forces. Unless the binary period is quite long,the inflowing gas through L_1 appears to move almost orthogonally to the line joining the centres of the two stars.

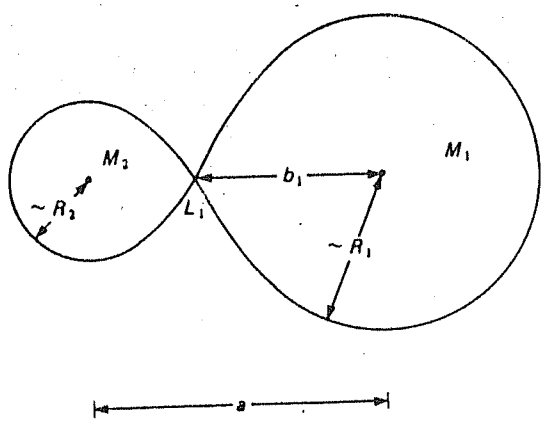

Fig. 1.1

The configuration of this is shown in Fig. (1.1). The incoming gas orbits the primary in the binary plane at a distance R_c such that the Keplerian orbit at R_c has the same angular momentum as the transferring gas had on passing L_1

$$V_\phi(R_c) = \left(\frac{GM_1}{R_1}\right)^{1/2} \qquad (1.1.1)$$

with $R_c V_\phi = b_1^2 \omega$, b_1 being the distance of L_1 from the centre of M_1 and $\omega = 2\pi/P$, P being the binary period. Simplifying and using Kepler's law

$$4\pi^2 a^3 = G(M_1 + M_2) P^2 \qquad (1.1.2)$$

one gets $R_c = (1+q)\, b_1^4/a^3$, q being the mass ratio M_2/M_1. This gives the necessary conditions on dimensions of the disk, once the mass and radius of the primary is known, along with the binary period. As the disk is composed of matter with bulk motion there could be dissipative processes giving rise to a redistribution of angular momentum and subsequent infall of the material from the disk onto the primary

surface. As the gas element starts at distances quite far from the primary, with very little binding energy, the total luminosity in steady state is

$$L_{disk} = \frac{GM_1\dot{M}}{2R} \qquad (1.1.3)$$

$\dot{M}$ being the accretion rate. This disk luminosity is just about half the accretion luminosity which is obtained when all the kinetic energy of infalling matter is given up at the stellar surface, $L_{acc} = \frac{GM_1\dot{M}}{R}$. Thus about half the kinetic energy of matter would be lost due to disk luminosity and the dissipative processes produce torque that transport angular momentum outward and finally away from the disk. However, the timescale over which this happens could be long enough (in fact depends on the nature of viscosity) so that one can conceive of disk configurations existing in equilibrium around the primary with the inner edge at R_c and the outer edge inside the Roche Lobe of the primary. Most of the disks are generally assumed to be thin, whereas there do exist discussions of thick disks with the inner edge being blown up by radiation pressure. In either case the gas in the inner regions of the disk would get heated up into temperatures $\sim 10^5$-10^6 ^oK and becomes a source for X-rays. Further these soft X-rays scattering with the hot relativistic electrons of the plasma, achieve greater energy by inverse Compton scattering and appears as hard X-rays observed in the X-ray binaries.

Lynden-Bell (1969) studied the accretion of matter by

massive black holes at the centre of galaxies as a possible mechanism of energy generation by quasars.Shakura (1972), Pringle and Rees (1972) and Shakura and Sunyaev (1973) have studied the accretion process using Newtonian dynamics whereas Novikov and Thorne (1973) have extended this study to include the effects of strong gravitational fields by having a general relativistic approach.They consider the formation of a disk around a compact object slowly spiralling onto the object as angular momentum is carried outward by viscosity.Molecular viscosity being too small to produce the required dissipation of energy to account for the observed luminosity, it is considered that there exist large anomalous viscosity whose origin may be turbulent or magnetic stress. Since the mechanism of producing viscosity by turbulence or magnetic field is not well understood,it is characterised by a parameter α given by

$$\alpha = \frac{v_t}{v_s} + \frac{H^2}{4\pi \rho v_s^2}$$

where

$\frac{\rho v_s^2}{2} = \frac{3}{2}\frac{\rho K \bar{T}}{m_p} + \varepsilon_r$ is the thermal energy density of matter, ε_r is the energy density of radiation, V_s is the sound velocity in the fluid and V_t is the characteristic turbulent velocity. All the dynamical variable connected with the accretion flow can be determined in terms of α, the accretion rate $\dot{M}$ at the outer boundary and the mass of the central object M and distance R from the central object. These models are known as α-models.Properties of the disk are largely independent of the central body except at the

inner boundary. If the object is a neutron star or white dwarf, matter have to be slowed down before it hits the star surface. The process by which it is slowed down determines the nature of the radiation spectrum.If the objects have magnetic fields associated with it,as we go nearer to the object the magnetic pressure increases more rapidly than gas pressure and when they are of comparable magnitude,the disks gets disrupted and matter starts flowing in quasi-radial orbits along the field lines.This process will also change the nature of radiation emitted from the inner regions of the disk.

Most of the accretion disk models had been constructed in the realm of Newtonian description of gravitation as it was always believed that the gravitational potential at the site of emission is rather small.However,in the description of accretion disks the effects of general relativity had been considered by Shakura and Sunyaev (1973),and Novikov and thorne (1973),Page and Thorne (1974) and several others, an integrated treatment of which may be found in Shapiro and Teukolsky (1984).The situation for considering general relativity in the accretion dynamics has gotten further strengthened with the discovery of quasiperiodic oscillations in the galactic X-ray sources. Paczynski (1987) has pointed out the relevance of the flow through r_{ms}, the marginally stable orbit for nonmagnetospheric disk accretion onto neutron stars,which requires the discussion of flow properties as described by general relativity.

In case the compact object is a black hole,it is very

pertinent to have the general relativistic formalism since the disk could reach almost upto 3m (1.5 times the Schwarzschild radius) with the help of external magnetic fields. The same would apply to the case of extremely compact neutron stars too.Whatever the emission mechanism be, it is evident that accretion in binary systems with self consistent electromagnetic fields in the presence of intense gravitational field is the physical phenomena whose dynamics has to be properly understood for constructing models.

1.3. Basic Theory of α-Disk Models

Assumptions

1. The disk is considered to be geometrically thin.At any point on the disk with radial distance R from the centre, the thickness of the disk H is such that $H/R \ll 1$.

2. Pressure gradients and heat flux along radial direction are neglected.Hence it can be safely assumed that matter follows Keplerian orbits. At a radius R from an object of mass M, the Keplerian angular velocity is given by

$$\Omega = \Omega_K(R) = \left(\frac{GM}{R^3}\right)^{1/2} \qquad (1.3.1)$$

and circular velocity $V_\phi = R\,\Omega_K(R)$.

3. Radial drift velocity V_R is small compared with V_ϕ ($V_R << V_\phi$) and is subsonic $V_R < V_S = \left(\frac{\partial P}{\partial \rho}\right)^{1/2}$.
Vertical component of the velocity V_Z is negligible.

$$V_z << V_R << V_\phi$$

The disk is characterised by a surface density $\Sigma(R,t)$ defined as the mass/unit area of the disk and is obtained by integrating the density in the Z-direction.
The equations of motion for a fluid element at radius R can be written as

$$R\frac{d\Sigma}{dt} + \frac{\partial}{\partial R}\left(R\Sigma V_R\right) = 0$$

(conservation of mass)

(1.3.2)

and

$$R\frac{\partial}{\partial t}\left(\Sigma R^2\Omega\right) + \frac{\partial}{\partial R}\left(R\Sigma V_R R^2\Omega\right) = \frac{1}{2\pi}\frac{\partial G}{\partial R}$$

(conservation of angular momentum)

(1.3.3)

where G(R, t) is the torque acting due to viscosity and is given by the expression

$$G(R,t) = 2\pi R\nu\Sigma R^2\frac{\partial\Omega}{\partial R}$$

(1.3.4)

These equations can be used to obtain the equation for the time evolution of the surface density as given by

$$\frac{\partial\Sigma}{\partial t} = \frac{3}{R}\frac{\partial}{\partial R}\left\{R^{1/2}\frac{\partial}{\partial R}\left[\nu\Sigma R^{1/2}\right]\right\}$$

(1.3.5)

and radial velocity

$$v_R = -\frac{3}{\Sigma R^{1/2}} \frac{\partial}{\partial R}\left[\nu \Sigma R^{1/2}\right] . \qquad (1.3.6)$$

If ν is known, all other dynamical variables of the disk can be determined in terms of ν. The standard α-disk is characterised by the viscosity relations

$$\nu = \alpha c_s H \qquad (1.3.7)$$

where c_s is the sound speed in the disk, H is the thickness of the disk and $\alpha \leq 1$. If magnetic fields are present α is increased by $\alpha \sim \frac{v_A^2}{c_s^2}$ where v_A is the Alfven speed in the disk. For steady state one can get the following relations.

Accretion rate

$$\dot{M} = -2\pi R \Sigma v_R , \qquad (1.3.8)$$

$$\nu\Sigma = \frac{\dot{M}}{3\pi}\left[1 - (R_g/R)^{\frac{1}{2}}\right] , \qquad (1.3.9)$$

where R_g is the Schwarzschild radius of the object.

Viscous dissipation per unit surface area

$$D(R) = \frac{3GM\dot{M}}{8\pi R^3}\left[1 - (R_g/R)^{\frac{1}{2}}\right] , \qquad (1.3.10)$$

Luminosity of the disk

$$L_{disk} = \frac{GM\dot{M}}{2R_g} . \qquad (1.3.11)$$

The vertical structure of the disk is obtained from

hydrostatic equilibrium in the Z-direction (cylindrical polar coordinates)

$$\frac{1}{\rho}\frac{\partial P}{\partial z} = \frac{\partial}{\partial z}\left[\frac{GM}{(R^2+z^2)^{\frac{1}{2}}}\right] \qquad (1.3.12)$$

which for Z <<R gives

$$\frac{1}{\rho}\frac{\partial P}{\partial z} = -\frac{GMz}{R^3} \qquad (1.3.13)$$

with the solution

$$\rho(z,R) = \rho_c(R)\exp(-z^2/H^2) \qquad (1.3.14)$$

where we have taken $P \sim \rho c_s^2$. Half thickness H is given by

$$H = c_s^2 R/GM . \qquad (1.3.15)$$

For the thin disk definiton to hold we need $c_s << \left(\frac{GM}{R}\right)^{1/2}$ i.e.,local Keplerian velocity should be highly supersonic.

1.4. Time Dependence of α-Disks

Lightman (1974) and Lightman and Eardly (1974) have studied the time dependence of α-disk models to understand the stability of time dependent disk models and the variability of mass deposition rate as a possible explanation for the observed periodicity in the X-ray source HerX-1.They obtained an 'evolution equation' for the surface density Σ of the disk,which when solved can be

used to calculate all other disk structure variables.It was found that, in the inner region of the disk,where radiation pressure dominates the gas pressure,an instability which leads to clumping of matter into rings occurs.This shows the break down of α-disk model at the inner edge and makes it necessary to revise the basic assumptions behind this model. One important assumption is that the disk is geometrically thin everywhere,which need not be true always. If the disk cannot radiate away all the radiation produced in the inner region,pressure gradient forces will develop in the vertical direction leading to bulging of the disk and formation of thick disk structure with thickness comparable to radial distance.

1.5. Thick Disks

The theory of thick accretion disks is relatively less understood compared to that of thin disks.Thick disks are formed when the accretion rate is large enough to produce luminosities of the order of or more than Eddington luminosity, where the Eddington luminosity is the luminosity at which radiation pressure on free electron balances gravity and is given by $L_E = \frac{4\pi G M m_p c^2}{\sigma_T}$ with σ_T being the Thomson scattering cross section.As already mentioned, this leads to the formation of pressure gradient forces which supports disks with thickness comparable to its radial distance. Another reason for the study of thick accretion disk is that, they provide a mechanism by which

particles can be accelerated to very high velocities in the narrow funnels that they possess,due to the large radiation pressure gradients that exist there.Thus thick disks can explain at the same time both the energy generation mechanism as well as the obsreved jets in objects like active galactic nuclei.

One of the earliest studies of thick disk is that of Fishbone and Moncrief (1976). They studied stationary, axisymmetric, purely azimuthal flow of isentropic fluid in an arbitrary stationary, axisymmetric gravitational field, and as a special case obtained solutions for a fluid disk around Kerr black hole without taking self gravity of the disk into account. For constant angular momentum per unit mass, it was shown that disks have considerable thickness in the direction perpendicular to the equatorial plane. Following this, Abramowicz et al (1978) have given an analytical theory of the hydrodynamical structure of accretion disks around compact objects, using a pseudo-Newtonian potential $\psi = \frac{GM}{R - R_g}$,which reproduces most features of a Schwarzschild metric.They showed that, for a disk with constant angular momentum density,the surface of the disk lie on equipotential surfaces and the inner edge of the marginally stable orbit shows a cusp located at the equatorial plane (Fig. 1.2) between r_{ms} and r_{mb}. Paczynski and Witta (1980) and Jaroszynski et al (1980) have worked out details of thick accretion disk models which can produce super Eddington luminosities with large accretion rates. In the models of Abramowicz et al,the gas

falls over the cusp with no dissipation of angular momentum. Accretion is driven by pressure gradient forces and there is no need of any viscosity whereas Paczynski and Witta considered generation of energy by viscous dissipation. Abramowicz et al (1980) in their study of thick accretion disk using Newtonian dynamics have shown that, super Eddington luminosities ($L \backsim 100\ L_E$) do not change the equilibrium configuration of the disk. Rees et al (1982) have studied ion supported torus around massive blackholes accreting gas at subcritical rates in a galactic nuclei and shown that, the inner regions of such disks can collimate a pair of relastivistic jets comprising electrons,positrons and electromagnetic fields.The acceleration of the jets is possible by tapping the rotational energy of the blackhole through electromagnetic interactions. Sikora (1981) studied the effects of absorption and re-emission of radiation from the surface of the disk and have computed upper limits for the total luminosities and collimation of radiation from thick radiation supported disks. Chakraborty and Prasanna (1982) have clearly underlined the necessity of using General Relativity by comparing the meridional structue of thick disk in Newtonian and GR formalisms,and showing that the cusp at the inner edge forms only when GTR effects are considered.

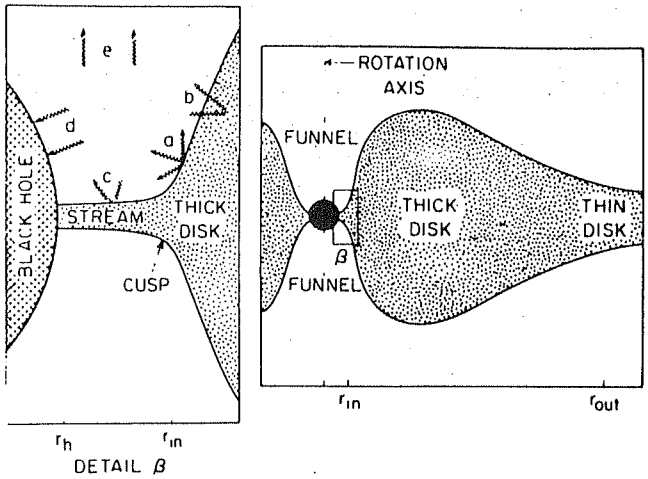

Fig 1.2.

1.6. Magnetic Accretion Disks

White dwarfs and neutron stars generally possess surface magnetic fields of the order of 10^7 G and 10^{12} G respectively. Even though a black hole cannot have intrinsic magnetic field asociated with it, external currents can produce a field around it.It is generally accepted that, magnetic fields can play the role of viscosity in transferring angular momentum and further acting as a dissipation mechanism. If the magnetic pressure is comparable with the gas pressure, which is possible in various circumstances in the inner regions of the disk,the disk gets disrupted, and the matter flow acquires a quasiradial nature following the magnetic field lines.The emitted spectrum can also be significantly modified when magentic fields are present.

Lynden-Bell (1969) has considered magnetic fields as a possible mechanism of viscosity. As a magnetic field is sheared by an initially perpendicular displacement, the

component across the shear is left unchanged whereas the one down the shear gets continually amplified till the magnetic pressure becomes equal to the gas pressure.The resulting magnetic stress can be estimated to be equal to $W_{r\phi} \sim H_r \times H_\phi / 8\pi \sim H^2/8\pi \sim \rho \frac{GM}{r}$. Shakura and Sunyaev (1973) have shown that it is possible to incorporate viscosity produced by magnetic fields in the α-prescription, the contribution to α being V_A^2/C_s^2 where V_A is the Alfven velocity.

Eardly and Lightman (1975) have formulated a detailed self consistent model for magnetic viscosity in an accretion disk around Kerr blackhole.The magnetic field is amplified by shear and dissipated by reconnection,leading to a chaotic field configuration in steady state consisting of magnetic cells which reconnect with each other.The integratged shear stress is obtained in terms of the magnetic flux. Based on the microscopic formulation of transport processes in a plasma,Ichimaru (1976) has studied the turbulence generated by differential rotation and its decay through current dissipation due to anomalous magnetic viscosity. Blandford (1976) gave a model of an accretion disk, where it is shown that, if the material carries a vertical component of magnetic field (parallel to the rotation axis), then a magnetosphere can form above and below the disk. Analytical solutions for such a force-free geometry was obtained, which has the property that energy and angular momentum can be extracted from the disk without invoking any separate viscous torques.Blandford and Znajek

(1977) studied the case of a rotating black hole threaded by magnetic field lines produced by currents flowing in an equatorial disk and showed that if the induced potential difference is too large then electron-positron pairs will be produced leading to the creation of a force free magnetosphere, and energy and angular momentum can be extracted electromagnetically.

Bisnovatyi-Kogan and Ruzmaikin (1974,1976) studied the variation of magnetic field in spherically symmetric accretion flow of infinitely conducting fluid in Schwarzschild geometry and made estimates of synchroton radiation from such flow.Also they showed that considerable part of the radiation was formed in the relativistic region $r < (2.5 \text{ to } 7.7)\ R_g$. Further, they have obtained two dimensional magnetohydrodynamic solutions of accretion of matter onto a blackhole in the Newtonian case and obtained the structure of the disk and the spectrum of outgoing radiation for the cases of laminar disks with Coulomb mechanism of dissipation and that for turbulent disks.

The problem of magnetic accretion onto neutron stars was studied by Pringle and Rees (1972),for non-axisymmetric magnetic fields showing that, if the star has a magnetic field and is spinning slowly,accretion takes place along field lines, and X-rays will be emitted thermally from regions near the magnetic poles of the neutron star,the radiation being pulsed with a frequency equal to the rotation period of the star.On the other hand,no accretion takes place when either magnetic field is very strong or

the star is rotating very rapidly.Lamb et al (1973) showed that in a magnetic disk around a rotating star,the stellar magnetic field is screened by the currents flowing in the accretion plasma in regions far away from star,whereas in closer regions, the stellar field forces matter to corotate with the star. The position of Alfven surface,where the transition between the two regions occurs,is dependent on the flow pattern and the strength of the stellar field. Ghosh et al (1977) showed that in accretion of matter by neutron star with the axis of stellar magnetic field aligned with the rotation axis,within the Alfven radius,the flow of matter is described by magnetohydrodynamics.Matter in this region moves along the field lines when viewed from the frame corotating with the star.Considering the case of Keplerian disk outside the magnetosphere,they showed that, it is possible to have a strong spin up torque exerted on the star by the disk.Further they obtained solutions for the matter flow and configuration of magnetic field inside the magnetosphere, both of them showing dependence on the angular momentum transport to the star by accreting matter. By matching the solution of flow in the regions outside and inside the magnetosphere,they obtained torque acting on the star and further calculated bounds on the accretion torque. Extending their study Ghosh and Lamb (1978,1979) showed that the stellar magnetic field cannot be completely screened by the disk plasma and the coupling between the two exerts a torque on the star.They calculated the total accretion torque, which shows a periodic change which is in

accordance with the observed period changes in pulsating X-ray sources. In the case of steady, axisymmetric disk accretion by aligned rotator, a detailed structure of the vertical and radial structure of the transition zone was obtained. They calculated the effective conductivity of the disk plasma under steady state condition and the effective dissipation which is in agreement with that expected from magnetic flux reconnection.

Aly (1980) obtained the structure of magnetic field resulting from distortion of stellar field by currents flowing in the disk with a perfectly conducting plasma, whereas Kundt and Robnik (1980) obtained the field line structures by numerical methods.Review articles by Gerhard Bornet (1980) and S.Hayakawa (1986) give a detailed account of production of X-rays from accreting neutron stars where the effect of magnetic field on accretion flow is reviewed. Kaburaki (1986,1987) has studied the structure of Keplerian disks threaded by magnetic field lines and showed that the azimuthal velocity of the disk plasma is somewhat reduced from the Keplerian value due to the pressure gradient forces exerted by the magnetic field.Magnetic stress acts as viscous stress and extracts angular momentum from the disk. The solutions are obtained in terms of the electrical conductivity, $\eta = c^2/4\pi\sigma$ which depends on the half thickness of the disk and corresponds to specifying the effective kinematic viscosity $\nu = \alpha c_s H$ in the standard α-models. In another paper Kaburaki and Itoh (1987) have proposed an analytical model for ionized jets from young

stars, where the azimuthal component of the magnetic field which is generated by accretion disks around the object plays an essential role in collimation and long travel distance of the jets.

In Chapter III we present a general formalism for the study of plasma disks around slowly rotating compact objects. The study of the dynamics and structure of plasma disks of infinite conductivity with only azimuthal velocity nonzero around a stationary compact object is presented in Chapter IV,and that of a plasma disk of finite conductivity with nonzero azimuthal and radial velocity in Chapter V. Finally in Chapter VI, we give results of the study of a plasma disk of infinite conductivity with only azimuthal velocity nonzero around a slowly rotating compact object.

1.7. Luminosity Function of Radiation from Accretion Disk

When the matter circulating along the Keplerian orbit gradually falls inward,half of the energy released will be converted into radiation from the disk,the other half being carried into the accreting star's surface as kinetic energy of the matter and is released there.Thus accretion disks are expected to have atleast two emission regions with different characteristics of emissions.The observed X-ray spectra of low mass binary X-ray sources indeed show two spectral components, a hard component and a soft component (Mitsuda et al 1984;White et al 1986).A detailed account of the emission characteristics of accreting neutron stars is

given by Hayakawa (1986). Page and Thorne (1974) gave a model for a geometrically thin accretion disk rotating around Kerr black hole taking the effect of general relativity into account. Luminet (1979) adapted the result obtained by Page and Thorne to calculate the distribution of bolometric flux as seen by observers at various angles above the plane of the disk. Hanawa (1989) showed that taking into account general relativity significantly modifies the results obtained in a Newtonian model.Compared to the Newtonian model,the colour temperature is less by a factor of 3 in the general relativistic model.Also observed maximum temeprature has a strong dependence on radial distance ($T_{col} \propto r^{-3/4}$) in the Newtonian model,whereas it has only a weak dependence on radial distance in the general relativistic model. In Chapter IV, we give the results of our study of the dependence of the luminosity function for different azimuthal velocity structures.

Figure Captions

Fig. 1.1 : Accretion disk formation in Binary star system

Fig. 1.2 : Formation of cusp in the inner region of thick disk

CHAPTER II

EFFECT OF RADIATION REACTION ON THE MOTION OF CHARGED PARTICLES IN ELECTROMAGNETIC FIELDS AROUND COMPACT OBJECTS

2.1. Introduction

The dynamics of charged particle motion in electromagnetic fields surrounding blackholes had been studied extensively by several authors,a review of which is given in Prasanna (1980). In these studies,it was shown clearly that, in the presence of magnetic fields it is possible to have stable orbits for charged particles very close to the event horizon of a black hole.Negative energy orbits of particles in magnetic fields around compact

objects wherein the possibility of energy extraction in the sense of Penrose process exists has been studied by Prasanna and Dadhich (1982),Prasanna (1983) and Dhurandhar and Dadhich (1984). Prasanna and Rawal (1983) studied charged particle trajectories in electromagnetic fields near compact objects in the framework of Rosen's bimetric theory of gravity.

However, in all these studies, the discussion was restricted to the class of orbits wherein the radiation emission effects of the charged particles were not considered. The trajectories of particles whose energy and angular momentum were constants throughout were considered and it was found that they have stable orbits under varying circumstances. A particle in orbit around a blackhole will radiate as it is accelerated and will loose energy and angular momentum.A radiating charged particle experiences a force which is proportional to the rate of change of acceleration and is known as radiation reaction. It is important to see the effect of this force on the motion of charged particles in the context of a plasma disk around compact objects, because the possibility of having a stable disk depends on how long the charged particle can stay in orbit.

2.2. Equation of Motion for Radiating Charged Particle

The concept of radiation reaction was first introduced by Lorentz as a damping force that appeared in the

equations of motion of the electron loosing energy by radiation. However, the special relativistic expression was first obtained by Abraham, and is known as the Abraham four vector (Rohrlich 1965) represented as

$$R^i = \frac{2e^2}{3c^3}\left(\dot{a}^i - u^i a_j a^j\right) \tag{2.2.1}$$

wherein the acceleration $a^i = \frac{du^i}{ds}$, u^i being the 4-velocity defined as $\frac{dx^i}{ds}$; the overhead dot denotes the derivative with respect to the affine parameter s and $ds^2 = g_{ij}dx^i dx^j$ is the background metric.

The Lorentz-Dirac equation for the motion of charged particle in an electromagnetic field is given by

$$M_0 a^i = \frac{e}{c} F^i_j u^j \tag{2.2.2}$$

where $F_{ij} = A_{j,i} - A_{i,j}$ is the electromagnetic field tensor with A_i being the four potential.

By including the radiation reaction term, the equation of motion for the radiating charged particle is given by

$$M_0 a^i = \frac{e}{c} F^i_j u^j - \frac{2e^2}{3c^3}\left(\dot{a}^i - u^i a_j a^j\right) \tag{2.2.3}$$

For a general curved spacetime, this equation can be written as

$$M_0 a^i = \frac{e}{c} F^i_j u^j - \frac{2e^2}{3c^3}\left(\frac{Da^i}{Ds} - u^i a_j a^j\right) \tag{2.2.4}$$

where the acceleration a^i is defined by

$$a^i = \frac{Du^i}{Ds} = u^i_{;j} u^j = \frac{du^i}{ds} + \Gamma^i_{jk} u^j u^k \qquad (2.2.5)$$

with Γ^i_{jk} the Christoffel symbols.

Since R^i contains the term $\frac{Da^i}{Ds}$, the equation of motion is a third order differential equation, which in general leads to runaway solutions. However, here we consider an approximate case only, where a^i in the expression for R^i is replaced by the approximate form $a^i \simeq (e/Moc) F^i{}_j u^j$, thus reducing the equations of motion to a second order differential equation.

The term $\frac{Da^i}{Ds}$ in expression (2.2.4) can be written as

$$\frac{Da^i}{Ds} = \frac{D}{Ds}\left[\frac{e}{Moc} F^i_j u^j\right] = \frac{e}{Moc}\left[F^i_j u^j\right]_{;k} u^k$$

$$= \frac{e}{Moc}\left[F^i_{j;k} u^k + \frac{e}{Moc} F^i_j F^j_k u^k\right] \qquad (2.2.6)$$

where we have used equation (2.2.2).

Using the relation $F^i_{p;\,j} = F^i_{p,\,j} - \Gamma^m_{jp} F^i_m + \Gamma^i_{mj} F^m_p$ in (2.2.6) and then substituting it in (2.2.4), the equation of motion can be written explicitly as

$$\frac{du^i}{ds} = -\Gamma^i_{jk} u^j u^k + (e/Moc) F^i_j u^j$$

$$-\frac{2e^2}{3c^3}\left\{\left(\frac{e}{Moc}\right)\left[F^i_{pj}u^j - \Gamma^m_{pj}F^i_m u^j + \Gamma^i_{mj}F^m_p u^j\right]u^p u^j\right.$$

$$+ (e/Moc)^2 F^i_p F^p_j u^j$$

$$\left. - u^i (e/Moc)^2 F_{pk} F^p_l u^k u^l\right\}$$

(2.2.7)

Considering the motion of charged particle in an electromagnetic field superposed on the Schwarzschild background;

$$ds^2 = (1-2m/r)^{-1}dt^2 - (1-2m/r)dr^2 - r^2d\theta^2 - r^2\sin^2\theta\, d\phi^2$$

(2.2.8)

the four components of the equation of motion can be written as

$$\frac{du^r}{ds} = \frac{m}{r^2}\left(1-\frac{2m}{r}\right)^{-1}u^{r^2} + r\left(1-\frac{2m}{r}\right)u^{\theta^2}$$

$$+ r\left(1-\frac{2m}{r}\right)\sin^2\theta\, u^{\phi^2} - \frac{mc^2}{r^2}\left(1-\frac{2m}{r}\right)u^{t^2}$$

$$+ (e/Moc)\left[F^r_\phi u^\phi + F^r_\theta u^\theta\right]$$

$$-\frac{2e^2}{3c^3 M_0}\left(e/M_0c\right)\Big\{ F^r_{\theta,r}\,u^r u^\theta + F^r_{\theta,\theta}\,u^{\theta 2} + F^r_{\phi,r}\,u^\phi u^r$$

$$+ F^r_{\phi,\theta}\,u^\phi u^\theta + \sin\theta\cos\theta\, F^r_\phi\, u^{\phi 2} - \frac{2}{r} F^r_\phi\, u^\phi u^r$$

$$- 2\cot\theta\, F^r_\phi\, u^\phi u^\theta - \frac{m}{r^2}\left(1-\frac{2m}{r}\right)^{-1}\left[F^r_\theta u^\theta + F^r_\phi u^\phi\right] u^r$$

$$- r\left(1-\frac{2m}{r}\right)\sin^2\theta\left[F^\phi_r u^r + F^\phi_\theta u^\theta\right] u^\phi$$

$$- r\left(1-\frac{2m}{r}\right)\left[F^\theta_r u^r + F^\theta_\phi u^\phi\right] u^\theta$$

$$+ \left(e/M_0c\right)\left[\left(F^r_\theta F^\theta_r + F^r_\phi F^\phi_r\right) u^r + F^r_\theta F^\theta_\phi u^\phi + F^r_\phi F^\phi_\theta u^\theta\right]$$

$$- \left(e/M_0c\right)^2 u^r F_{km} F^k{}_r\, u^m u^l \Big\}$$

(2.2.9)

$$\frac{du^\theta}{ds} = -\frac{2}{r} u^r u^\theta + \sin\theta\cos\theta\, u^{\phi 2} + \left(e/M_0c\right) F^\theta_\phi u^\phi$$

$$- \frac{2e^2}{3M_0c^3}\left(e/M_0c\right)\Big\{ F^\theta_{r,r}\,u^{r2} + F^\theta_{r,\theta}\,u^r u^\theta$$

$$+ F^\theta_{\phi,r}\,u^\phi u^r + F^\theta_{\phi,\theta}\,u^\phi u^\theta + \left[\frac{m}{r^2}\left(1-\frac{2m}{r}\right)^{-1} u^{r2}\right.$$

$$+ r\left(1-\frac{2m}{r}\right) u^{\theta 2} + r\left(1-\frac{2m}{r}\right)\sin^2\theta\, u^{\phi 2} + \left.\frac{mc^2}{r^2}\left(1-\frac{2m}{r}\right) u^{t2}\right] F^\theta_r$$

$$- \left[\frac{2}{r} u^r u^\phi + 2\cot\theta\, u^\theta u^\phi\right] F^\theta_\phi + \left[F^r_\theta u^\theta + F^r_\phi u^\phi\right]\frac{u^\theta}{r}$$

$$+ \left[F^\theta_r u^r + F^\theta_\phi u^\phi\right]\frac{u^r}{r} - \left[F^\phi_r u^r + F^\phi_\theta u^\theta\right]\sin\theta\cos\theta\, u^\phi$$

$$+ (e/Moc)\Big[\Big(F^{\theta}{}_{r} F^{r}{}_{\theta} + F^{\theta}{}_{\phi} F^{\phi}{}_{\theta}\Big) u^{\theta}$$

$$+ \quad F^{\theta}{}_{r} F^{r}{}_{\phi} u^{\phi} + F^{\theta}{}_{\phi} F^{\phi}{}_{r} u^{r}\Big]$$

$$- u^{\theta} (e/Moc)\; F^{k}{}_{m} F_{kl} u^{m} u^{l}\Big\}$$

(2.2.10)

$$\frac{du^{\phi}}{ds} = -\frac{2}{r} u^{r} u^{\phi} - 2\, cot\theta\, u^{\theta} u^{\phi}$$

$$+ (e/Moc)\Big[F^{\phi}{}_{r} u^{r} + F^{\phi}{}_{\theta} u^{\theta}\Big]$$

$$- \frac{2e^2}{3Moc^3} (e/Moc)\Big\{ F^{\phi}{}_{r,r} u^{r^2} + F^{\phi}{}_{\theta,\theta} u^{\theta^2} + F^{\phi}{}_{r,\theta} u^{r} u^{\theta} +$$

$$+ F^{\phi}{}_{\theta,r} u^{\theta} u^{r} + \Big[\frac{m}{r^2}\Big(1-\frac{2m}{r}\Big)^{-1} u^{r^2} + r\Big(1-\frac{2m}{r}\Big) u^{\theta^2}$$

$$+ r\Big(1-\frac{2m}{r}\Big) \sin^2\theta\, u^{\phi^2} - \frac{mc^2}{r^2}\Big(1-\frac{2m}{r}\Big)\Big] F^{\phi}{}_{r}$$

$$- \frac{2}{r} F^{\phi}{}_{\theta} u^{\theta} u^{r} + \sin\theta \cos\theta\, F^{\phi}{}_{\theta} u^{\phi^2}$$

$$+ \frac{1}{r}\Big[F^{r}{}_{\theta} u^{\theta} u^{\phi} + F^{r}{}_{\phi} u^{\phi^2} + F^{\phi}{}_{r} u^{r^2} + F^{\phi}{}_{\theta} u^{\theta} u^{r}\Big]$$

$$+ cot\theta\Big[F^{\theta}{}_{r} u^{r} u^{\phi} + F^{\theta}{}_{\phi} u^{\phi^2} + F^{\phi}{}_{r} u^{r} u^{\theta} + F^{\phi}{}_{\theta} u^{\theta^2}\Big]$$

$$+ (e/Moc)\Big[F^{\phi}{}_{r} F^{r}{}_{\theta} u^{\theta} + \Big(F^{\phi}{}_{r} F^{r}{}_{\phi} + F^{\phi}{}_{\theta} F^{\theta}{}_{\phi}\Big) u^{\phi} + F^{\phi}{}_{\theta} F^{\theta}{}_{r} u^{r}\Big]$$

$$- u^{\phi}(e/M_0c)\ F_{kl}F^{k}{}_{m}u^{l}u^{m}\Big\} \qquad (2.2.11)$$

and

$$\frac{du^t}{ds} = -\frac{2m}{r^2}\left(1-\frac{2m}{r}\right)^{-1}u^r u^t - \frac{2e^2}{3M_0c^3}(e/M_0c)\Big\{\frac{m}{r^2}\left(1-\frac{2m}{r}\right)^{-1}\left[F^r_{\theta}u^{\theta}+F^r_{\phi}u^{\phi}\right]u^t - (e/M_0c)\,u^t F_{kl}F^{k}{}_{m}u^{l}u^{m}\Big\} \qquad (2.2.12)$$

with

$$F^{k}_{m}F_{kl}u^{m}u^{l} = \left[F^r_{\phi}F_{r\phi}+F^{\theta}_{\phi}F_{\theta\phi}\right]u^{\phi 2} + F^{\phi}_{\theta}F_{\theta\phi}u^{\theta 2} + F^{\phi}_{r}F_{\phi r}u^{r 2} + \left[F^{\phi}_{r}F_{\phi\theta}+F^{\phi}_{\theta}F_{\phi r}\right]u^{\theta}u^{r} \qquad (2.2.13)$$

Assuming the electromagnetic field to be of purely magnetostatic in nature and dipolar at infinity, one can use for F_{ij}, the components obtained by Ginzburg and Ozernoi (1964) as used by Prasanna and Varma (1977) the vector potential A_i given by A_i $(0,0,A\phi,0)$ with

$$A\phi = -\frac{3\mu \sin^2\theta}{8m^3}\left[r^2 \ln\left(1-\frac{2m}{r}\right) + 2m(r+m)\right] \qquad (2.2.14)$$

and the associated magnetic field components are

$$F_{r\phi} = -\frac{3\mu \sin^2\theta}{4m^2}\left[\frac{r}{m}\ln\left(1-\frac{2m}{r}\right) + \left(1-\frac{2m}{r}\right)^{-1} + 1\right] \qquad (2.2.15)$$

$$F_{\theta\phi} = -\frac{3\mu r^2}{4m^3}\sin\theta\cos\theta\left[\ln\left(1-\frac{2m}{r}\right) + \frac{2m^2}{r^2} + \frac{2m}{r}\right] \qquad (2.2.16)$$

Using these in the system of equations (2.2.5) to (2.2.11) one will have the general equations with the appropriate radiation reaction term. However, considering the particles to be confined to the equatorial plane ($\theta = \pi/2$) of the compact object, one knows the nature of orbits without the reaction term as discussed by Prasanna and Varma (1977), in terms of the effective potential. As the equations are a coupled set of second order nonlinear differential equations, they may at best be solved numerically using proper initial conditions.

If we consider the radiation reaction as a perturbation to the motion of the particle with energy E and angular momentum L as constants of motion, the initial conditions can be obtained from the first integrals of motion for such a system. As given by Prasanna and Varma, the lagrangian for the motion of charged particle in electromagnetic fields is given by

$$\mathcal{L} = \left[g_{ij} u^i_0 u^j_0 + \frac{e}{c} A_i u^i_0\right] \qquad (2.2.17)$$

where the suffix o denotes unperturbed quantities. If the background metric g_{ij} and potential A_i are stationary and axisymmetric, two first integrals of motion may be written corresponding to the two ignorable coordinates t and ϕ of the coordinate chart (t, r, θ, ϕ) as

$$u^t_o = -\left[g_{\phi\phi}(E + eA_t) + g_{t\phi}(L - eA_\phi) \right] / D \tag{2.2.18}$$

$$u^\phi_o = \left[g_{\phi t}(E + eA_t) + g_{t\phi}(L - eA_\phi) \right] / D \tag{2.2.19}$$

with

$$D = g_{\phi\phi} g_{tt} - g_{t\phi}^2 \tag{2.2.20}$$

Using the normalization condition for velocity one more integral of motion can be obtained as

$$(u^r_o)^2 = \frac{1}{g_{rr} D} \left\{ -D + g_{tt}(L - eA_\phi)^2 + g_{\phi\phi}(E + eA_t)^2 + 2g_{t\phi}(E + eA_t)(L - eA_\phi) \right\} \tag{2.2.21}$$

For the motion of charged particle confined to the equatorial plane one can consider $u^\theta = 0$ and equation (2.2.18) to (2.2.21) give the required initial values of u^r, u^ϕ, and u^t.

The complete set of differential equations for this case in terms of the dimensionless parameters

$$\sigma = \frac{cs}{m}, \quad \rho = r/m, \quad \tau = \frac{ct}{m}$$

$$\lambda = \frac{3e\mu}{4M_0c^2m^2}, \quad l = \frac{L}{mc}$$

and

$$\beta = 2e^2 / 3M_0c^2m$$

are given as

$$\frac{d^2\rho}{d\sigma^2} = \frac{1}{\rho^2}(1-2/\rho)^{-1}\left(\frac{d\rho}{d\sigma}\right)^2 + (\rho-2)\left(\frac{d\varphi}{d\sigma}\right)^2 - \frac{1}{\rho^2}(1-2/\rho)\left(\frac{d\tau}{d\sigma}\right)^2$$

$$+ \lambda(1-2/\rho)\left[\rho\ln(1-2/\rho) + (1-2/\rho)^{-1}+1\right]\left(\frac{d\varphi}{d\sigma}\right)$$

$$+ \beta\lambda\left\{\frac{1}{\rho^2}(1-2/\rho)\left[\rho\ln(1-2/\rho) + (1-2/\rho)^{-1}+1\right]\left(\frac{d\rho}{d\sigma}\right)\left(\frac{d\varphi}{d\sigma}\right)\right.$$

$$+ \frac{\lambda}{\rho^2}(1-2/\rho)\left[\rho\ln(1-2/\rho)+(1-2/\rho)^{-1}+1\right]^2\left(\frac{d\rho}{d\sigma}\right)$$

$$+ \frac{\lambda}{\rho^2}\left(\frac{d\rho}{d\sigma}\right)\left[\rho\ln(1-2/\rho)+(1-2/\rho)^{-1}+1\right]^2$$

$$\left.\times\left[\rho^2(1-2/\rho)\left(\frac{d\varphi}{d\sigma}\right)^2 + \left(\frac{d\rho}{d\sigma}\right)^2\right]\right\}.$$

(2.2.22)

$$\frac{d^2\phi}{d\sigma^2} = -\frac{2}{\rho}\left(\frac{d\rho}{d\sigma}\right)\left(\frac{d\varphi}{d\sigma}\right) - \frac{\lambda}{\rho^2}\left[\rho\ln(1-2/\rho)+(1-2/\rho)^{-1}+1\right]$$

$$-\beta\lambda\left\{\frac{1}{\rho^3}\left[\rho\ln(1-2/\rho)+\frac{2}{\rho}(1-2/\rho)^{-2}+2\right]\left(\frac{d\rho}{d\sigma}\right)^2\right.$$

$$-\frac{1}{\rho_2}\left[\rho\ln(1-2/\rho)+(1-2/\rho)^{-1}+1\right]\left[\frac{1}{\rho_2}(1-2/\rho)^{-1}\left(\frac{d\rho}{d\sigma}\right)^2\right.$$

$$\left.+(\rho-2)\left(\frac{d\phi}{d\sigma}\right)^2-\frac{1}{\rho_2}(1-2/\rho)\left(\frac{d\tau}{d\sigma}\right)^2\right]$$

$$+\frac{1}{\rho}\left[\rho\ln(1-2/\rho)+(1-2/\rho)^{-1}+1\right]\times$$

$$\left[(1-2/\rho)\left(\frac{d\phi}{d\sigma}\right)^2-\frac{1}{\rho_2}\left(\frac{d\rho}{d\sigma}\right)^2\right]$$

$$-\frac{\lambda}{\rho_2}(1-2/\rho)\left[\rho\ln(1-2/\rho)+(1-2/\rho)^{-1}+1\right]^2\left(\frac{d\phi}{d\sigma}\right)$$

$$-\frac{\lambda}{\rho_2}\left(\frac{d\phi}{d\sigma}\right)\left[\rho\ln(1-2/\rho)+(1-2/\rho)^{-1}+1\right]^2\left[\rho^2(1-2/\rho)\left(\frac{d\phi}{d\sigma}\right)^2+\left(\frac{d\rho}{d\sigma}\right)^2\right].$$

(2.2.23)

$$\frac{d^2\tau}{d\sigma^2}=-\frac{2}{\rho_2}(1-2/\rho)^{-1}\left(\frac{d\rho}{d\sigma}\right)\left(\frac{d\tau}{d\sigma}\right)$$

$$-\beta\lambda\left\{\frac{1}{\rho_2}\left[\rho\ln(1-2/\rho)+(1-2/\rho)^{-1}+1\right]\frac{d\phi}{d\sigma}\frac{d\tau}{d\sigma}\right.$$

$$-\frac{\lambda}{\rho_2}\left(\frac{d\tau}{d\sigma}\right)\left[\rho\ln(1-2/\rho)+(1-2/\rho)^{-1}+1\right]^2$$

$$\left.\times\left[\rho^2(1-2/\rho)\left(\frac{d\phi}{d\sigma}\right)^2+\left(\frac{d\rho}{d\sigma}\right)^2\right]\right\}.$$

(2.2.24)

2.3. Results and Discussion

As one can obtain self consistently the solutions of

orbit equations in terms of trajectories for particles with given initial conditions the plots so obtained would show the effects of radiation reaction. As the effect of the reaction term is cumulative one can only hope to see substantial effect only after a large number of revolutions. However, continued integration over several number of periods does not show any appreciable change in the orbit profiles from those obtained earlier without the R^i term. This clearly indicates that for the situation under consideration with the allowed values of dipolar magnetic field on the Schwarzschild background, the loss of energy due to radiation reaction seems to be negligibly small even over a large number of periods and thus there is no orbit loss for the particle. Thus the particles seem to continue in their stable orbits for sufficiently long time thus paving way for possible build up of structures which might lead to disklike configurations. With this in the background we proceed on to consider possible equilibrium configurations by just generalising the orbit equations without the radiation reaction term leading to fluid equations of motion obtained through the conservation of energy and momentum on a general curved space.

CHAPTER III

FORMALISM

In this chapter we describe a general formalism for discussing the structure and dynamics of plasma disks, around slowly rotating compact objects, having finite viscosity and conductivity (Prasanna and Bhaskaran (1989)).

3.1. Dynamics of Plasma Disks

The dynamical equations for the motion of fluid in a general curved background is obtained from the conservation laws $T^{ij}_{;j} = 0$ where T^{ij} is the appropriate energy momentum tensor. In general, the geometry of the spacetime should be obtained by solving the set of Einstein's equations

$G_{ij} = T_{ij}$. However, if the self gravity of the matter distribution is negligible compared with the gravitational field of the central object, the geometry of the spacetime can be taken to be that due to the central object only, which is given by the vacuum solution of Einstein's equations.

The spacetime outside a self-gravitating, rotating compact object is described exactly by the Kerr solution of Einstein's equations. Expressed in Boyer-Lindquist coordinates, it is written as

$$ds^2 = \left(\frac{\Delta - a^2\sin^2\theta}{\Sigma}\right) dt^2 + \frac{2a\sin^2\theta\,(r^2+a^2-\Delta^2)}{\Sigma}\,dt\,d\varphi - (B/\Sigma)\sin^2\theta\,d\varphi^2 - (\Sigma/\Delta)\,dr^2 - \Sigma\,d\theta^2 \qquad (3.1.1)$$

with

$$\Delta = r^2 + a^2 - 2mr$$

$$\Sigma = r^2 + a^2\cos^2\theta$$

and

$$B = (r^2+a^2)^2 - \Delta a^2\sin^2\theta$$

For the convenience of comparing the results with the observations in local inertial frames, one should be able to transform the geometrical variables into variables in a

local Lorentz frame. Two types of local frames can be defined. One, the local Lorentz frame (LLF) corresponding to an observer (defined through the principle of equivalence) at rest and the other, the locally nonrotating frame corresponding to an observer comoving with the disk. These transformatons can be carried out using orthonormal tetrads corresponding to the respective frames.

For any metric $ds^2 = g_{ij}dx^i dx^j$, an orthonormal tetrad can be defined through the relations

$$ds^2 = (\theta^0)^2 - (\theta^1)^2 - (\theta^2)^2 - (\theta^3)^2 \,, \qquad (3.1.2)$$

θ^a the one form being defined as

$$\theta^a = \lambda^a_i \, dx^i \,, \qquad \begin{pmatrix} a = 0, 1, 2, 3 \\ i = t, r, \theta, \varphi \end{pmatrix} .$$

λ^a_i are the components of the tetrad and are related to the metric coefficients through the relation

$$g_{ij} = \eta_{ab} \lambda^a_i \lambda^b_j \,; \quad g^{ij} = \eta^{ab} \lambda^i_a \lambda^j_b \,. \qquad (3.1.3)$$

The Kerr metric can be written in the following two tetrad forms:

$$ds^2 = \left[\left(\frac{\Delta\Sigma}{B}\right)^{1/2} dt\right]^2 - \left[\left(\frac{\Sigma}{\Delta}\right)^{\frac{1}{2}} dr\right]^2 - \left[\Sigma^{\frac{1}{2}} d\theta\right]^2$$

$$+ \left[\frac{B^{1/2} \sin\theta}{\Sigma^{1/2}} \left(d\varphi + \frac{2amr}{B} dt\right)\right]^2 \qquad (3.1.4)$$

and

$$ds^2 = \left(\frac{\Delta}{\Sigma}\right)\left[dt + a\sin^2\theta\, d\phi\right]^2 - \left(\frac{\Sigma}{\Delta}\right) dr^2$$

$$- \Sigma\, d\theta^2 - \frac{\sin^2\theta}{\Sigma}\left[(r^2+a^2)\, d\phi + a\, dt\right]^2$$

(3.1.5)

Metric (3.1.4) gives the tetrad for the locally nonrotating frame as

$$\lambda^{a}_{i}\,(LNRF) =$$

$$\begin{bmatrix} \left(\frac{\Delta\Sigma}{B}\right)^{1/2} & 0 & 0 & 0 \\ 0 & \left(\Sigma/\Delta\right)^{1/2} & 0 & 0 \\ 0 & 0 & (\Sigma)^{1/2} & 0 \\ \frac{2amr\sin\theta}{(B\Sigma)^{1/2}} & 0 & 0 & \left(B/\Sigma\right)^{\frac{1}{2}}\sin\theta \end{bmatrix}$$

(3.1.6)

Similarly from metric (3.1.5), the tetrad for the local lorentz frame can be obtained as

$$\lambda^{\mu}_{i\,(LLF)} =$$

$$\begin{bmatrix} \left(\frac{\Delta}{\Sigma}\right)^{1/2} & 0 & 0 & -\left(\frac{\Delta}{\Sigma}\right)^{1/2} a\sin^2\theta \\ 0 & (\Sigma/\Delta)^{\frac{1}{2}} & 0 & 0 \\ 0 & 0 & \Sigma^{1/2} & 0 \\ -\frac{a\sin^2\theta}{\Sigma^{1/2}} & 0 & 0 & \frac{(r^2+a^2)\sin\theta}{\Sigma^{1/2}} \end{bmatrix} \qquad (3.1.7)$$

As we are interested in the study of plasma disks around slowly rotating compact objects only, it will suffice to use the linearised form of the Kerr metric written as (neglecting terms of second order in a)

$$ds^2 = \left(1-\frac{2m}{r}\right)^{-1} dt^2 - \left(1-\frac{2m}{r}\right)^{-1} dr^2 - r^2 d\theta^2 - r^2\sin^2\theta\, d\varphi^2 + \frac{4am}{r}\sin^2\theta\, d\varphi\, dt \,. \qquad (3.1.8)$$

The associated orthonormal tetrads for this metric are

$$\lambda^{\mu}_{i\,(LNRF)} = \begin{bmatrix} \left(1-\frac{2m}{r}\right)^{1/2} & 0 & 0 & 0 \\ 0 & \left(1-\frac{2m}{r}\right)^{-1/2} & 0 & 0 \\ 0 & 0 & r & 0 \\ -\frac{2am}{r^2}\sin\theta & 0 & 0 & r\sin\theta \end{bmatrix} \qquad (3.1.9)$$

and

$$\lambda^{q}_{i\,(LLP)} =$$

$$\begin{bmatrix} \left(1-\frac{2m}{r}\right)^{1/2} & 0 & 0 & -a\left(1-\frac{2m}{r}\right)^{\frac{1}{2}}\sin^2\theta \\ 0 & \left(1-\frac{2m}{r}\right)^{-1/2} & 0 & 0 \\ 0 & 0 & r & 0 \\ -\frac{a\sin^2\theta}{r} & 0 & 0 & r\sin\theta \end{bmatrix} \qquad (3.1.10)$$

The components of the affine connections for this metric are given by

$$\Gamma^{r}_{rr} = -\frac{m}{r^2}\left(1-\frac{2m}{r}\right)^{-1}$$

$$\Gamma^{r}_{\theta\theta} = -r\left(1-\frac{2m}{r}\right)$$

$$\Gamma^{r}_{\varphi\varphi} = -r\left(1-\frac{2m}{r}\right)\sin^2\theta$$

$$\Gamma^{r}_{tt} = \frac{m}{r^2}\left(1-\frac{2m}{r}\right)$$

$$\Gamma^{r}_{\varphi t} = \frac{am}{r^2}\left(1-\frac{2m}{r}\right)\sin^2\theta$$

$$\Gamma^{\theta}_{r\theta} = \frac{1}{r}$$

$$\Gamma^{\theta}_{\varphi\varphi} = -\sin\theta\cos\theta.$$

$$\Gamma^{\theta}_{\varphi t} = -\frac{2am}{r^3}\left(1-\frac{2m}{r}\right)\sin\theta\cos\theta$$

$$\Gamma^{\varphi}_{r\varphi} = \frac{1}{r}$$

$$\Gamma^{\varphi}_{\theta\varphi} = \cot\theta$$

$$\Gamma^{t}_{rt} = \frac{m}{r^2}\left(1-\frac{2m}{r}\right)^{-1}$$

$$\Gamma^{t}_{r\varphi} = \frac{3am}{r^2}\left(1-\frac{2m}{r}\right)^{-1}\sin^2\theta$$

(3.1.11)

The components of electromagnetic fields and of the velocity can be expressed in the respective frames through the following transformation laws

$$v^{\alpha} = \frac{\lambda^{\alpha}_{(\beta)}\, v^{(\beta)} + c\,\lambda^{\alpha}_{(t)}}{\lambda^{t}_{(\beta)}\, v^{(\beta)} + c\,\lambda^{t}_{(t)}}$$

(3.1.12)

and

$$F_{ij} = \lambda^{(a)}_{i}\,\lambda^{(b)}_{j}\,F_{(a)(b)}$$

(3.1.13)

where the indices with brackets represent the components in the local frame and V^{α} is the spatial 3-velocity vector defined through the relation $u^{\alpha} = v^{\alpha}u^{t}/c$ (Prasanna 1982), where α takes values 1,2,3.

For the case of the linearized Kerr metric the

components of velocity and electromagnetic fields in the two frames are given by the expressions:

LNRF

$$V^{r} = \left(1 - \frac{2m}{r}\right) V^{(r)}$$

$$V^{\theta} = \frac{1}{r}\left(1 - \frac{2m}{r}\right)^{1/2} V^{(\theta)}$$

$$V^{\phi} = \frac{1}{r \sin\theta}\left(1 - \frac{2m}{r}\right)^{1/2} V^{(\phi)}$$

(3.1.14)

$$E_r = E_{(r)} - \frac{2am}{r^2}\left(1 - \frac{2m}{r}\right)^{-1/2} \sin\theta\, B_{(\theta)}$$

$$E_\theta = r\left(1 - \frac{2m}{r}\right)^{1/2} E_{(\theta)} + \frac{2am}{r} \sin\theta\, B_{(r)}$$

$$E_\phi = r\left(1 - \frac{2m}{r}\right)^{\frac{1}{2}} \sin\theta\, E_{(\phi)}$$

$$B_r = r^2 \sin\theta\, B_{(r)}$$

$$B_\theta = r\left(1 - \frac{2m}{r}\right)^{-1/2} \sin\theta\, B_{(\theta)}$$

$$B_\phi = r\left(1 - \frac{2m}{r}\right)^{-1/2} B_{(\phi)}$$

(3.1.15)

LLF

$$V^{\hat{r}} = \frac{(1-\frac{2m}{r})\,V^{(r)}}{\left[1+\frac{a}{r_c}(1-\frac{2m}{r})^{1/2}\sin\theta\, V^{(\varphi)}\right]}$$

$$V^{\hat{\theta}} = \frac{\frac{1}{r}(1-\frac{2m}{r})^{1/2}V^{(\theta)}}{\left[1+\frac{a}{r_c}(1-\frac{2m}{r})^{1/2}\sin\theta\, V^{(\varphi)}\right]}$$

$$V^{\hat{\varphi}} = \frac{\frac{1}{r\sin\theta}(1-\frac{2m}{r})^{1/2}V^{(\varphi)} + \frac{a\epsilon}{r^2}}{\left[1+\frac{a}{r_c}(1-\frac{2m}{r})^{1/2}\sin\theta\, V^{(\varphi)}\right]}$$

$$E\hat{r} = E(r) + \frac{a}{r}(1-\frac{2m}{r})^{-1/2}\sin\theta\, B(\theta)$$

$$E\hat{\theta} = r(1-\frac{2m}{r})^{1/2}E(\theta) - \frac{a}{r}\sin\theta\, B(r)$$

$$E\hat{\varphi} = r(1-\frac{2m}{r})^{1/2}\sin\theta\, E(\varphi)$$

$$B\hat{r} = r^2\sin\theta\, B(r) - ar(1-\frac{2m}{r})^{1/2}\sin^2\theta\, E(\theta)$$

$$B\hat{\theta} = r(1-\frac{2m}{r})^{-1/2}\sin\theta\, B(\theta) + a\sin^2\theta\, E(r)$$

$$B\hat{\varphi} = r(1-\frac{2m}{r})^{-1/2}B(\varphi) \qquad (3.1.16)$$

Here we have used the electric and magnetic field vectors defined as

$$E_\alpha = F_{\alpha t} \quad \text{and}$$

$$B_\alpha = \varepsilon_{\alpha\beta\gamma} F_{\beta\gamma} \qquad (3.1.17)$$

(without any summation).

The energy momentum tensor for an imperfect fluid with the associated electromagnetic field is given by (neglecting the heat conduction)

$$T^{ij} = (\rho + \bar{p}) u^i u^j - \bar{p} g^{ij} + 2\eta_s \sigma^{ij} - E^{ij} \qquad (3.1.18)$$

with

$$\bar{p} = p - (\eta_b - 2/3\eta_s) \Theta \; ; \quad \Theta = u^i{}_{;i}, \qquad (3.1.19)$$

$$\sigma^{ij} = \frac{1}{2}(u^{i;k} h^j_k + u^{j;k} h^i_k) - \frac{1}{3} \Theta h^{ij}, \qquad (3.1.20)$$

and

$$h^{ij} = g^{ij} - u^i u^j, \qquad (3.1.21)$$

σ^{ij}, Θ and h^{ij} representing the shear tensor, the coefficient of expansion and the projection tensor respectively and η_b and η_s are the coefficients of bulk and shear viscosity respectively. The electromagnetic stress tensor E^{ij} is related to the field tensor $F_{ij} = A_{i,j} - A_{i,j}$ through

$$E^{ij} = F^{ik} F^{j}{}_{k} - \frac{1}{4} g^{ij} F_{kl} F^{kl} .$$

(3.1.22)

The dynamical equations for the magnetofluid is obtained from the conservation laws

$$T^{ij}{}_{;j} = 0$$

(3.1.23)

together with the Maxwell's equations

$$F^{ik}{}_{;k} = - J^{i} \quad ; \quad F_{[ij,k]} = 0$$

(3.1.24)

Supplemented with the generalized Ohm's law for the current four vector

$$J^{i} = \varepsilon u^{i} + \sigma F^{i}{}_{k} u^{k}$$

(3.1.25)

where ε is the charge density and σ is the electrical conductivity. In general, the conductivity in a plasma will be a tensor quantity, but here we consider it as a scalar only.

As a special case we consider the shear viscosity to be zero ($\eta_s = 0$) and use equation (2.1.18) in (2.1.23) to get the momentum and continuity equations.Written in terms of the 3-velocity vector defined earlier, we get (Prasanna 1982)

$$\left(\rho+\frac{\bar{p}}{c^2}\right)(u^t)^2\left[\frac{dv^\alpha}{dt}+c^2\left(\Gamma^\alpha_{tt}-\frac{v^\alpha}{c}\Gamma^t_{tt}\right)\right.$$

$$\left.+2cv^\beta\left(\Gamma^\alpha_{t\beta}-\frac{v^\alpha}{c}\Gamma^t_{t\beta}\right)+v^\beta v^\gamma\left(\Gamma^\alpha_{\beta\gamma}-\frac{v^\alpha}{c}\Gamma^t_{\beta\gamma}\right)\right]$$

$$+\left(g^{ti}\frac{v^\alpha}{c}-g^{\alpha i}\right)\frac{\partial\bar{p}}{\partial x^i}$$

$$=\left(F^\alpha{}_k-F^t{}_k\frac{v^\alpha}{c}\right)\bar{J}^k_k\,, \qquad (3.1.26)$$

$$\left(\rho+\bar{p}/c^2\right)\left[v^\alpha{}_{,\alpha}+\Gamma^\alpha_{t\alpha}-\left(\Gamma^t_{t\alpha}-\Gamma^\beta_{\beta\alpha}\right)v^\alpha-\Gamma^t_{\alpha\beta}v^\alpha\frac{v^\beta}{c}\right]$$

$$+\frac{\partial}{\partial t}\left(\rho-\frac{\bar{p}}{c^2}\right)+v^\alpha\frac{\partial}{\partial x^\alpha}\left(\rho-\bar{p}/c^2\right)$$

$$+\frac{1}{c^2u^{t2}}\left[g^{tt}\frac{\partial\bar{p}}{\partial t}+cg^{t\alpha}\frac{\partial\bar{p}}{\partial x^\alpha}+F^t_k\bar{J}^k-2F_{ik}\bar{J}^k_i u^t\right].$$

(3.1.27)

For the case of the linearised Kerr metric these equations reduces to

$$\left(\rho+\bar{p}/c^2\right)u^{t2}\left[\frac{dv^r}{dt}+\frac{me^2}{r^2}\left(1-\frac{2m}{r}\right)-\frac{2ame}{r^2}v^\varphi\left(1-\frac{2m}{r}\right)\sin^2\theta\right.$$

$$-\frac{3m}{r^2}\left(1-\frac{2m}{r}\right)^{-1}v^{r2}-(r-2m)\left[v^{\theta2}+\sin^2\theta v^{\varphi2}\right]$$

$$\left.+\frac{6am}{cr^2}\left(1-\frac{2m}{r}\right)^{-1}\sin^2\theta\,v^r v^\varphi\right]+\left(1-\frac{2m}{r}\right)\frac{\partial\bar{p}}{\partial r}$$

$$+ \left(1-\frac{2m}{r}\right)^{-1}\left[\frac{v^r}{c^2}\frac{\partial \bar{p}}{\partial t} + \frac{2am}{cr^3}v^r\frac{\partial \bar{p}}{\partial \varphi}\right] = \left(F^r_k - F^t_k\frac{v^r}{c}\right)J^k$$

(3.1.28)

$$\left(\rho + \frac{\bar{p}}{c^2}\right)u^{t2}\left[\frac{dv^\theta}{dt} + \frac{2}{r}\left(1-\frac{2m}{r}\right)^{-1}\left(1-\frac{3m}{r}\right)v^r v^\theta\right.$$

$$- \sin\theta\cos\theta\, v^{\varphi 2} + \frac{2am}{r^3}\sin\theta\, v^\varphi\left\{2c\cos\theta\right.$$

$$\left.\left. + 3v^r\frac{v^\theta}{c}\, r\sin\theta\left(1-\frac{2m}{r}\right)^{-1}\right\}\right]$$

$$+ \frac{1}{r^2}\frac{\partial \bar{p}}{\partial \theta} + \left(1-\frac{2m}{r}\right)^{-1}\frac{v^\theta}{c^2}\left\{\frac{\partial \bar{p}}{\partial t} + \frac{2ame}{r^3}\frac{\partial \bar{p}}{\partial \varphi}\right\}$$

$$= \left(F^\theta{}_k - F^t_k\frac{v^\theta}{c}\right)J^k$$

$$\left(\rho + \bar{p}/c^2\right)u^{t2}\left[\frac{dv^\varphi}{dt} + \frac{2}{r}\left(1-\frac{2m}{r}\right)^{-1}\left(1-\frac{3m}{r}\right)v^r v^\varphi\right. \quad (3.1.29)$$

$$+ 2\cot\theta\, v^\theta v^\varphi + \frac{2ame}{r^3}\left\{-2\cot\theta\, v^\theta\right.$$

$$\left.\left. + \left(1-\frac{2m}{r}\right)^{-1}\frac{v^r}{r}\left(1+\frac{3v^{\varphi 2}}{c^2}r^2\sin^2\theta\right)\right\}\right]$$

$$+ \left(v^\varphi - \frac{2ame}{r^3}\right)\frac{1}{c^2}\frac{\partial \bar{p}}{\partial t}\left(1-\frac{2m}{r}\right)^{-1} + \frac{1}{r^2\sin^2\theta}\frac{\partial \bar{p}}{\partial \varphi}$$

$$+ \frac{2amv^{\varphi}}{cr^3}\left(1-\frac{2m}{r}\right)^{-1}\frac{\partial \bar{p}}{\partial \varphi} = \left(F^{\varphi}{}_{k} - F^{t}{}_{k}\frac{v^{\varphi}}{c}\right)\bar{J}^{k}{}_{e} \qquad (3.1.30)$$

and

$$\left(\rho + \bar{p}/c^2\right)\left[\frac{\partial v^{r}}{\partial r} + \frac{\partial v^{\theta}}{\partial \theta} + \frac{\partial v^{\varphi}}{\partial \varphi} - \frac{2m}{r^2}\left(1-\frac{2m}{r}\right)^{-1}v^{r}\right.$$

$$\left. + \frac{2}{r}v^{r} + \cot\theta\, v^{\theta} + \frac{6am}{cr^2}\left(1-\frac{2m}{r}\right)^{-1}\sin^2\theta\, v^{r}v^{\varphi}\right]$$

$$+ \frac{\partial}{\partial t}\left(\rho - \bar{p}/c^2\right) + v^{\alpha}\frac{\partial}{\partial x^{\alpha}}\left(\rho - \bar{p}/c^2\right)$$

$$+ \frac{1}{c^2u^{t2}}\left\{\left(1-\frac{2m}{r}\right)^{-1}\left[\frac{\partial \bar{p}}{\partial t} + \frac{2ame}{r^3}\frac{\partial \bar{p}}{\partial \varphi}\right]\right.$$

$$\left. + \left(F^{t}{}_{k}\bar{J}^{k} - 2F_{ik}\bar{J}^{k}u^{i}u^{t}\right)\right\} . \quad = 0 \qquad (3.1.31)$$

Using the relation

$$g_{ij}u^{i}u^{j} = 1 \qquad (3.1.32)$$

u^{t} can be expressed in terms of the spatial velocity components as

$$u^{t2} = \left(1-\frac{2m}{r}\right)^{-1}\left(1 - v^2/c^2\right)^{-1} \qquad (3.1.33)$$

where $v^2 = v^{(r)2} + v^{(\theta)2} + v^{(\varphi)2}$, bracket around the indices representing components in the locally nonrotating frame.

Using Maxwell's equation (2.1.24), the current J^{i} can be written as

$$J^r = -\frac{1}{r^2 \sin\theta}\left(1-\frac{2m}{r}\right)\frac{\partial}{\partial\theta}(\sin\theta B_\varphi) + \frac{1}{r^2\sin^2\theta}\left(1-\frac{2m}{r}\right)\frac{\partial B_\theta}{\partial\varphi} + \frac{\partial E_r}{\partial t} + \frac{2am}{r^3}\left(\frac{\partial E_r}{\partial\varphi} - \frac{\partial B_\theta}{\partial t}\right) \tag{3.1.34}$$

$$J^\theta = \frac{1}{r^2}\frac{\partial}{\partial r}\left[\left(1-\frac{2m}{r}\right)B_\varphi\right] - \frac{1}{r^4\sin^2\theta}\frac{\partial B_r}{\partial\varphi} + \frac{1}{r^2}\left(1-\frac{2m}{r}\right)^{-1}\frac{\partial E_\theta}{\partial t} + \frac{2am}{r^3}\left(\frac{\partial E_\theta}{\partial\varphi} + \frac{\partial B_r}{\partial t}\right) \tag{3.1.35}$$

$$J^\phi = \frac{1}{r^4\sin\theta}\frac{\partial}{\partial\theta}\left(\frac{B_r}{\sin\theta}\right) - \frac{1}{r^2\sin^2\theta}\frac{\partial}{\partial r}\left[\left(1-\frac{2m}{r}\right)B_\theta\right] + \frac{1}{r^2\sin^2\theta}\left(1-\frac{2m}{r}\right)^{-1}\frac{\partial E_\varphi}{\partial t} - \frac{2am}{r^2}\left[\frac{\partial}{\partial r}(E_r/r) + \frac{1}{r^2\sin\theta}\left(1-\frac{2m}{r}\right)^{-1}\frac{\partial}{\partial\theta}(\sin\theta E_\theta)\right]$$

$$J^t = -\frac{1}{r^2}\left[\frac{\partial}{\partial r}(r^2E_r) + \frac{1}{\sin\theta}\left(1-\frac{2m}{r}\right)^{-1}\left\{\frac{\partial}{\partial\theta}(\sin\theta E_\theta) + \frac{1}{\sin\theta}\frac{\partial E_\varphi}{\partial\varphi}\right\}\right] \tag{3.1.36}$$

$$- \frac{2am}{r^2}\left[\frac{1}{r^3\sin\theta}\left(1-\frac{2m}{r}\right)^{-1}\frac{\partial}{\partial\theta}(\sin\theta B_r) - \frac{\partial}{\partial r}\left(\frac{B_\theta}{r}\right)\right] \tag{3.1.37}$$

Maxwell's equation gives four more equations:

$$\frac{\partial B_r}{\partial r} + \frac{\partial B_\theta}{\partial \theta} + \frac{\partial B_\varphi}{\partial \varphi} = 0 \qquad (3.1.38)$$

$$\frac{\partial B_r}{\partial t} + \frac{\partial E_\varphi}{\partial \theta} - \frac{\partial E_\theta}{\partial \varphi} = 0 \qquad (3.1.39)$$

$$\frac{\partial B_\theta}{\partial t} + \frac{\partial E_r}{\partial \varphi} - \frac{\partial E_\varphi}{\partial r} = 0 \qquad (3.1.40)$$

$$\frac{\partial B_\varphi}{\partial t} + \frac{\partial E_\theta}{\partial r} - \frac{\partial E_r}{\partial \theta} = 0 \qquad (3.1.41)$$

Together with the Maxwell's equations (2.1.34) to (2.1.41) and the expression for u^t, the set of equations (2.1.28) to (2.1.31) constitutes the set of equations governing a magnetofluid supported on the background geometry of a slowly rotating compact object.

3.2. X-Ray Emission from a Geometrically Thin Disk

Page and Thorne (1974) obtained an explicit algebraic expression for the radial dependence of the time averaged

energy flux emitted from the disk's surface.Assuming the disk to reside on the equatorial plane of a Kerr black hole and be thin with its material moving in nearly circular geodesics with negligible heat transport in the radial direction, they obtain the time averaged flux of radient energy emitted from the disk surface to be

$$f = \frac{3}{2m}\,\frac{1}{x^2(x^3-3x+2a_*)}\left\{x - x_0 + \frac{3}{2}a_* \ln(x/x_0)\right.$$

$$-\frac{3(x_0-a_*)^2}{x_1(x_1-x_2)(x_1-x_3)}\ln\left(\frac{x-x_1}{x_0-x_1}\right)$$

$$-\frac{3(x_2-a_*)^2}{x_2(x_2-x_1)(x_2-x_3)}\ln\left(\frac{x-x_2}{x_0-x_2}\right)$$

$$\left.-\frac{3(x_3-a_*)^2}{x_3(x_3-x_1)(x_3-x_2)}\ln\left(\frac{x-x_3}{x_0-x_3}\right)\right\}$$

(3.2.1)

wherein $a^* = a/m$, $x = (r/m)^{1/2}$, $x_0 = \left(\frac{r_{ms}}{m}\right)^{1/2}$ with r_{ms} the radius of the innermost stable geodesic orbit (marginally stable orbit) and x_1, x_2 and x_3 the three roots of the cubic equation $x^3 - 3x + 2a^* = 0$.Luminet (1979) and later Hanawa (1989) obtained the expression for Schwarzschild space time (a=0) given as

$$F = \frac{3GM\dot{M}}{8\pi r^3}\left(1-\frac{3m}{r}\right)^{-1}\left\{1-\sqrt{\frac{6m}{r}}+\sqrt{\frac{3m}{4r}}\ln\left(\frac{1+\sqrt{3m/r}}{1-\sqrt{3m/r}}\cdot\frac{1-\sqrt{2}/2}{1+\sqrt{2}/2}\right)\right\}$$

(3.2.2)

where $\dot{M}$ is the accretion rate,the flux being measured by a

local observer comoving with the gas in the disk.The effective temperature of the disk as a function of radial distance can be obtained from the relation

$$T_{eff} = (F/\sigma)^{1/4} \qquad (3.2.3)$$

where σ is the Stefan Boltzman constant.

As the gas emitting radiation is rotating around the central object, the radiation that the distant observer receives will be redshifted or blueshifted according to whether the radiation is emitted from the approaching part of the disk or from the receeding part.Also,the intense gravitational field at the site of emission contributes a gravitational redshift. The amount of redshift will depend on the velocity of rotation, angle of inclination of the disk to the line of sight and the mass of the central object. Hanawa obtained analytical expressions for the redshift for the two extreme cases, i.e., when the inclination angle i=0 or $\pi/2$ for radiation from a disk rotating with a velocity

$$V_\phi = \left[\frac{GM/r}{1 - \frac{2GM}{rc^2}} \right]^{1/2} \qquad (3.2.4)$$

and calculated the corresponding temperature distribution. The expression for the observed temperature can be rewritten in terms of a general rotational velocity V_ϕ as

$$T_{obs} = 1.11 \left(\frac{T_{col}/T_{obs}}{1.5}\right)\left(\frac{g(\mathcal{R}, \mathcal{R}_g)}{0.15}\right)\left(\frac{M}{1.4 M_\odot}\right)^{-1/2}\left(\frac{\dot{M}}{10^{18}\ gm\ s^{-1}}\right)^{1/4} keV \qquad (3.2.5)$$

where

$$\mathcal{R}_g = GM/c^2$$

and

$$g(x) = g_0(x)$$

$$= x^{-3/4}(1-3/x)^{-1/4}\left\{1-\sqrt{6}/x + \sqrt{3}/4x \ln\left(\frac{1+\sqrt{3}/x}{1-\sqrt{3}/x}\cdot\frac{1-\sqrt{2}/2}{1+\sqrt{2}/2}\right)\right\}^{\frac{1}{4}}$$

$$\times (1-2/x)^{1/2}\left(1-\frac{v_\phi^2}{c^2}\right)^{1/2},$$

$$g_\pm(x) = x^{-3/4}(1-3/x)^{-1/4}(1-2/x)^{1/2}(1-v_\phi^2/c^2)^{1/2}\left[1 \pm v_\phi/c\right] \qquad (3.2.6)$$

$$\times\left\{1-\sqrt{6}/x + \sqrt{3}/4x \ln\left(\frac{1+\sqrt{3}/x}{1-\sqrt{3}/x}\cdot\frac{1-\sqrt{2}/2}{1+\sqrt{2}/2}\right)\right\}^{1/4}$$

(3.2.7)

The + sign corresponds to the blueshifted part and the - sign to the redshifted part of the emission. Equations (3.2.5) to (3.2.7) can be used to obtain the radial dependence of temperature distribution in a thin accretion disk with an azimuthal velocity V^ϕ.

CHAPTER IV

PLASMA DISK AROUND A SCHWARZSCHILD BLACK HOLE WITH NON-ZERO AZIMUTHAL VELOCITY : STRUCTURE AND LUMINOSITY

4.1. Introduction

In the third chapter we gave the general formalism for studying plasma disks around slowly rotating compact objects. In this chapter we consider the case of a stationary and axisymmetric disk around a nonrotating (a=0) compact object, having only its azimuthal velocity nonzero. We assume a magnetic field which is dipolar at infinity and look for equilibrium configurations of the fluid in the gravitational field of the compact object such that at the

inner boundary of the fluid, the hydrostatic pressure is balanced by the magnetic bouyancy. Furthermore, we shall assume the fluid to be infinitely conducting plasma with zero net charge,and having only its azimuthal component of spatial 3-velocity nonzero. We obtain the equilibrium configurations for a disk of incompressible fluid confined to the equatorial plane of the compact object and further study the nature of luminosity flux functions for the class of velocity fields (Bhaskaran and Prasanna (1989a)).

4.2. Disk Structure

The dyanmical equations governing the structure of such a configuration is given by the set of equations (3.1.28) to (3.1.41), with a=0 and $\frac{\partial f}{\partial \varphi} = \frac{\partial f}{\partial t} = 0$, f being any function.

Due to axisymmetry and stationarity, the toroidal component of electric field E_φ is zero and the systems of equations for the magnetic and electric field components reduces to

$$\frac{\partial B_r}{\partial r} + \frac{\partial B_\theta}{\partial \theta} = 0 \qquad (4.2.1)$$

$$\frac{\partial E_r}{\partial \theta} - \frac{\partial E_\theta}{\partial r} = 0 \qquad (4.2.2)$$

$$J^r = -\frac{1}{r^2 \sin\theta}\left(1-\frac{2m}{r}\right)\frac{\partial}{\partial\theta}(\sin\theta B_\varphi), \qquad (4.2.3)$$

$$J^\theta = \frac{1}{r^2}\frac{\partial}{\partial r}\left[\left(1-\frac{2m}{r}\right)B_\varphi\right], \qquad (4.2.4)$$

$$J^\varphi = \frac{1}{r^2\sin\theta}\frac{\partial}{\partial\theta}\left[B_r/\sin\theta\right] - \frac{1}{r^2\sin^2\theta}\frac{\partial}{\partial r}\left[\left(1-\frac{2m}{r}\right)B_\theta\right], \qquad (4.2.5)$$

$$J^t = -\frac{1}{r^2}\left[\frac{\partial}{\partial r}(r^2 E_r) + \frac{1}{\sin\theta}\left(1-\frac{2m}{r}\right)^{-1}\frac{\partial}{\partial\theta}(\sin\theta E_\theta)\right]. \qquad (4.2.6)$$

Since the charge density ε_q is zero and the electrical conductivity σ is infinite the generalized Ohm's law (3.1.25) gives the force free condition

$$F^i_k u^k = 0. \qquad (4.2.7)$$

For V^r and V^θ zero, this gives the two relations between the electric and magnetic field components

$$E_r = \frac{V^\varphi}{c} B_\theta \quad ; \quad E_\theta = -\frac{V^\varphi}{c} B_r . \qquad (4.2.8)$$

As the magnetic field is assumed to be dipolar at infinity, one has the simple solution

$$B_r = B_0 \frac{R_c^3}{r} \sin\theta\cos\theta ;$$

$$B_\theta = \frac{B_0}{2}\frac{R_c^2}{r^2}\sin^2\theta , \qquad (4.2.9)$$

with B_0 being the surface field of the compact object with

radius R_e. In terms of the LNRF components, one has the field given by

$$B(r) = B_0 (R_e/r)^3 \cos\theta ;$$

$$B(\theta) = \frac{B_0}{2} (R_e/r)^3 \sin\theta \left(1-\frac{2m}{r}\right)^{1/2} . \qquad (4.2.10)$$

Using (4.2.8) in (4.2.2) an equation for V^{ϕ} can be obtained, which expressed in LNRF components is given by

$$\sin\theta \frac{\partial V^{(\phi)}}{\partial\theta} - 3\cos\theta V^{(\phi)} + \frac{2m}{r}\left(1-\frac{2m}{r}\right)^{-1}\cos\theta V^{(\phi)}$$

$$+ 2r\cos\theta \frac{\partial V^{(\phi)}}{\partial r} = 0 \qquad (4.2.11)$$

which has the solution

$$V^{(\phi)} = K\left(1-\frac{2m}{r}\right)^{-1/2} r^{\left(\frac{3-n}{2}\right)} \sin^n\theta \qquad (4.2.12)$$

where K and n are arbitrary constants. As V^r and V^{θ} are zero, the momentum and continuity equations reduce to

$$\left(\rho + \frac{p}{c^2}\right) u^{t^2}\left[\frac{mc^2}{r^2}\left(1-\frac{2m}{r}\right) - r\left(1-\frac{2m}{r}\right)\sin^2\theta V\varphi^2\right] ;$$

$$+ \left(1-\frac{2m}{r}\right)\frac{\partial p}{\partial r} = F^r{}_k \bar{J}^k/c , \qquad (4.2.13)$$

$$-\left(\rho + p/c^2\right) u^{t^2} \sin\theta\cos\theta V.\varphi^2 + \frac{1}{r^2}\frac{\partial p}{r\theta} = F^{\theta}{}_k \bar{J}^k/c , \qquad (4.2.14)$$

$$\left(F^{\varphi}{}_k - F^t{}_k V^{\varphi}/c\right) \bar{J}^k/c = 0 , \qquad (4.2.15)$$

$$F^t_k \bar{J}^k - 2F_{ik}\bar{J}^k u^i u^t = 0 \quad . \tag{4.2.16}$$

Here we have $\bar{P} = P$ as $V^{\mathfrak{r}}$ and V^{θ} are zero.

Since $\bar{E}_{\phi} = 0$, the two constraint equations (4.2.15) and (4.2.16) together give the relation

$$B_{\theta} J^{\mathfrak{r}} - B_{\mathfrak{r}} J^{\theta} = 0 \Rightarrow (B \times J)_{\phi} = 0 \tag{4.2.17}$$

As $B_{\mathfrak{r}}$ is zero on the equatorial plane $\theta = \pi/2$, (4.2.17) would require J^r to be zero on $\theta = \pi/2$ plane. However, as $V^{\mathfrak{r}}$ and V^{θ} are zero, if we assume the currents J^r and J^{θ} also to be zero, then both the constraints (4.2.15) and (4.2.16) would be identically satisfied. The first two Maxwell's equations (4.2.3) and (4.2.4) give two equations for B_{ϕ}, the toroidal component of the magnetic field as given by

$$\frac{\partial}{\partial \theta}(\sin\theta\, B_{\phi}) = 0 \qquad \text{and}$$

$$\frac{\partial}{\partial \mathfrak{r}}\left[\left(1 - \frac{2m}{\mathfrak{r}}\right) B_{\phi}\right] = 0 \tag{4.2.18}$$

which has a solution of the form

$$B_{\phi} = \frac{k_1 \left(1 - \frac{2m}{\mathfrak{r}}\right)^{-1}}{\sin\theta} \tag{4.2.19}$$

k_1 being a constant.

However, with $J^{\mathfrak{r}}$ and J^{θ} zero, B_{ϕ} does not enter into any dynamical equation, and for the present case one can choose B_{ϕ} to be zero without any loss of generality. Using the expressions for $B_{(r)}$, $B_{(\theta)}$ and $V^{(\phi)}$ and equation (4.2.8) in the remaining two Maxwell's equations (4.2.5)

and (4.2.6), we get $E_{(r)}$, $E_{(\theta)}$, $J^{(\varphi)}$ and $J^{(t)}$ as given by

$$E_{(r)} = \frac{k B_0 R_c^3}{2 r^{(\frac{n+3}{2})}} \sin^{(n+1)}\theta$$

$$E_{(\theta)} = -\frac{k B_0 R_c^3}{r^{(\frac{n+3}{2})}} \left(1-\frac{2m}{r}\right)^{-1/2} \sin^n\theta \cos\theta \qquad (4.2.20)$$

$$\bar{J}^{(\varphi)} = -\frac{3m B_0 R_c^3}{r^5} \sin\theta \qquad (4.2.21)$$

$$\bar{J}^{(t)} = -\frac{k B_0 R_c^3}{r^{(\frac{n+5}{2})}} \left(1-\frac{2m}{r}\right)^{-1/2} \sin^{n-1}\theta \left\{\left[\left(1-\frac{n}{4}\right)\left(1-\frac{2m}{r}\right)+1\right]\right.$$

$$\left.\sin^2\theta - (n+1)\cos^2\theta\right\} \qquad (4.2.22)$$

Now we are left with r and θ components of the momentum equations only. Expressed in the LNRF components, these can be written as

$$\left(\rho + p/c^2\right)\left(1-\frac{v^{(\varphi)2}}{c^2}\right)^{-1}\left[\frac{mc^2}{r^2} - \left(1-\frac{2m}{r}\right)\frac{v^{(\varphi)2}}{r}\right]$$

$$+ \left(1-\frac{2m}{r}\right)\frac{\partial p}{\partial r} = \frac{1}{c}\left(1-\frac{2m}{r}\right)^{1/2}\left[B_{(\theta)}\bar{J}^{(\varphi)} - E_{(r)}\bar{J}^{(t)}\right] \qquad (4.2.23)$$

(4.2.24)

$$\left(\rho + \frac{p}{c^2}\right)\left(1 - \frac{v^{(\varphi)2}}{c^2}\right)^{-1} \frac{v^{(\varphi)2}}{r} \cot\theta - \frac{1}{r}\frac{\partial p}{\partial \theta}$$

$$= \frac{1}{cr}\left[B(r)\, j^{(\varphi)} - E(\theta)\, j^{(t)}\right] \qquad (4.2.25)$$

where we have used the relation

$$u^{t2} = \left(1 - \frac{2m}{r}\right)^{-1}\left(1 - \frac{v^2}{c^2}\right)^{-1} \qquad (4.2.26)$$

For the special case of a disk of incompressible fluid (with density $\rho = \rho_0$, a constant), confined to the equatorial plane ($\theta = \pi/2$) of the compact object, these equations can be written as

$$\frac{\partial p}{\partial \theta} = 0 \qquad (4.2.27)$$

$$\frac{d}{dr}(\rho_0 c^2 + p) + \left[1 - \frac{2m}{r} - \frac{K^2 r^{3-n}}{c^2}\right]^{-1}\left[\frac{mc^2}{r^2} - K^2 r^{2-n}\right](\rho_0 c^2 + p)$$

$$= \frac{B_0 R_c^6}{2c\, r^7}\left[\frac{K^2}{r^{n-3}}\left\{\left(\frac{1-n}{4}\right) + \left(1 - \frac{2m}{r}\right)^{-1}\right\} - \frac{3m}{r}\right] \qquad (4.2.28)$$

Introducing a dimensionless parameter $\beta = \frac{K^2 m^{3-n}}{c^2}$, one can write the velocity as

$$\left(\frac{v^{(\varphi)}}{c}\right)^2 = \beta R^{3-n}(1 - 2/R)^{-1}$$

$$\text{where } R = r/m \qquad (4.2.29)$$

such that when n=4, $\beta = 1$ corresponds to the usual

relativistic Keplerian velocity. It is clear from this expression that, in order to keep $V^{(\phi)} \ll c$, the disk will have a constraint either on its inner edge or outer edge depending upon whether $n>3$ or $n<3$. For example, for $n=4$, the inner edge should be beyond $2+\beta$, and thus for relativistic Keplerian orbit with $\beta = 1$, the inner edge must be outside $r=3m$. On the other hand if $\beta < 1$, it is possible to have the inner edge extended within $r=3m$. For $n<3$, as $V^{(\phi)}$ increases with R, β has to be very small ($\beta \ll 1$) to have plausible equilibrium configurations.

Figure (4.1) shows the velocity profiles for the case $n<3$ and Figure(4.2) the corresponding pressure profiles obtained through numerically integrating equation (4.2.29). It is clear that as velocity increases with R, the pressure profiles too show increasing trend outwords and that it is unlikely that one could have disklike configuration for these values of n when the fluid is incompressible.

With $n=3$, the velocity profiles for different β (Figure 4.3) show a trend, where in the velocity drops slightly and remains almost a constant. The corresponding pressure profiles (Figure 4.4) show again increasing trend depending upon the value of β and thus may not be realizable as disk configuration.

As may be expected with $n=4$ and above the velocity profiles show a smooth decrease outwards whose rate of decrease is governed by β (Figure 4.5) and the pressure profiles show a reasonable behaviour (decreasing outwards) (Figure 4.6). However, if β is very small as may be seen

from Figures (4.7) and (4.8) the velocity saturates at a very low value beyond $\beta \sim 10^{-2}$ and thus the corresponding pressure profiles also do not show any change.

When n=4, $\beta \sim 10^{-2}$, the inner edge of the disk can extend to within r < 3m region. However, when the inner edge is very near to the horizon, the pressure drops to zero rather abruptly whereas if it is slightly away (r > 2.3 m), the pressure distribution again shows a possible realizable disk configuration (Figure 4.9). Figure (4.10) gives a representative diagram of the pressure profiles for differnt densities when n and β are kept fixed.

4.3. Luminosity Flux from the Disk

The luminosity function associated with the radiative flux from the disk for Schwarzschild geometry is given by equation (3.2.2). As analyzed by Hanawa (1989), the energy observed by the distant observer $\mathcal{E}_{DO}$, measured in terms of the generalized velocity profile (4.2.12) for different inclination angle i is given by

$$\mathcal{E}_{DO} \mid \mathcal{E}_{LO} = \left[1 - 2/R - \beta R^{3-n}\right]^{1/2} \tag{4.3.1}$$

for i=0 and

$$\left(\mathcal{E}_{DO} \mid \mathcal{E}_{LO}\right)_{max} = \left[1 - 2/R - \beta R^{3-n}\right]^{-\frac{1}{2}} (1-2/R)^{1/2} \kappa$$

$$\left[(1-2/R)^{+1/2} + \beta^{\frac{1}{2}} R^{\frac{3-n}{2}}\right] \tag{4.3.2}$$

$$(\varepsilon_{D0}/\varepsilon_{L0})_{min} = \left[1-2/R-\beta R^{3-n}\right]^{-\frac{1}{2}}(1-2/R)^{\frac{1}{2}}\left[(1-2/R)^{\frac{1}{2}}-\beta^{\frac{1}{2}}R^{\frac{3-n}{2}}\right]$$

(4.3.3)

for $i = \pi/2$. With this the observed temperature T_{obs} expressed in terms of the ratios of colour temperature T_{col} to effective temperature T_{eff} is given by, (Hanawa 1989)

$$T_{obs} = 1.11\left[\frac{T_{col}/T_{eff}}{1.5}\right]\left(\frac{g(R)}{0.252}\right)\left(\frac{M}{1.4M_{\odot}}\right)^{-\frac{1}{2}}\left(\frac{\dot{M}}{10^{18}\,g\,s^{-1}}\right)^{1/4}\ keV$$

(4.3.4)

with

$$g(R) = g_0(R) = R^{-3/4}(1-3/R)^{-1/4}\left[1-2/R-\beta R^{3-n}\right]^{\frac{1}{2}}$$

$$\times\left\{1-\sqrt{6}/R+\sqrt{3/4}R\ln\left(\frac{1+\sqrt{3}/R}{1-\sqrt{3}/R}\ \frac{1-\sqrt{2}/2}{1+\sqrt{2}/2}\right)\right\}^{\frac{1}{4}}$$

(4.3.5)

for i=0, while for $i = \pi/2$, we have

$$g_{max}(R) = g_+(R) = R^{-3/4}(1-2/R)^{\frac{1}{2}}(1-3/R)^{-1/4}\left(1-2/R-\beta R^{3-n}\right)$$

$$\times\left[(1-2/R)^{\frac{1}{2}}+\beta^{\frac{1}{2}}R^{\frac{(3-n)}{2}}\right]\left\{1-\sqrt{6}/R+\sqrt{\frac{3}{4R}}\ln\left(\frac{1+\sqrt{3}/R}{1-\sqrt{3}/R}\cdot\frac{1-\sqrt{2}/2}{1+\sqrt{2}/2}\right)\right\}^{\frac{1}{4}}$$

(4.3.6)

and

$$g_{min}(R) = g_{-}(R) =$$

$$= R^{-3/4}(1-2/R)^{\frac{1}{2}}(1-3/R)^{-1/4}\left[1-2/R-\beta R^{3-n}\right]\left[(1-2/R)+\beta^{\frac{1}{2}}R^{\frac{3-n}{2}}\right]$$

$$\times\left\{1-\sqrt{6}/R+\sqrt{\frac{3}{4R}}\ln\left(\frac{1+\sqrt{3}/R}{1-\sqrt{3}/R}\cdot\frac{1-\sqrt{2}/2}{1+\sqrt{2}/2}\right)\right\}^{1/4}$$

(4.3.7)

The Newtonian limit of these functions is just given by

$$g_N(R) = R^{-3/4}$$

(4.3.8)

Figures (4.11) to (4.19) show profiles of the function g for various values of n and β. It is clear from the plots that with general relativistic contribution a single blackbody curve could fit the emission features particularly from the inner regions of the disk, whereas the Newtonian limit would require a superposition of several different (multicolour) blackbody spectra to match the theoretical curve. Figure (4.13) with n=4 and β =1 corresponds exactly to the case discussed by Hanawa and thus comparing this with other figures one can see the differences that occur due to the variation in the velocity from the usual relativistic Keplerian value. Figures (4.15) and (4.16) give the curves for $g_o(R)$ for different values of n with (4.15) for $n>3$ and (4.16) for $n<3$. As one sees $g_o(R)$ shows the same trend for all situations except that the peak value seems to decrease with increasing n. Fixing n and changing the values of β one finds for g(R) (Figures

4.17, 4.18 and 4.19), whereas for n=4, there is a slight difference in the curves for changes in β, with n=5, there is hardly any change for different β.

If we consider the plots for g+ and g- which in fact refer to the different contributions from the redshift factor (the approaching part giving rise to blueshift while the receding part gives rise to redshift) the difference between the cases n>3 and n<3 is indeed large, particularly for g+.

4.4. Results and Discussion

The inclusion of the magnetic field in the discussion of the thin disk configuration straightaway renders the possibility of the inner edge of the disk extending to regions much closer to the 'event horizon', unlike in the absence of the magnetic field when in Schwarzschild background the inner edge has to be beyond r=6m, the last stable orbit for tardyons. This obviously requires a discussion in the framework of general relativity as Newtonian treatment is hardly appropriate for regions very close to a highly collapsed central object. The class of solutions discussed for the velocity field with varying values of n and β (which reflects in the values of associated angular momentum of the fluid element) shows appropriately that with outwardly increasing velocity distributions one has a runaway situation (increasing pressure profiles) whereas with $v^{(\phi)}$ decreasing outwards,

the disk equilibrium with the magnetic field looks more reasonable.

Hanawa (1989), following the earlier studies due to Luminet and others,has discussed the possible scenario for the radiative flux from a thin disk possibly applicable to the study of emission from low mass X-ray binaries.In view of the discussion given by Paczynski (1987) in the context of Quasi Periodic Oscillation of binary X-ray sources,one could conceive a situation having a highly compact Neutron star (radius $\sim$ 2.5 to 3m) and a thin fluid disk surrounding it. For such a scenario the analysis as made here - showing the existence of equilibrium configuration is of direct relevance, for, the extension of these discussions including viscosity as well as radial velocity component, would then describe the flow through the sonic point. Regarding the profiles for the 'g' function associated with the radiative flux and temperature profile, our investigation seems to show that it is not very sensitive to variations from the relativistic Keplerian distributions (Figures 4.17 and 4.18) except when the inclination angle is different from zero.For $i = \pi/2$ as shown in the plots,the component coming from the blueshift factor seems to be very sensitive to the variation in the n and β values for $n<3$.

The electrical field which has only non-zero radial component is rather small,unless $n<0$,and is consistent with the current system, participates effectively alongwith the gravitational and centrifugal forces in giving rise to the equilibrium pressure profiles.

Figure Captions

Fig. 4.1 : Velocity profiles for $n < 3$

Fig. 4.2 : Pressure profiles for $n < 3$

Fig. 4.3 : Velocity profiles for $n = 3$

Fig. 4.4 : Pressure profiles for $n = 3$

Fig. 4.5 : Velocity profile for $n \geq 4$

Fig. 4.6 : Pressure profile for $n \geq 4$

Fig. 4.7 : Velocity profiles for $n \simeq 4$, different β

Fig. 4.8 : Pressure profiles for $n = 4$, different β

Fig. 4.9 : Pressure profile for $n = 4$, $\beta = 10^{-2}$ for different positions of inner edge

Fig. 4.10 : Pressure profiles for different ρ_0

Fig. 4.11 : Luminosity flux function $g(R)$ for $n = 1$, $\beta = 3 \times 10^{-4}$

Fig. 4.12 : Luminosity flux function $g(R)$ for $n = 3$, $\beta = 3 \times 10^{-1}$

Fig. 4.13 : Luminosity flux function $g(R)$ for $n = 4$, $\beta = 1$

Fig. 4.14 : Luminosity flux function $g(R)$ for $n = 5$, $\beta = 3$

Fig. 4.15 : Luminosity flux function $g_0(R)$ for $n > 3$

Fig. 4.16 : Luminosity flux function $g_0(R)$ for $n < 3$

Fig. 4.17 : Luminosity flux function $g_0(R)$ for $n = 4$, different β

Fig. 4.18 : Luminosity flux function $g_0(R)$ for $n = 1$, different β

Fig. 4.19 : Luminosity flux function $g_0(R)$ for $n = 5$, different β

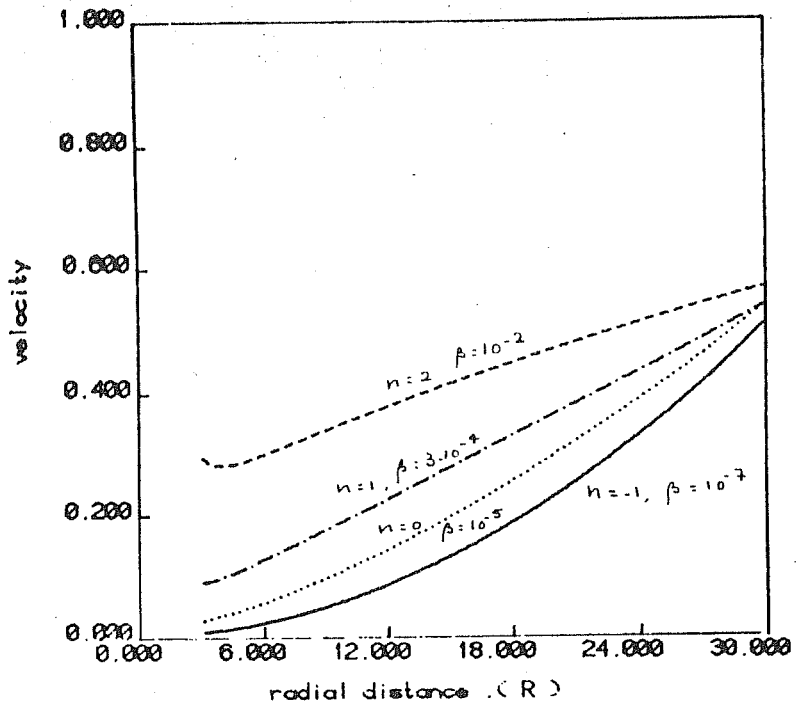
1.000
0.800
0.600
0.400
0.200
0.000
velocity
n = 2, β = 10⁻²
n = 1, β = 3.10⁻⁴
n = 0, β = 10⁻⁵
n = -1, β = 10⁻⁷
0.000
6.000
12.000
18.000
24.000
30.000
radial distance (R)

Fig. 4. 1

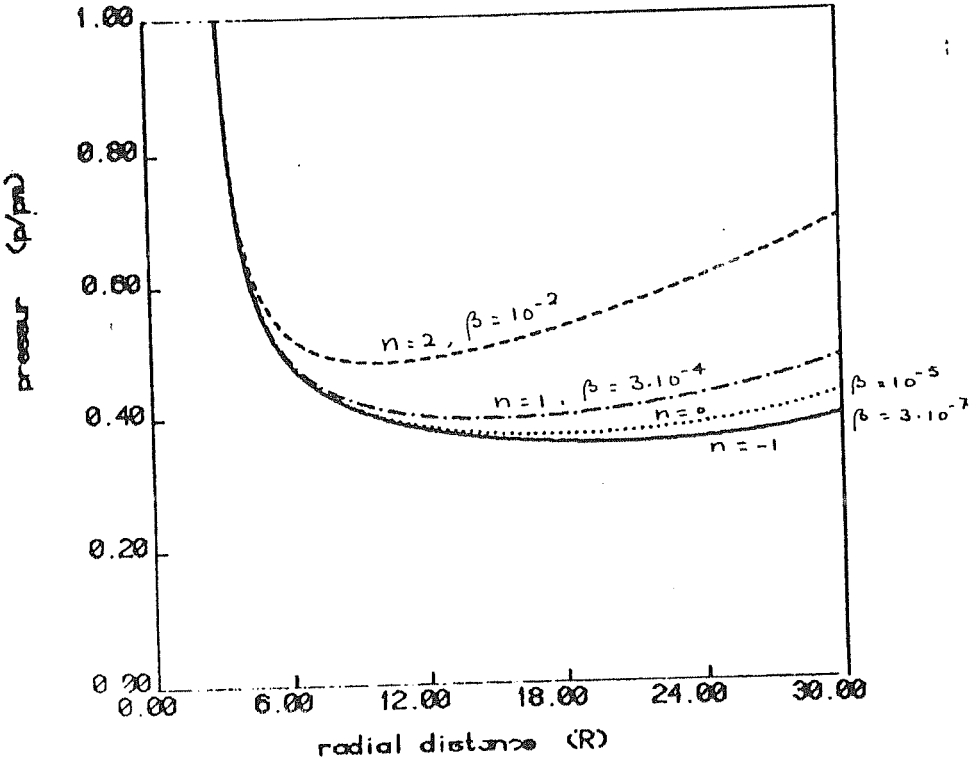
1.00
0.80
0.60
0.40
0.20
0.00
pressur (p/ρ₀)
n = 2, β = 10⁻²
n = 1, β = 3.10⁻⁴
n = 0
n = -1
β = 10⁻⁵
β = 3.10⁻⁷
0.00
6.00
12.00
18.00
24.00
30.00
radial distance (R)

Fig. 4. 2

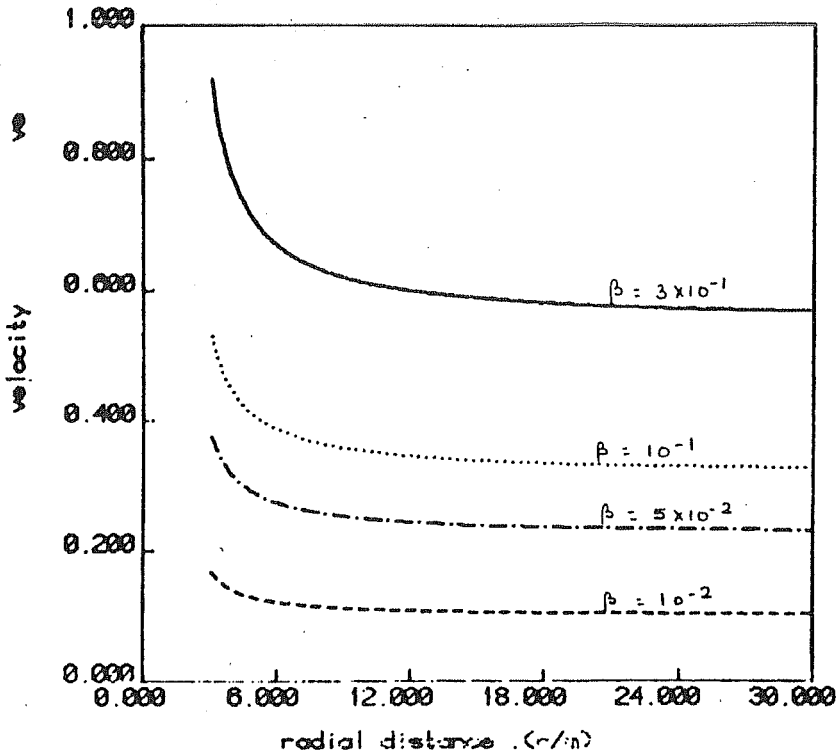

Fig. 4.3 n = 3.

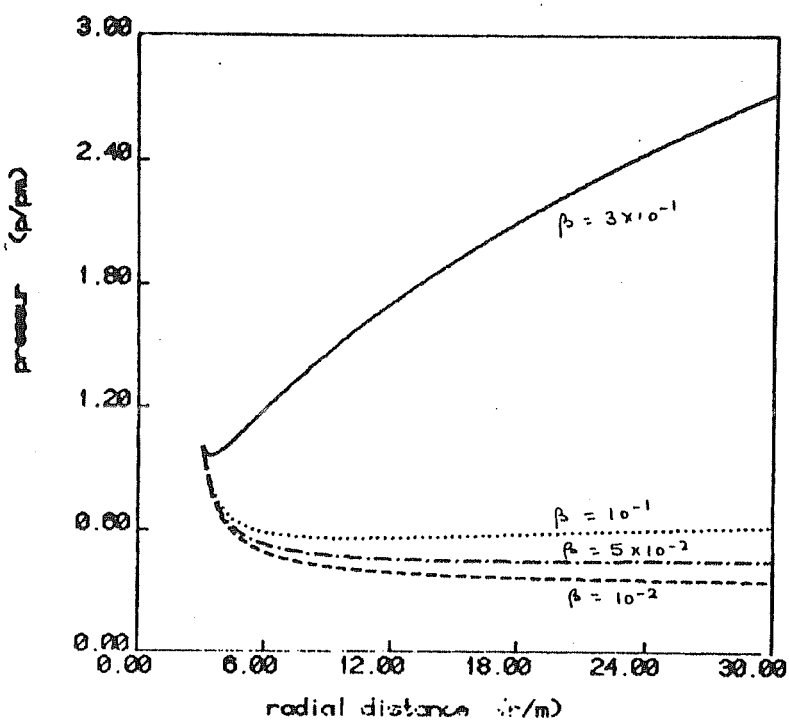

Fig 4.4 n = 3

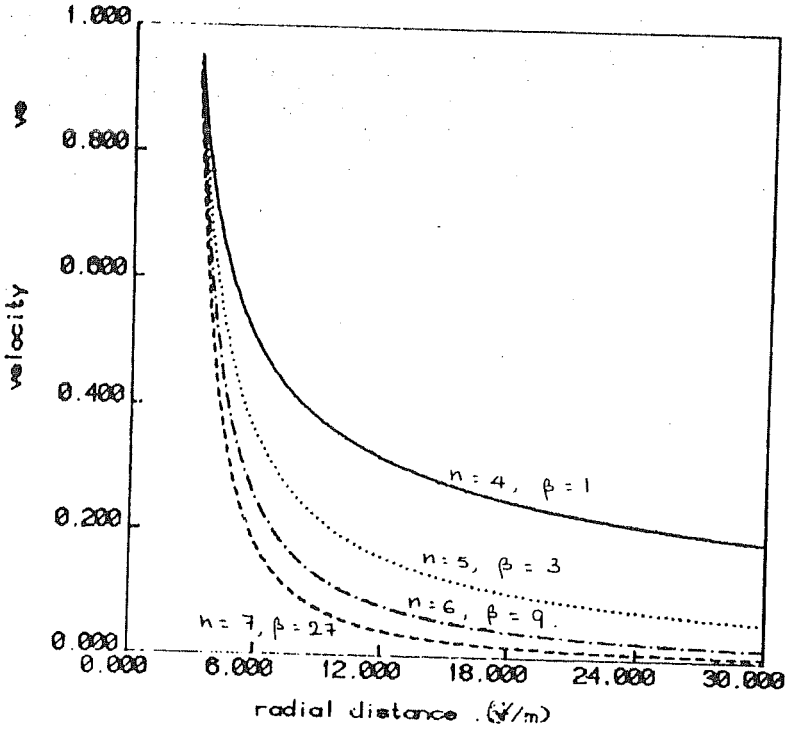
1.000
0.800
0.600
0.400
0.200
0.000
velocity
n = 4, β = 1
n = 5, β = 3
n = 6, β = 9
n = 7, β = 27
0.000
6.000
12.000
18.000
24.000
30.000
radial distance (r/m)

Fig. 4.5

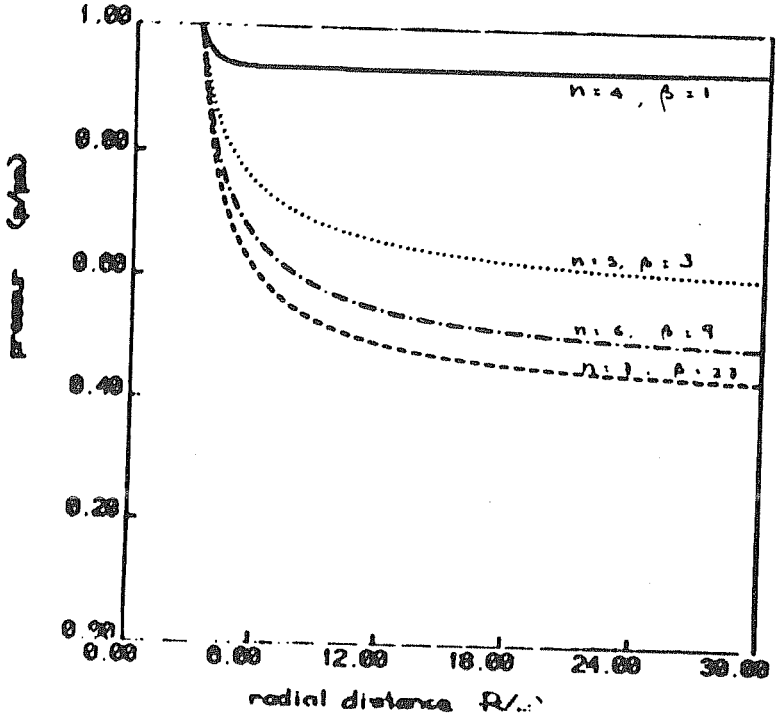
1.00
0.80
0.60
0.40
0.20
0.00
n = 4, β = 1
n = 5, β = 3
n = 6, β = 9
0.00
6.00
12.00
18.00
24.00
30.00
radial distance

Fig. 4.6

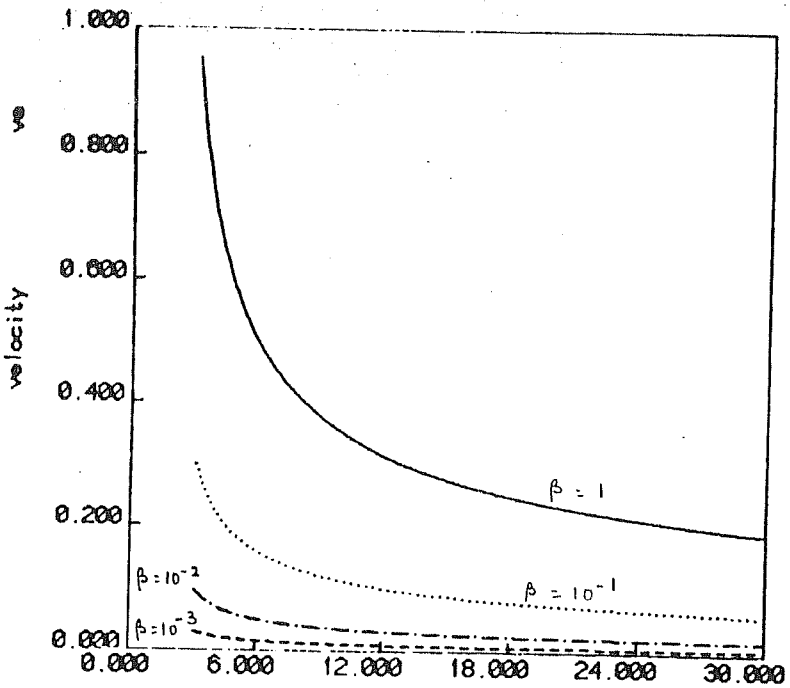

n = 4.

Fig. 4.7

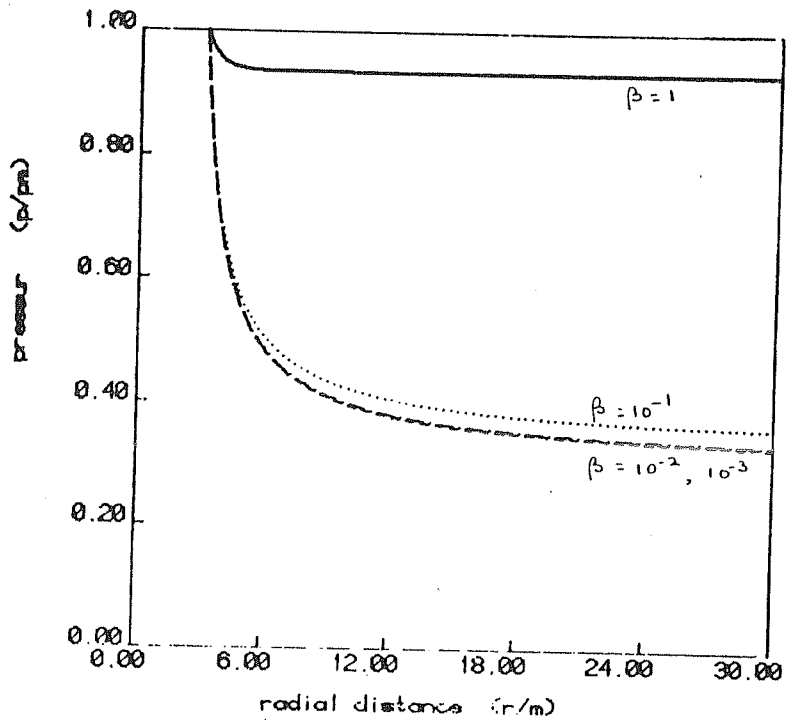

n = 4.

Fig. 4.8

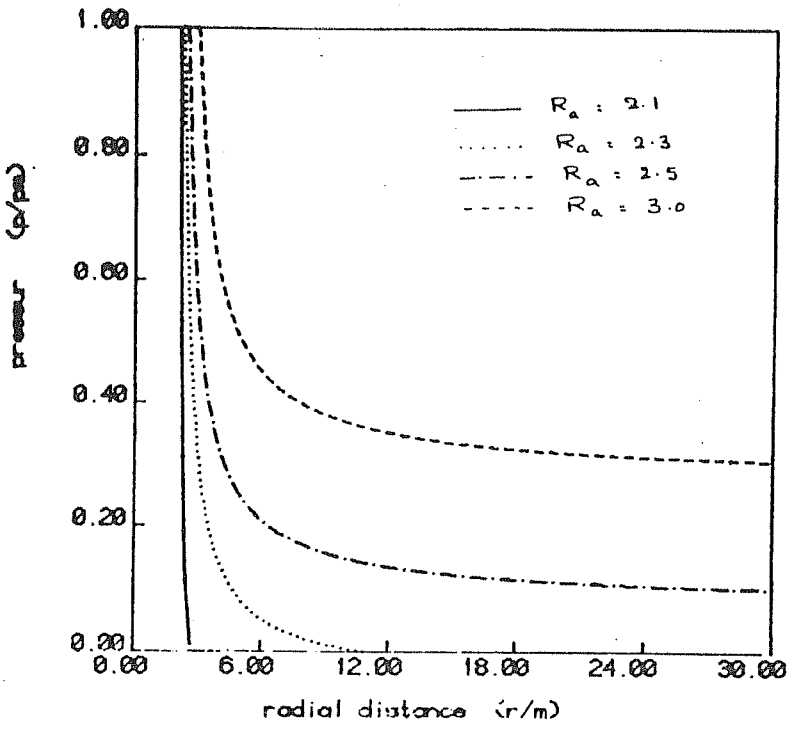

Fig. 4.9 $n = 4$, $\beta = 10^{-2}$

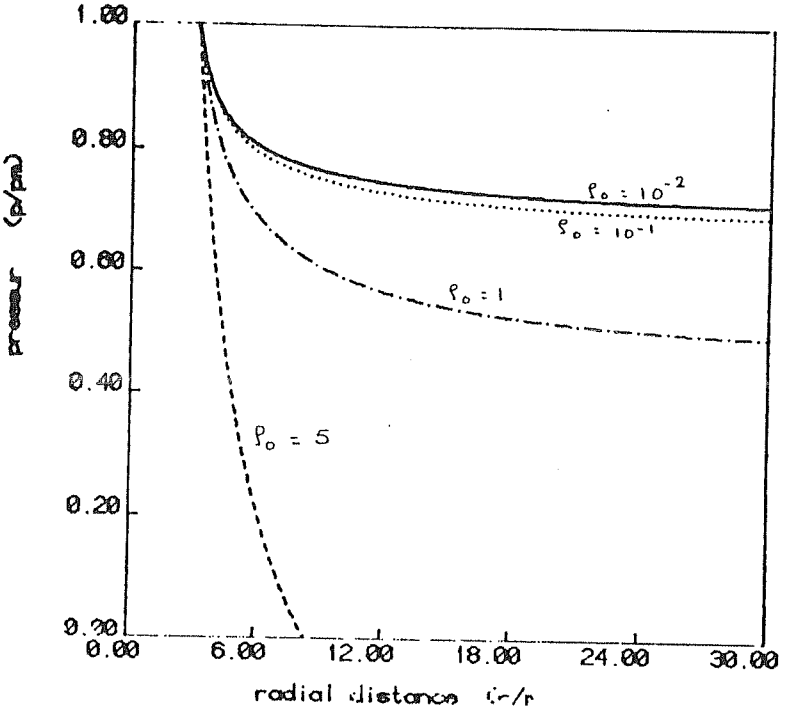

Fig 4.10 $\beta = 3$, $n = 5$

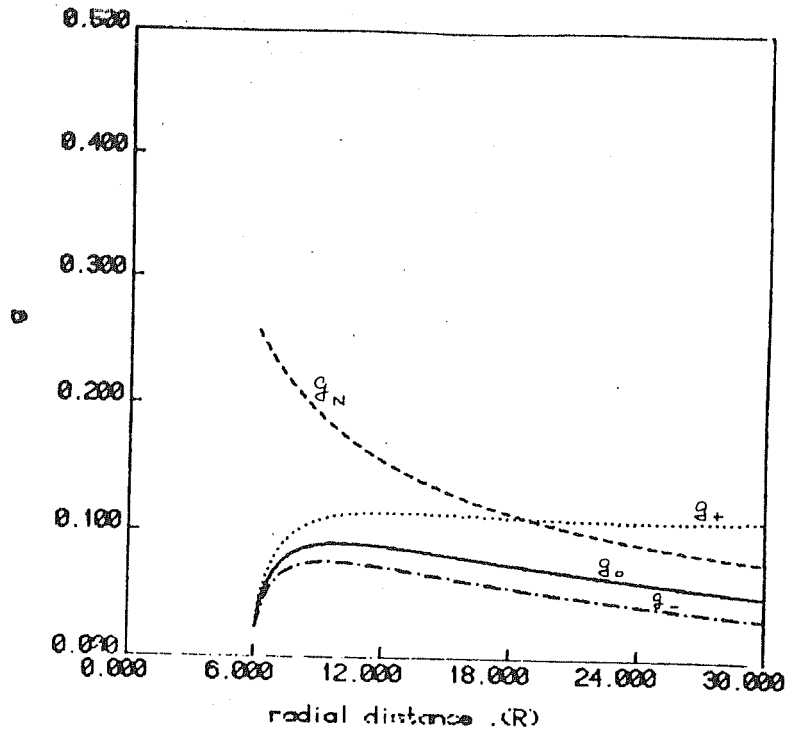

Fig. 4.11 $n = 1$, $\beta = 3 \cdot 10^{-4}$

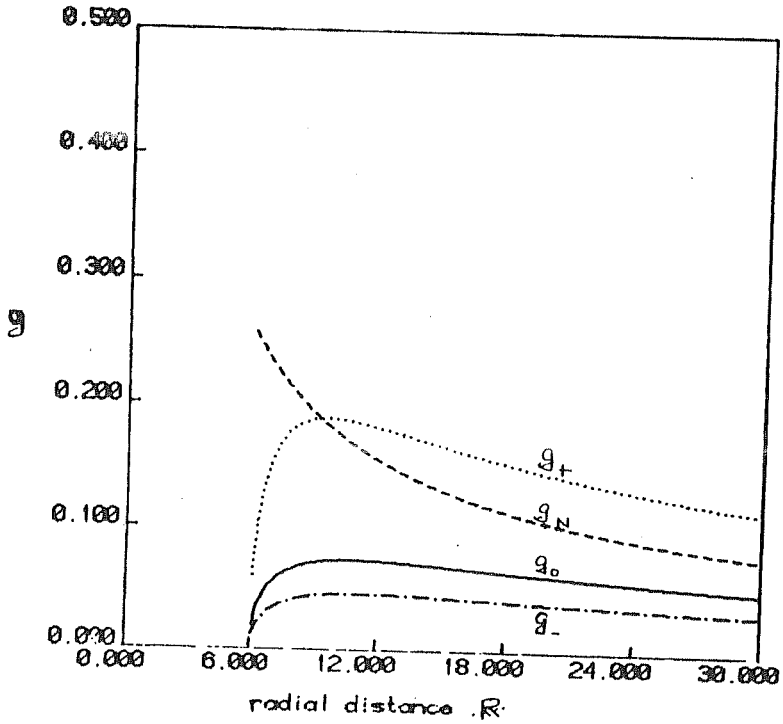

Fig. 4.12 $n = 3$, $\beta = 3 \times 10^{-1}$.

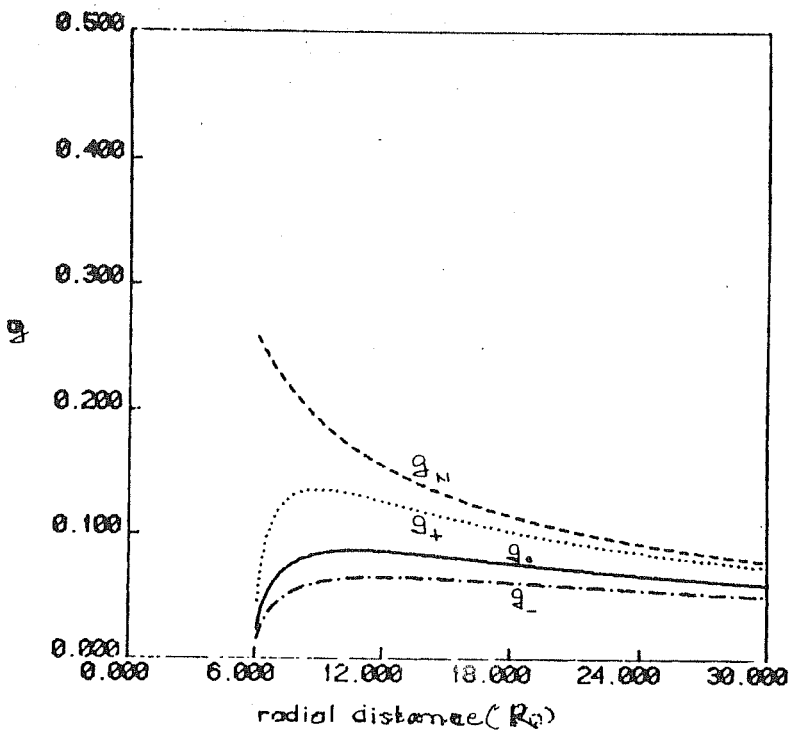

Fig.4.13 $n = 4$, $\beta = 1$

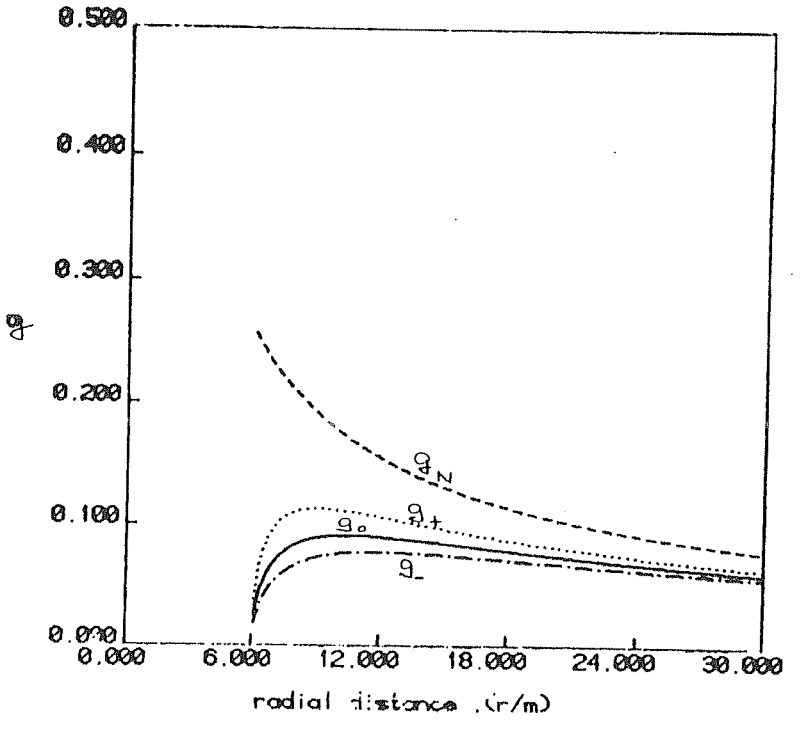

Fig.4.14 $n = 5$, $\beta = 3$.

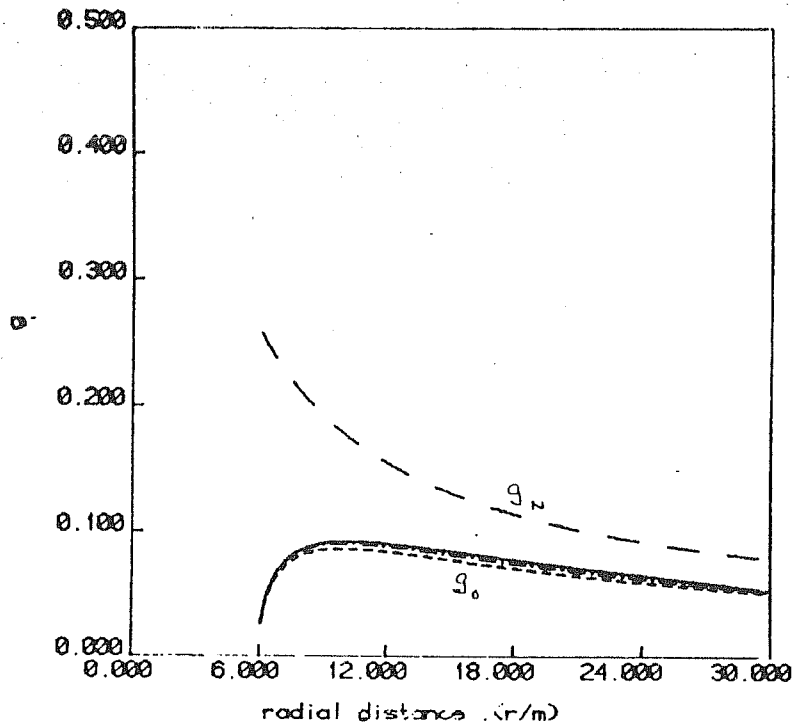

Fig 4.15 n = 3, 4 .. 7

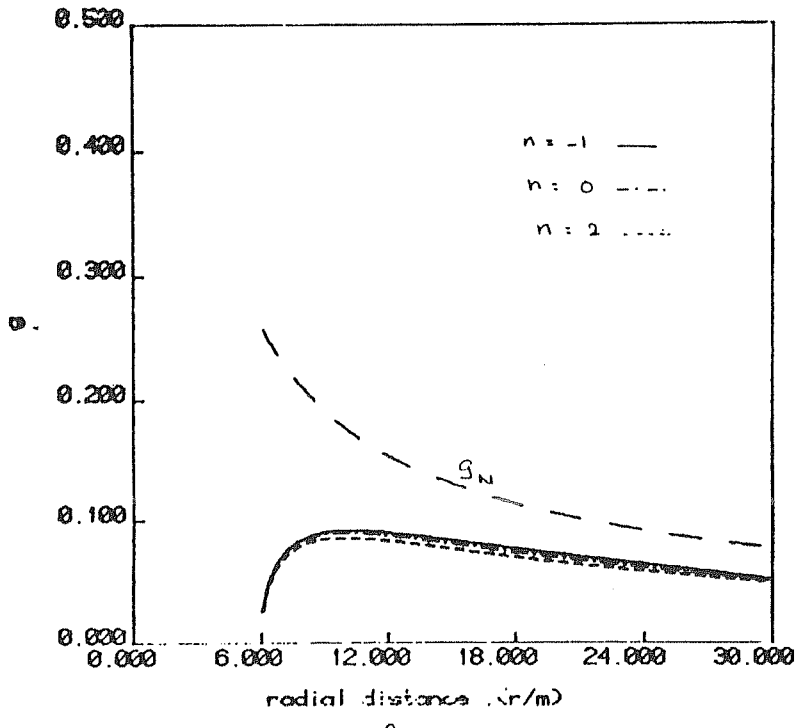

Fig 4.16 $g_0(R)$ for n = -1, 0, 1, 2.

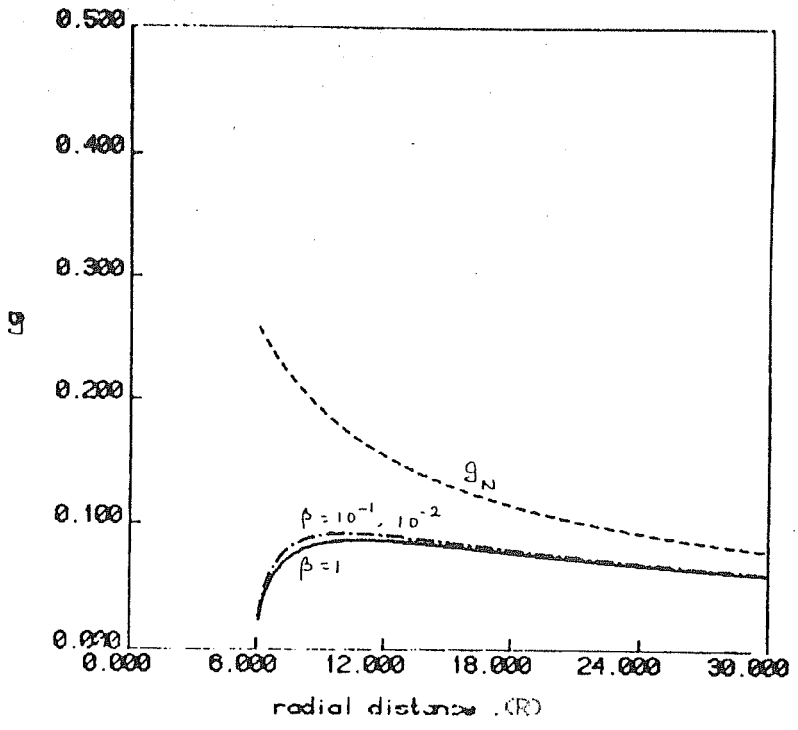

Fig. 4.17 $g_0(R)$ for $n = 4$

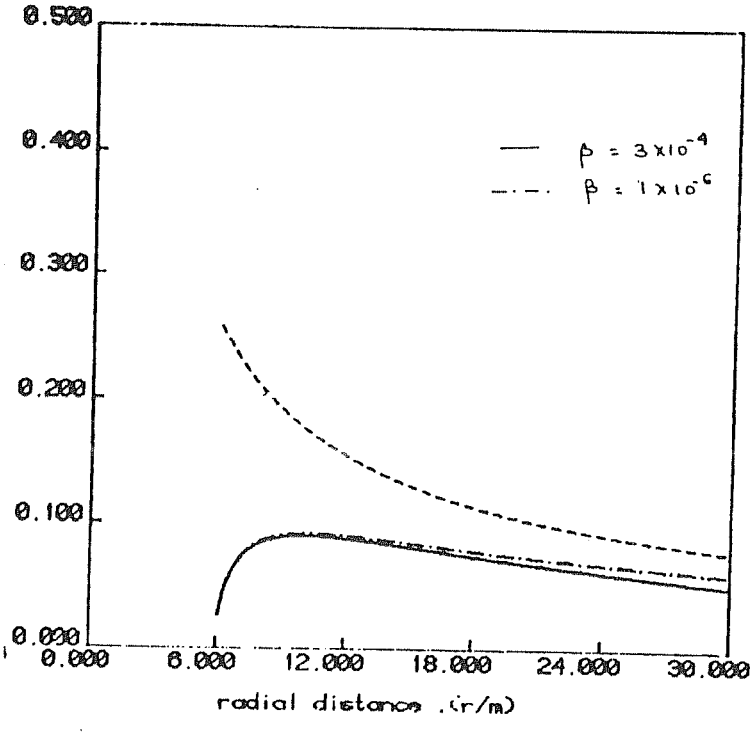

Fig. 4.18 $n = 1$, $g_0(R)$ for different β.

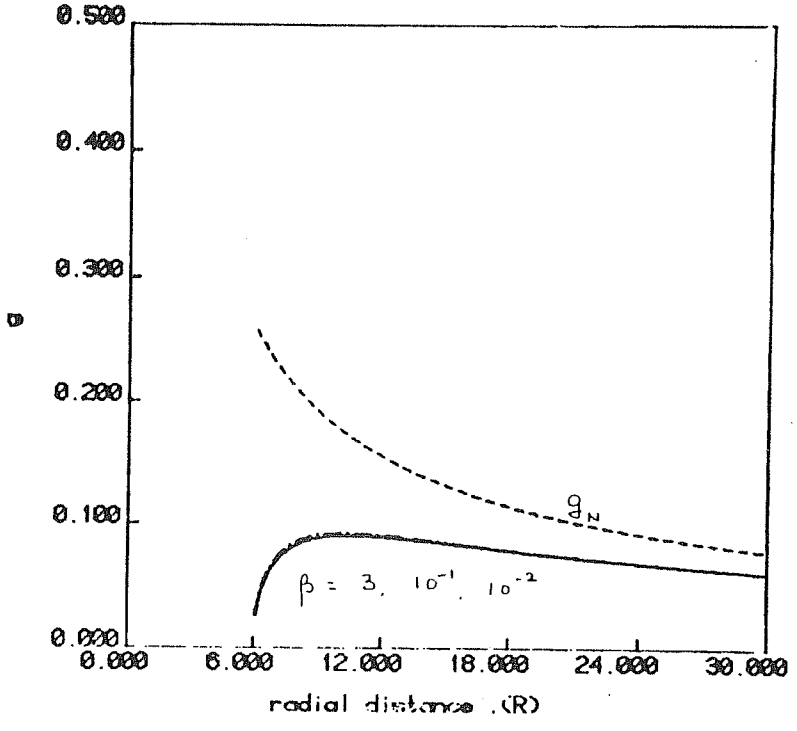

Fig 4: 19 $g_0(R)$ for $n = 5$

CHAPTER V

PLASMA DISK AROUND SCHWARZSCHILD BLACKHOLE WITH RADIAL AND AZIMUTHAL VELOCITY

5.1. Introduction

In many of the standard models of accretion disks (Abramowicz et. al. 1978,Kozlovski et. al. 1978) the fluid flow is restricted to the azimuthal direction only with the inherent assumption that the radial and meridional components of velocity are negligible in comparison with the azimuthal one.Recently Kuwahara (1978) has studied the relativistic accretion tori around Schwarzschild blackhole considering all the three components of flow velocity to be

nonzero and has found that though the radial and meridional velocities play a minor role in the structure of the tori, they play an important role in determining the accretion rate and the angular momentum transport due to shear stress. However, the study is incomplete.without taking into account the role of electromagnetic fields that could coexist with any such fluid configurations.

In Chapter IV, we have described the study of the structure and equilibrium configurations for a disk of incompressible fluid, where the flow was restricted to the azimuthal directions only.The importance of considering the magnetic field was easily realized by the fact that the inner edge of the disk can now reach almost upto 3m ($m = GM/c^2$) whereas one knows that in the pure Schwarzschild geometry the inner edge is necessarily beyond 6m.

In the present chapter we discuss the structure of the disk when both the radial and the azimuthal components of velocity are nonzero and the associated electromagnetic field being self-consistent for a finitely conducting disk, in the absence of the toroidal components of magnetic field (Bhaskaran and Prasanna (1989b)).

5.2. Disk Structure

The present discussion being for the case of a plasma disk with finite conductivity and having only the coefficient of bulk viscosity to be non-zero ($\eta_b \neq 0$) with the central compact object static (a=0) the system of

governing equations are given by:

the continuity equation:

$$(\rho+\frac{\bar{p}}{c^2})\left[\frac{\partial v^r}{\partial r}-\frac{2m}{r^2}(1-\frac{2m}{r})^{-1}v^r+\frac{2}{r}v^r\right]+v^r\frac{\partial}{\partial r}(\rho-\bar{p}/c^2)$$

$$=-\frac{1}{c^2u^{t2}}\left\{F^t_k\bar{J}^k+2(F_{rk}v^r+F_{\phi k}v^\phi)u^{t2}\bar{J}^k\right\}$$

(5.2.1)

the momentum equation:

$$(\rho+\frac{\bar{p}}{c^2})u^{t2}\left[v^r\frac{\partial v^r}{\partial r}+\frac{mc^2}{r^2}(1-\frac{2m}{r})-\frac{3m}{r^2}(1-\frac{2m}{r})^{-1}v^{r2}\right.$$

$$\left.-(r-2m)\sin^2\theta\, v^{\phi 2}\right]+(1-\frac{2m}{r})\frac{\partial\bar{p}}{\partial r}$$

$$=(F^r_k-F^t_k\frac{v^r}{c})\bar{J}^k/c\quad,\qquad(5.2.2)$$

$$-(\rho+\frac{\bar{p}}{c^2})\sin\theta\cos\theta\, v^{\phi 2}u^{t2}+\frac{1}{r^2}\frac{\partial\bar{p}}{\partial\theta}=F^\theta_k\bar{J}^k/c\quad,\qquad(5.2.3)$$

$$(\rho+\bar{p}/c^2)u^{t2}\left[v^r\frac{\partial v^\phi}{\partial r}+\frac{2}{r}(1-\frac{2m}{r})^{-1}(1-\frac{3m}{r})v^rv^\phi\right]$$

$$=(F^\phi_k-F^t_k\frac{v^\phi}{c})\bar{J}^k/c\quad.$$

(5.2.4)

and the Maxwell's equations:

$$-\frac{1}{r^2\sin\theta}(1-\frac{2m}{r})\frac{\partial}{\partial\theta}(\sin\theta B_\phi)=\bar{J}^r$$

(5.2.5)

$$\frac{1}{r^2}\frac{\partial}{\partial r}\left[(1-\frac{2m}{r})B_\phi\right]=\bar{J}^\theta$$

(5.2.6)

$$\frac{1}{r^4 \sin\theta}\frac{\partial}{\partial\theta}\left[\frac{B_r}{\sin\theta}\right] - \frac{1}{r^2\sin^2\theta}\frac{\partial}{\partial r}\left[\left(1-\frac{2m}{r}\right)B_\theta\right] = J^\phi$$

(5.2.7)

$$\frac{1}{r^2}\frac{\partial}{\partial r}\left(r^2 E_r\right) - \frac{1}{r^2\sin\theta}\left(1-\frac{2m}{r}\right)^{-1}\frac{\partial}{\partial\theta}\left(\sin\theta\, E_\theta\right) = J^t$$

(5.2.8)

$$\frac{\partial E_\theta}{\partial r} - \frac{\partial E_r}{\partial\theta} = 0$$

(5.2.9)

$$\frac{\partial B_r}{\partial r} + \frac{\partial B_\theta}{\partial\theta} = 0$$

(5.2.10)

and the Ohm's law

$$J^i = \sigma F^i{}_k u^k$$

(5.2.11)

As the toroidal component of the magnetic field has been assumed to be zero ($B_\varphi = 0$), (5.2.5) and (5.2.6) give

$$J^r = 0 \quad \text{and} \quad J^\theta = 0$$

(5.2.12)

Using these conditions in (5.2.11) we are led to the relation between E and B fields:

$$E_r = \frac{v^\phi}{c} B_\theta$$

and

$$E_\theta = -\frac{v^\phi}{c} B_r$$

(5.2.13)

whereas from (5.2.4) we get the equation for v^ϕ

$$\frac{\partial V^{\phi}}{\partial r} + \frac{2}{r}\left(1-\frac{2m}{r}\right)^{-1}\left(1-\frac{3m}{r}\right)V^{\phi} = 0 \qquad (5.2.14)$$

whose solution is given by

$$V^{\phi} = \frac{L(\theta)}{r^2}\left(1-\frac{2m}{r}\right) \qquad (5.2.15)$$

The 'θ' dependence of V^{ϕ} may be obtained through consistency conditions for defining J^{ϕ} and J^{t} through Ohm's law and this requires $L(\theta) = L/\sin^2\theta$ where L is a constant. Thus we have for the azimuthal component of the velocity the structure

$$V^{\phi} = \frac{L}{r^2\sin^2\theta}\left(1-\frac{2m}{r}\right) \qquad (5.2.16)$$

Using this V^{ϕ} in (5.2.13) and substituting so obtained E_r and E_θ in (5.2.9) (which says curl E=0) we obtain two equations for B_r and B_θ which are solved to get the general solutions

$$B_r = -A r^{k-1}\left(1-\frac{2m}{r}\right)^{-k/2}\sin^{k-1}\theta\cos\theta \qquad (5.2.17)$$

$$B_\theta = A r^{k}\left(1-\frac{3m}{r}\right)\left(1-\frac{2m}{r}\right)^{-\frac{k}{2}-1}\sin^{k}\theta \qquad (5.2.18)$$

and consequently the electric field is given by

$$E_r = \frac{AL}{c} r^{k-2}\left(1-\frac{3m}{r}\right)\left(1-\frac{2m}{r}\right)^{-k/2}\sin^{k-2}\theta \qquad (5.2.19)$$

$$E_\theta = \frac{AL}{c} r^{k-3}\left(1-\frac{2m}{r}\right)^{-\frac{k}{2}+1}\sin^{k-3}\theta\cos\theta \qquad (5.2.20)$$

with A and k being arbitrary constants. Using these E and B

fields one can calculate the non-zero current components J^{ϕ} and J^{t} and are given by

$$J^{\phi} = -\frac{\sigma}{r^2 \sin^2\theta} B_0 V^r u^t , \tag{5.2.21}$$

$$J^{t} = -\sigma \left(1-\frac{2m}{r}\right)^{-1} V^{\phi} V^r B_0 u^t . \tag{5.2.22}$$

Thus we have solved for the electromagnetic field and the azimuthal velocity exactly. The remaining equations to be considered are the equation of continuity and the two momentum equations and part of the Ohm's law concerning J^{ϕ} and J^{t}, as given in (5.2.21) and (5.2.22). Consistency of (5.2.21) and (5.2.22) with the Maxwell's equations (5.2.7) and (5.2.8) lead us to the exact solution for V^r as given by

$$V^r u^t = -\frac{e^2}{4\pi G}\frac{1}{r^2}\left\{ km + (2-k)(r-2m)\left[1+\cot^2\theta\left(1-\frac{3m}{r}\right)^{-1}\right]\right\}, \tag{5.2.23}$$

wherein

$$u^{t^2} = \left(1-\frac{2m}{r}\right)^{-1}\left(1-V^2/c^2\right)^{-1}, \quad V^2 = V^{(r)^2} + V^{(\phi)^2} \tag{5.2.24}$$

the parenthesis around an index indicating the LNRF component. Expressing the remaining equations in terms of LNRF components we have now the system

$$\left(\rho + \bar{p}/c^2\right)\left[\frac{\partial V^{(r)}}{\partial r} + \frac{2V^{(r)}}{r}\right] + V^{(r)}\frac{\partial}{\partial r}\left(\rho - \bar{p}/c^2\right)$$

$$= \frac{2\sigma}{c^4} u^t V^{(r)^2} B_{(\theta)}^2 \left(1 - \frac{V^{(\phi)^2}}{c^2}\right), \tag{5.2.25}$$

$$\left(\rho+\frac{\bar{P}}{c^2}\right)\left(1-\bar{v}^2/c^2\right)^{-1}\left[v^{(r)}\frac{\partial v^{(r)}}{\partial r}+\frac{mc^2}{r^2}\left(1-\frac{2m}{r}\right)^{-1}\left(1-\frac{v^{(\varphi)2}}{c^2}\right)\right.$$

$$\left.-\frac{1}{r}v^{(\varphi)2}\right]+\frac{\partial\bar{P}}{\partial r}=-\frac{\sigma}{c^2}u^t B^{(\theta)2}v^{(r)}\left(1-\frac{v^{(\varphi)2}}{c^2}\right)$$

(5.2.26)

and

$$\left(\rho+\frac{\bar{P}}{c^2}\right)\left(1-\bar{v}^2/c^2\right)^{-1}v^{(\varphi)2}\cot\theta+\frac{\partial\bar{P}}{\partial\theta}=$$

$$-\sigma v^{(r)}u^t B^{(r)}B^{(\theta)}\left(1-\frac{v^{(\varphi)2}}{c^2}\right)$$

(5.2.27)

wherein

$$v^{(r)}=\left(1-\frac{2m}{r}\right)^{-1}v^r,$$

$$v^{(\varphi)}=r\sin\theta\left(1-\frac{2m}{r}\right)^{-1/2}v^\varphi,$$

$$B^{(r)}=\frac{1}{r^2\sin\theta}B_r,$$

$$B^{(\theta)}=\frac{1}{r\sin\theta}\left(1-\frac{2m}{r}\right)^{1/2}B^\theta. \qquad (5.2.28)$$

From (5.2.25) and (5.2.26) one can easily obtain the relation

$$\left(\rho+\frac{\bar{P}}{c^2}\right)r^2v^{(r)}=C_1\left(1-\frac{2m}{r}\right)^{-1}\left(1-\bar{v}^2/c^2\right),$$

which indeed is the relativistic generalisation of the equation for the accretion rate and thus one has

$$\left(\rho+\frac{\bar{P}}{c^2}\right)\left(1-\frac{2m}{r}\right)\left(1-\bar{v}^2/c^2\right)^{-1}r^2v^{(r)}=-\dot{M}$$

(5.2.29)

the parameter C_1 being identified with $-\dot{M}$, which may be a function of θ. With this we now have just two equations and two unknowns in P and ρ.

$$(\rho + \bar{p}/c^2)(1-v^2/c^2)^{-1}\left\{-\frac{c^2}{2}(1-\frac{2m}{r})\frac{\partial}{\partial r}\left[(1-\frac{2m}{r})^{-1}(1-v^2/c^2)\right]\right\}$$

$$+ \frac{\partial \bar{p}}{\partial r} = -\frac{\sigma}{c^2} u^t B(\theta)^2 v^{(r)}\left(1-\frac{v^{(\varphi)^2}}{c^2}\right)$$

(5.2.30)

and (5.2.27). Using (5.2.29), they may be written as

$$\frac{\dot{M}c^2}{2}\frac{1}{r^2 v^{(r)}}\frac{\partial}{\partial r}\left[(1-\frac{2m}{r})^{-1}(1-v^2/c^2)\right] + \frac{\partial \bar{p}}{\partial r}$$

$$= -\frac{\sigma}{c^2} B(\theta)^2 v^{(r)} u^t \left(1-\frac{v^{(\varphi)^2}}{c^2}\right)$$

(5.2.31)

$$-\frac{\dot{M}\cot\theta\, v^{(\varphi)^2}}{r^2 v^{(r)}}(1-\frac{2m}{r})^{-1} + \frac{\partial \bar{p}}{\partial \theta} = -\sigma B(r) B(\theta) v^{(r)} u^t \left(1-\frac{v^{(\varphi)^2}}{c^2}\right)$$

(5.2.32)

The integrability condition for $\bar{P}$ viz., $\frac{\partial}{\partial \theta}$(5.2.31) = $\frac{\partial}{\partial r}$(5.2.32) would give a differential equation for $\dot{M}$ and thus one can in principle have a complete set of solution for $\dot{M}, \bar{p}$ and ρ.

Special Case: thin disk approximation $\theta = \pi/2$. With this we have

$$v^{(\varphi)} = \frac{L}{r}(1-\frac{2m}{r})^{1/2}$$

$$v^{(r)} u^t = -\frac{c^2}{4\pi\sigma}(1-\frac{2m}{r})^{-1}\left\{\frac{km}{r^2} + \frac{1}{r}(2-k)(1-\frac{2m}{r})\right\}$$

$$B(\theta) = A\, r^{k-2}(1-\frac{2m}{r})^{-\frac{(k+1)}{2}}(1-\frac{3m}{r})$$

$$\frac{\partial \bar{P}}{\partial \theta} = 0$$

and

$$\frac{d\bar{P}}{dr} = -\frac{\dot{M}c^2}{r^2 v^{(r)} u^t} \frac{d}{dr}\left[\left(1-\frac{2m}{r}\right)^{-1/2}\left(1-v^2/c^2\right)^{1/2}\right]$$

$$-\frac{\sigma}{c^2} B_{(\theta)}^2 v^{(r)} u^t \left(1-v^{(\varphi)2}/c^2\right)$$

(5.2.33)

which on integration gives after using (5.2.29) again the equation for ρ

$$\rho c^2 = (k-2)\dot{M}(4\pi\sigma)\int \frac{\left(1-\frac{2m}{r}\right)^{-1/2}\left(1-v^2/c^2\right)^{1/2} dr}{\left[km+(2-k)(r-2m)\right]^2}$$

$$-\frac{1}{4\pi}\int \frac{B_{(\theta)}^2}{r^2}\left[km+(2-k)(r-2m)\right]\left(1-\frac{2m}{r}\right)^{-1}\left(1-\frac{v^{(\varphi)2}}{c^2}\right)dr$$

(5.2.34)

For different values of k one can evaluate the density profiles and consequently the pressure profile from (5.2.29) for a given accretion rate $\dot{M}$.

5.3. Structure of the Magnetic Field

In order to get the structure of the complete magnetic field inside and outside the disk one has to consider a proper solution for a poloidal magnetic field in the Schwarzschild background. Using the general approach of Ginzburg and Ozernoi (1964), Prasanna and Varma (1977) have

expressed the vacuum solution of a magnetic field dipolar at infinity as given by

$$B(r) = -B_0\left[\ln\left(1-\frac{2m}{r}\right)+\frac{2m}{r}\left(1+m/r\right)\right]\cos\theta \qquad (5.3.1)$$

$$B(\theta) = B_0\frac{m}{r}\left(1-\frac{2m}{r}\right)^{1/2}\left[\left(1-\frac{2m}{r}\right)^{-1}+\ln\left(1-\frac{2m}{r}\right)+1\right]\sin^2\theta \qquad (5.3.2)$$

Demanding the continuity of the magnetic field lines across the disk through matching (5.2.17) and (5.2.18) with (5.3.1) and (5.3.2) one can express the constant A in terms of the constant $B_0 = (3\mu/4m)$. Approximating from the expression for the dipole moment of a magnetised star at its surface having surface field strength B_s and the radius R we can use for B_0 the expression $(3B_s/4)(R/m)^3$, R the radius being expressed in the units of $m = MG/c^2$. Figures (5.1) and (5.2) show a typical profile of the magnetic field structure without and with the disk. For the purpose of illustration the meridional structure of the disk is presumed to extend to about 15^0 on either side of the equatorial plane.

5.4. Results and Discussions

The integration of the equation for the density (5.2.34) involves a boundary condition as well as the knowledge of the accretion rate $\dot{M}$ and of the electrical conductivity σ. While the second term can be integrated analytically for different values of k, the first term can be integrated numerically and thus the profiles of density

and pressure be obtained. One other factor to be kept in mind is that the velocity should not exceed c and this restriction for the Schwarzschild geometry imposes the restriction on the constant angular momentum l = L/cm to be less than $3\sqrt{3}$. As the formation of the disk is through accretion (normally from the companion of the compact star in a binary) of matter flowing in through the inner Lagrange point, for any realistic model one should have the outer edge of the accretion disk located at a distance r_b less than b_1 the distance of L_1 from the centre of the primary (the compact object).Using the approximate relation as given by Plavec and Kratochvil (Frank et al 1985),

$$b_1 = (0.5 - 0.227 \log q) a \qquad (5.4.1)$$

with q being the mass ratio M_2/M_1 and 'a' the distance between the centres of the two stars,one can work out for a typical binary with the period-mass relation

$$4\pi^2 a^3 = G(M_1 + M_2) M_\odot P^2,$$

P being the binary period. If $M_1 \sim 2M_\odot$ and $M_2 \sim 1M_\odot$ and $P \sim 10$ days (typical for X-ray binary) a $\sim 2\times10^5$ kms and $b_1 \sim 1.13\times10^5$ kms.With this in mind we chose r = 50m (m = MG/c^2) which places the disk around the primary well within the Roche lobe.As the constant k in our expression for the electromagnetic field was kept free we can now choose some typical values for k and then integrate for the density.

(a) k = 2

$$B(\ell) = A\left(1-\frac{3m}{\ell}\right)\left(1-\frac{2m}{\ell}\right)^{-3/2}$$

$$E(\ell) = \frac{AL}{c\ell}\left(1-\frac{3m}{\ell}\right)\left(1-\frac{2m}{\ell}\right)^{-1}$$

$$\rho c^2 = \frac{A^2}{4\pi}\frac{1}{12}\left[19-\frac{90m}{\ell}+\frac{108m^2}{\ell^2}\right]\left(1-\frac{2m}{\ell}\right)^{-3}$$

$$+\frac{A^2}{4\pi}\frac{L^2}{m^2c^2}\frac{1}{16}\left[72\frac{m^4}{\ell^4}+\frac{48m^3}{\ell^3}-\frac{88m}{\ell}+33\right]\left(1-\frac{2m}{\ell}\right)^{-2}$$

$$+\frac{A^2}{4\pi}\frac{L^2}{m^2c^2}\frac{11}{8}\ln\left(1-\frac{2m}{\ell}\right)-c_2$$

(b) k = 0

$$B(\ell) = \frac{A}{\ell^2}\left(1-\frac{3m}{\ell}\right)\left(1-\frac{2m}{\ell}\right)^{-1/2}$$

$$E(\ell) = \frac{AL}{c\ell^3}\left(1-\frac{3m}{\ell}\right)$$

$$\rho c^2 = -\frac{2\dot{M}c^2}{4(e^2/4\pi\sigma)}\int\frac{1}{\ell^2}\left(1-\frac{2m}{\ell}\right)^{-5/2}\left(1-v^2/c^2\right)^{1/2}d\ell$$

$$-\frac{A^2}{4\pi}\frac{1}{480m^4}\left[864\left(\frac{m}{\ell}\right)^5-180\left(\frac{m}{\ell}\right)^4+40\left(\frac{m}{\ell}\right)^3+30\left(\frac{m}{\ell}\right)^2\right.$$

$$\left.+30\left(\frac{m}{\ell}\right)+15\ln\left(1-\frac{2m}{\ell}\right)\right]$$

$$-\frac{A^2}{4\pi}\frac{L^2}{m^2c^2}\frac{m^2}{3\ell^6}\left[\left(1-\frac{3m}{\ell}\right)^2+\frac{6m}{7\ell}\left(1-\frac{3m}{\ell}\right)+\frac{6m^2}{23\ell^2}\right]-C_2$$

(c) $k = -2$

$$B(\infty) = \frac{A}{r^4}\left(1-\frac{3m}{r}\right)\left(1-\frac{2m}{r}\right)^{1/2}$$

$$E(r) = \frac{AL}{cr^5}\left(1-\frac{3m}{r}\right)\left(1-\frac{2m}{r}\right)$$

$$\rho c^2 = \frac{4\dot{M}c^2}{(e^2/4\pi\sigma)}\int \frac{\left(1-\frac{2m}{r}\right)^{-1/2}\left(1-v^2/c^2\right)^{1/2}}{(4r-10m)^2}\,dr$$

$$-\frac{A^2}{4\pi}\frac{2m}{9r^4}\left[\left(1-\frac{3m}{r}\right)^2+\frac{3m}{5r}\left(1-\frac{3m}{r}\right)+\frac{9}{55}\frac{m^2}{r^2}\right]$$

$$+\frac{A^2}{4\pi}\frac{L^2}{m^2c^2}\frac{2m^3}{11r^{11}}\left[\left(1-\frac{3m}{r}\right)^2\left(1-\frac{11m}{r}\right)\right.$$

$$\left.+\frac{m}{2r}\left(1-\frac{3m}{r}\right)\left(1-\frac{22m}{13r}\right)+\frac{3m^2}{26r^2}\left(1-\frac{11m}{7r}\right)\right]$$

$$+\frac{A^2}{4\pi}\frac{1}{2r^8}\left\{\left(1-\frac{3m}{r}\right)^2\left(1-\frac{16m}{r}\right)+\frac{2m}{3r}\left(1-\frac{3m}{5r}\right)\left(1-\frac{8m}{6r}\right)\right.$$

$$\left.-\frac{m^2}{5r^2}\left(1-\frac{16m}{11r}\right)\right\}$$

$$-\frac{A^2}{4\pi}\frac{L^2}{m^2c^2}\frac{2m^2}{5r^{10}}\left\{\left(1-\frac{3m}{r}\right)^2\left[1-\frac{40m}{11r}+\frac{10m^2}{3r^2}\right]\right.$$

$$+\frac{6m}{11r}\left(1-\frac{3m}{r}\right)\left[1-\frac{10m}{3r}+\frac{110m^2}{39r^3}\right]$$

$$\left.+\frac{3m^2}{r^2}\left[\frac{1}{220}-\frac{2}{143}\frac{m}{r}+\frac{1}{91}\frac{m^2}{r^2}\right]\right\}-C_2$$

d) k = -1

$$B(\theta) = \frac{A}{r^3}\left(1-\frac{3m}{r}\right)$$

$$E(\theta) = \frac{AL}{cr^4}\left(1-\frac{3m}{r}\right)\left(1-\frac{2m}{r}\right)^{1/2}$$

$$\rho_c^2 = \frac{3\dot{M}c^2}{(e^2/4\pi\epsilon)}\int \frac{\left(1-\frac{2m}{r}\right)^{-1/2}\left(1-v^2/c^2\right)^{1/2}dr}{(3r-4m)^2}$$

$$+\frac{A^2}{4\pi}\frac{1}{m^6}\left\{-\frac{9}{16}\left(\frac{m}{r}\right)^8+\frac{3}{28}\left(\frac{m}{r}\right)^7-\frac{1}{48}\left(\frac{m}{r}\right)^6\right.$$

$$-\frac{1}{80}\left(\frac{m}{r}\right)^5-\frac{1}{128}\left(\frac{m}{r}\right)^4-\frac{1}{192}\left(\frac{m}{r}\right)^3-\frac{1}{256}\left(\frac{m}{r}\right)^2$$

$$\left.-\frac{1}{256}\left(\frac{m}{r}\right)-\frac{1}{512}\ln\left(1-\frac{2m}{r}\right)\right\}$$

$$-\frac{A^2}{4\pi}\frac{L^2}{m^2c^2}\frac{1}{96r^6}\left[1-\frac{27}{5}\frac{m}{r}+\frac{81}{11}\frac{m^2}{r^2}\right]$$

$$-\frac{A^2}{4\pi}\frac{1}{2r^6}\left[1-\frac{36}{7}\frac{m}{r}+\frac{54}{8}\frac{m^2}{r^2}\right]$$

$$+\frac{A^2}{4\pi}\frac{3L^2}{m^2c^2}m^2\left[\frac{1}{8r^8}\left(1-\frac{3m}{r}\right)^2\left(1-\frac{16}{9}\frac{m}{r}\right)\right.$$

$$\left.-\frac{m}{12r^9}\left(1-\frac{3m}{r}\right)\left(1-\frac{8m}{5r}\right)+\frac{m^2}{5r^2}\left(1-\frac{16}{11}\frac{m}{r}\right)\right\}-c_2.$$

wherein the constant C_2 is evaluated through the boundary condition.

Fixing L and obtaining A thorugh B_s the assumed surface magnetic field of the compact star one can obtain the relation between ρ_0 and $\dot{M}$ through the boundary condition that the pressure in the disk at the outer edge is equal to the magnetic pressure at that point plus one-third the energy density at that point

$$(P)_{ab} = (P_M)_{ab} + \frac{\rho_0 c^2}{3} \qquad (5.4.7)$$

by using (5.2.29).Hence fixing one of them the other may be evaluated and subsequently the density and the corresponding pressure profiles are obtained. The set of results are presented in tables and figures as detailed below.

Table (5.1) gives the approximate position of the inner edge X_A as a function of the angular momentum l for different values of k.As shown in the corresponding Figures (5.3)-(5.5), the pressure profiles for k=2 and 0 decrease inwards for $l = 3\sqrt{3}$,whereas for k = -2,-1 there is no such pathology, and the pressure has a reasonable profile decreasing outwards and saturating as one moves away from the inner edge. As evident from the table for k = 0 and 2, the inner edge stays quite far away from 3 for $l = 3\sqrt{3}$ whereas for lower values of l the inner edge can reach farther inwards. Figure (5.6) gives a typical density

profile for k = -2, for different values of l, which however are not significantly different.

Table (5.2) gives the positions of inner edge as a function of the conductivity σ which seems to have a minimum plausible value of 10^3. As k changes from 2 to -2, one sees the minimum allowed σ for reasonable pressure profiles is about 10^3 which also depends on correlated values of B_o and ρ_o. Figures (5.7) and (5.8) show the typical profiles for pressure and density as a function of σ.

Table (5.3) shows the possible permitted values of l, σ and B_o for different k and ρ_o. Again for k = 0, -1, and -2 if ρ_o is less than some critical value for the same B_o, σ and l, the inner edge cannot reach beyond 6m. Figures (5.9) and (5.10) show the pressure profiles for k = -2, -1 whereas (5.11) gives the density profiles for k = -2.

Table (5.4) gives the variation with respect to the magnetic field and as may be seen the magnetic fields cannot be higher than a critical value for reasonable pressure behaviour. For instance with k = -1, l = 5, and $\sigma = 10^8$ if $B_o \sim 10^{11}$ the inner edge can reach upto 3.1 m, but still the pressure at that point shows an abrupt decrease from the steady value. However for $B_o \sim 10^{10}$, one can have a reasonable pressure profile with $X_A \sim$ 3m. Figure (5.12) shows the pressure profiles for k = -2 and different B_o wherein a plausible equilibrium configuration occurs only for $B_o \sim 10^8$ and for any higher value the pressure decreases at the inner edge.

Thus as may be seen from the set of tables and figures a possible disk-like equilibrium structures exist only for a right combination of k, ℓ, σ, B_0 and ρ_0. For a given magnetic field B_0 and angular momentum ℓ the density at the outer edge has to be reasonably high if one wants a disk-like configuration. For example, with $B_0 \sim 10^7$ if the disk inner edge has to reach upto $\sim$ 3m (within 6m, where GTR influence would be strong) then $\rho_0 \gtrsim 5\times10^{-10}$ gm/cc or 5×10^{21} particles/m^3 with the corresponding accretion rate $\dot{M} \gtrsim 7\times10^{11}$ gms/cc $\backsim 10^{-14}$ $M_\odot$/yr.

In conclusion we can say that accretion disks around very compact objects (radius < 3m) can be sustained provided one has a certain amount of magnetic field associated with the compact object which may be either due to the intrinsic field like in a neutron star or due to ring currents just outside the event horizon, which smoothly joins with the disk field existing due to the currents within the disk. It is very interesting to note that for possible stable configurations having reasonable accretion rate a <u>disk close to the surface</u> of a highly compact star (R $\sim$ 3m) is possible only when the surface magnetic field strength is lower than $\sim 10^{10}$ G. It may also be noted, that though the bulk viscosity coefficient does contribute through the non-zero radial velocity term, it does not seem to be very effective at this stage of the calculations.

Table Captions

Table 5.1 : Position of inner edge for different values of ℓ

Table 5.2 : Position of inner edge for different values of σ

Table 5.3 : Position of inner edge for different values of ρ_0

Table 5.4 : Position of inner edge for different values of β_0

Table 5.1

k	ℓ	σ	B_0	ρ_0	$\dot{M}$	XA
0	0.1×10^{0}	0.1×10^{7}	0.1×10^{8}	0.1×10^{-8}	0.1348×10^{13}	3.5
	0.1×10^{1}				0.1348×10^{13}	3.5
	0.3×10^{1}				0.1350×10^{13}	3.5
	0.5×10^{1}				0.1354×10^{13}	8.4
2	0.1×10^{-1}	0.1×10^{9}	0.1×10^{7}	0.1×10^{-5}	0.2808×10^{12}	3.5
	0.1×10^{0}				0.2808×10^{12}	3.5
	0.3×10^{1}				0.2808×10^{12}	3.5
	0.5×10^{1}				0.2813×10^{12}	4.5
	0.519×10^{1}				0.2823×10^{12}	4.9
-2	0.1×10^{0}	0.1×10^{9}	0.1×10^{11}	0.1×10^{-3}	0.2667×10^{16}	3.1
	0.1×10^{1}				0.2668×10^{16}	3.1
	0.3×10^{1}				0.2672×10^{16}	3.1
	0.5×10^{1}				0.2680×10^{16}	3.1
-1	0.1×10^{0}	0.1×10^{9}	0.1×10^{7}	0.1×10^{-5}	0.2008×10^{14}	3.1
	0.1×10^{1}				0.2008×10^{14}	3.1
	0.3×10^{1}				0.2011×10^{14}	3.1
	0.5×10^{1}				0.2017×10^{14}	3.1

Table 5.2

k	ℓ	σ	B_o	ρ_o	$\dot{M}$	XA
2	1.0	0.1×10^{4}	0.1×10^{9}	0.1×10^{-5}	0.2814×10^{17}	5.6
		0.5×10^{4}			0.5628×10^{16}	3.5
		0.1×10^{6}			0.2814×10^{15}	3.5
0	1.0	0.1×10^{4}	0.1×10^{11}	0.1×10^{-3}	0.1589×10^{21}	28.8
		0.5×10^{4}			0.2717×10^{20}	9.5
		0.8×10^{4}			0.1690×10^{20}	3.5
		0.1×10^{5}			0.1350×10^{20}	3.5
-1	5.0	0.1×10^{9}	0.1×10^{7}	0.1×10^{-3}	0.2017×10^{16}	3.1
		0.1×10^{7}			0.2017×10^{18}	3.1
		0.1×10^{5}			0.2026×10^{20}	3.1
		0.1×10^{4}			0.2754×10^{21}	3.1
-2	5.0	0.5×10^{4}	0.1×10^{11}	0.1×10^{-3}	0.5522×10^{20}	13.1
		0.7×10^{4}			0.3888×10^{20}	3.1
		0.1×10^{5}			0.2701×10^{20}	3.1
		0.1×10^{7}			0.2680×10^{18}	3.1
-1	5.0	0.1×10^{4}			0.2754×10^{21}	3.1
		0.1×10^{5}			0.2020×10^{20}	3.1
		0.1×10^{6}			0.2017×10^{19}	3.1
		0.1×10^{7}			0.2017×10^{18}	3.1

Table 5.3

k	l	σ	B_o	ρ_o	$\dot{M}$	XA
2	1.0	0.1×10^{9}	0.1×10^{11}	0.1×10^{-3}	0.3335×10^{14}	3.5
				0.1×10^{-2}	0.2861×10^{15}	3.5
				0.1×10^{-1}	0.2814×10^{16}	3.5
2	1.0	0.1×10^{9}	0.1×10^{6}	0.1×10^{-5}	0.2808×10^{12}	3.5
				0.1×10^{-7}	0.2808×10^{10}	3.5
				0.1×10^{-8}	0.2808×10^{9}	3.5
				0.1×10^{-11}	0.2814×10^{6}	3.5
0	1.0	0.1×10^{7}	0.1×10^{8}	0.1×10^{-8}	0.1348×10^{13}	3.5
				0.1×10^{-9}	0.1348×10^{12}	3.5
				0.1×10^{-10}	0.1348×10^{11}	3.5
				0.7×10^{-11}	0.9440×10^{10}	7.8
				0.5×10^{-11}	0.6743×10^{10}	9.5
0	1.0	0.1×10^{7}	0.1×10^{5}	0.1×10^{-17}	0.1351×10^{04}	17.5
				0.1×10^{-16}	0.1348×10^{05}	3.5
				0.1×10^{-14}	0.1348×10^{07}	3.5
-1	5.0	0.1×10^{9}	0.1×10^{11}	0.1×10^{-5}	0.2017×10^{14}	27.4
				0.2×10^{-5}	0.4055×10^{14}	9.0
				0.5×10^{-5}	0.1008×10^{15}	3.4
				0.1×10^{-4}	0.2017×10^{15}	3.1

Contd.

Table 5.3(Contd.)

k	l	σ	B_0	ρ_0	$\dot{M}$	XA
-2	5.0	0.1×10^{8}	0.1×10^{11}	0.1×10^{-7}	0.2680×10^{13}	14.1
				0.1×10^{-6}	0.2680×10^{14}	9.2
				0.1×10^{-5}	0.2680×10^{15}	3.3
				0.1×10^{-4}	0.2680×10^{16}	3.1
-2	5.0	0.1×10^{8}	0.1×10^{7}	0.1×10^{-13}	0.2680×10^{7}	3.3
				0.1×10^{-12}	0.2680×10^{8}	3.1
				0.1×10^{-11}	0.2680×10^{9}	3.1

Table 5.4

k	l	σ	B_0	ρ_0	$\dot{M}$	XA
-1	5.0	0.1×10^{9}	0.1×10^{11}	0.1×10^{-2}	0.2017×10^{17}	3.1
			0.5×10^{11}		0.2017×10^{17}	3.1
			0.1×10^{12}		0.2017×10^{17}	3.1
			0.5×10^{12}		0.2017×10^{17}	40.0
-1	5.0	0.1×10^{9}	0.1×10^{8}	0.1×10^{-8}	0.2017×10^{11}	3.1
			0.5×10^{8}		0.2017×10^{11}	3.1
			0.1×10^{9}		0.2017×10^{11}	3.1
			0.5×10^{9}		0.2017×10^{11}	40.9
-1	5.0	0.1×10^{9}	0.1×10^{9}	0.1×10^{-9}	0.2017×10^{10}	27.4
			0.1×10^{8}		0.2017×10^{10}	3.1
			0.5×10^{8}		0.2017×10^{10}	3.8
-1	5.0	0.1×10^{9}	0.1×10^{11}	0.1×10^{-3}	0.2017×10^{16}	3.1
			0.5×10^{11}		0.2017×10^{16}	3.8
			0.1×10^{12}		0.2017×10^{16}	27.4
-2	5.0	0.1×10^{5}	0.1×10^{11}	0.1×10^{-3}	0.2701×10^{20}	3.1
			0.5×10^{11}		0.2701×10^{20}	3.1
			0.1×10^{12}		0.2701×10^{20}	6.2
			0.5×10^{12}		0.2701×10^{20}	12.1
			0.1×10^{13}		0.2701×10^{13}	14.9

Contd.

Table 5.4 (Contd)

γ_k	l	σ	B_o	ρ_o	$\dot{M}$	XA
-2	5.0	0.1×10^{8}	0.7×10^{10}	0.1×10^{-9}	0.2683×10^{11}	25.6
			0.5×10^{10}		0.2682×10^{11}	23.3
			0.1×10^{10}		0.2680×10^{13}	14.1
			0.5×10^{9}		0.2680×10^{11}	11.0
			0.1×10^{9}		0.2680×10^{11}	3.3
-2	5.0	0.1×10^{8}	0.1×10^{13}	0.1×10^{-4}	0.2681×10^{16}	20.3
			0.5×10^{12}		0.2681×10^{16}	16.4
			0.1×10^{12}		0.2681×10^{16}	9.2
			0.5×10^{11}		0.2681×10^{16}	6.3
			0.1×10^{11}		0.2681×10^{16}	3.1

Figure Captions

Fig. 5.1 : Structure of magnetic field lines without the disk.

Fig. 5.2 : Structure of magnetic field lines with the disk

Fig. 5.3- 5.5 : Pressure profiles for different ℓ

Fig. 5.6 : Density profiles for different ℓ

Fig. 5.7 : Pressure profiles for different σ

Fig. 5.8 : Density profiles for different σ

Fig. 5.9 - 5.10 : Pressure profiles for different ρ_0

Fig. 5.11 : Density profiles for different ρ_0

Fig. 5.12 : Pressure profiles for different B_0

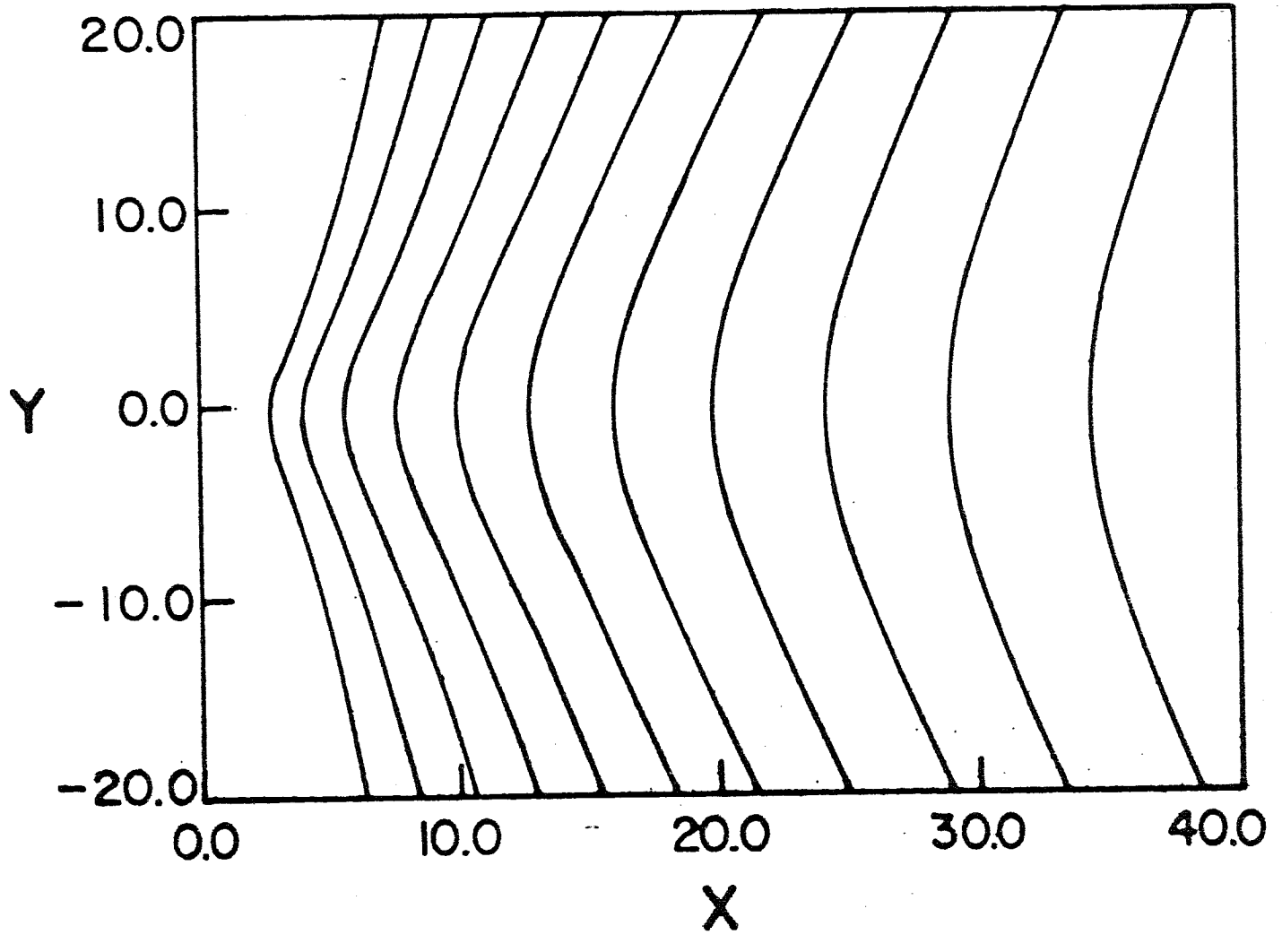

Fig. 5.1

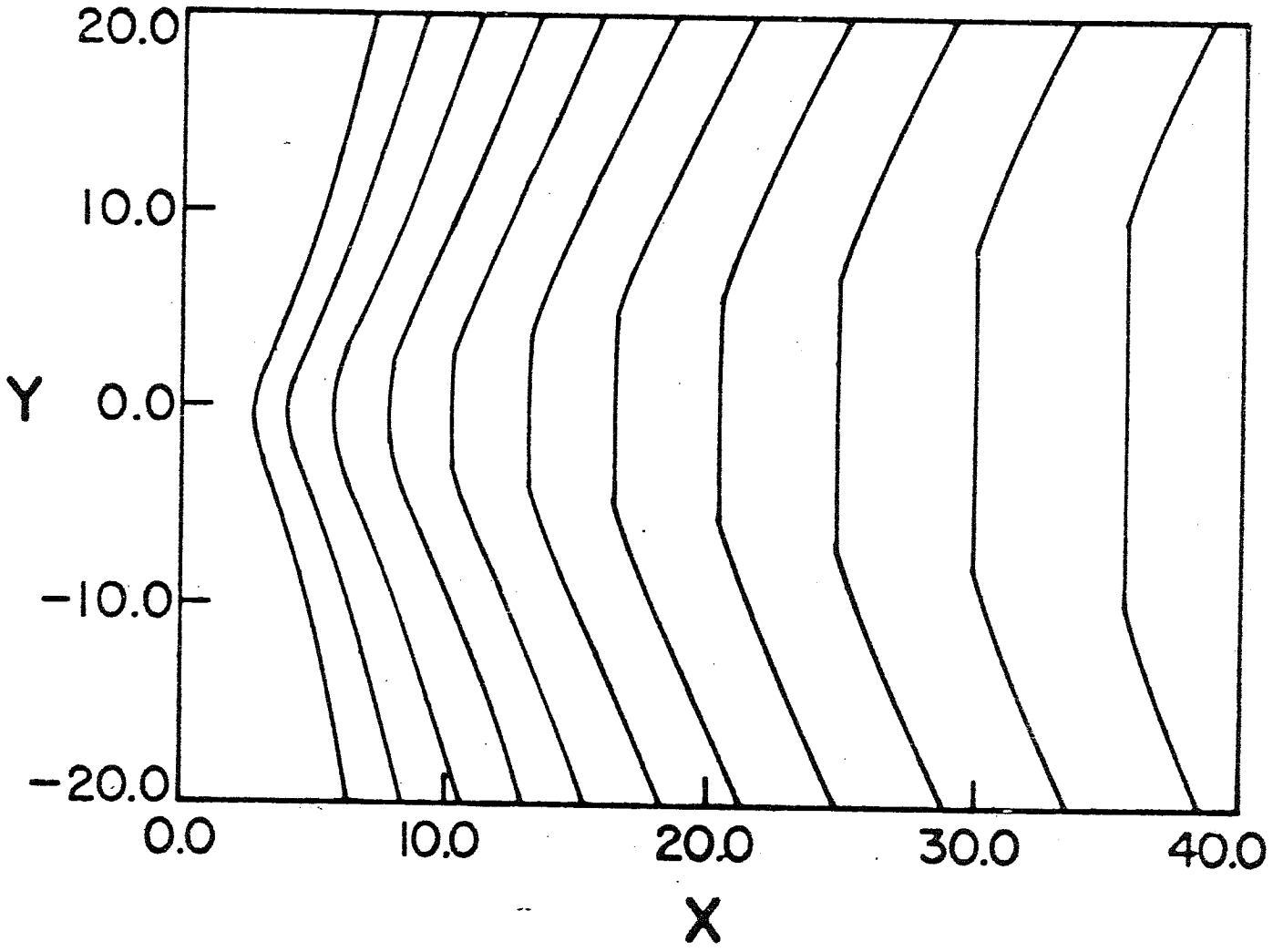

Fig. 5.2

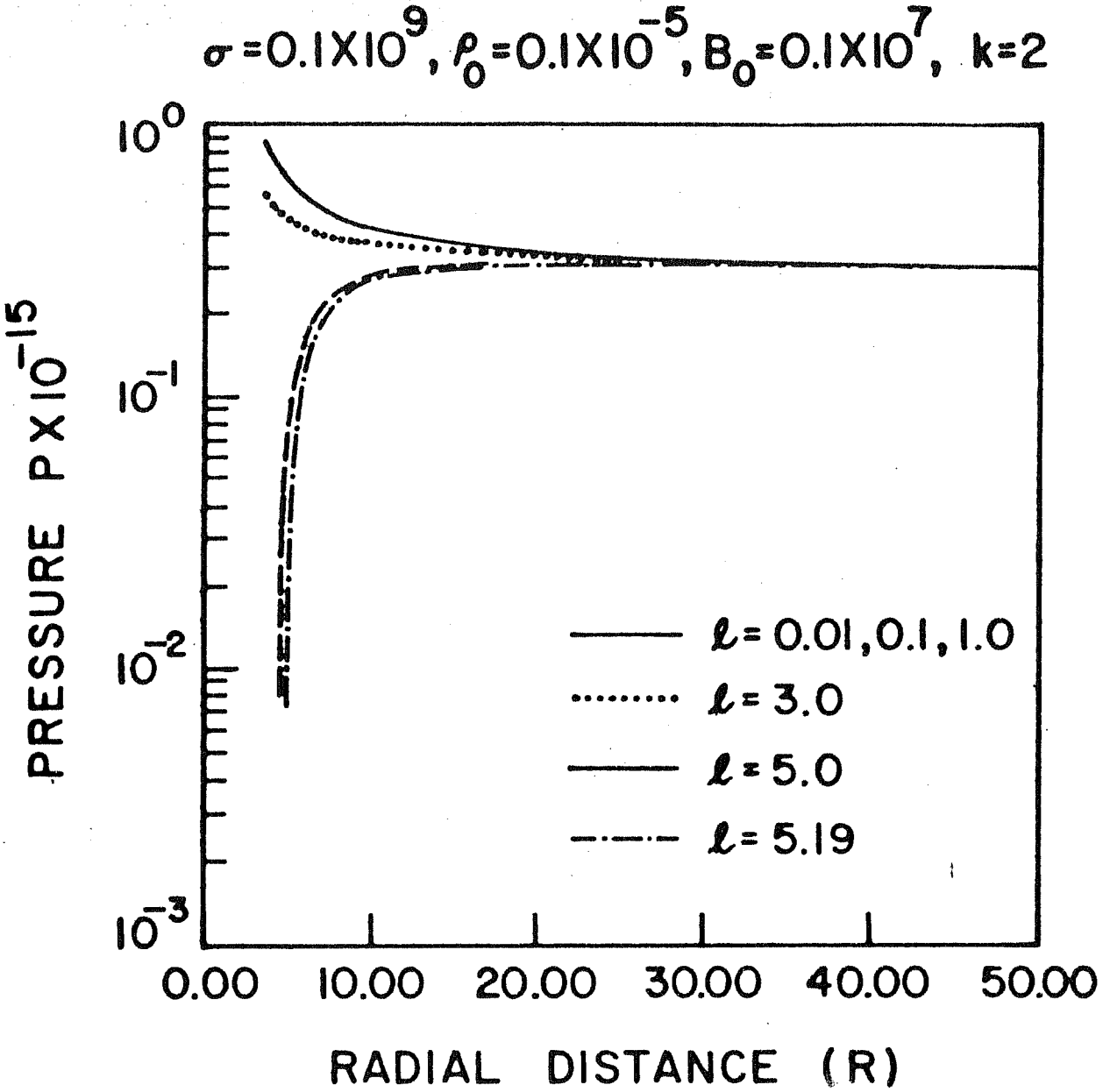
σ=0.1X10^9, ρ0=0.1X10^-5, B0=0.1X10^7, k=2
PRESSURE P X 10^-15
10^0
10^-1
10^-2
10^-3
0.00
10.00
20.00
30.00
40.00
50.00
RADIAL DISTANCE (R)
ℓ= 0.01, 0.1, 1.0
ℓ= 3.0
ℓ= 5.0
ℓ= 5.19

Fig. 5.3

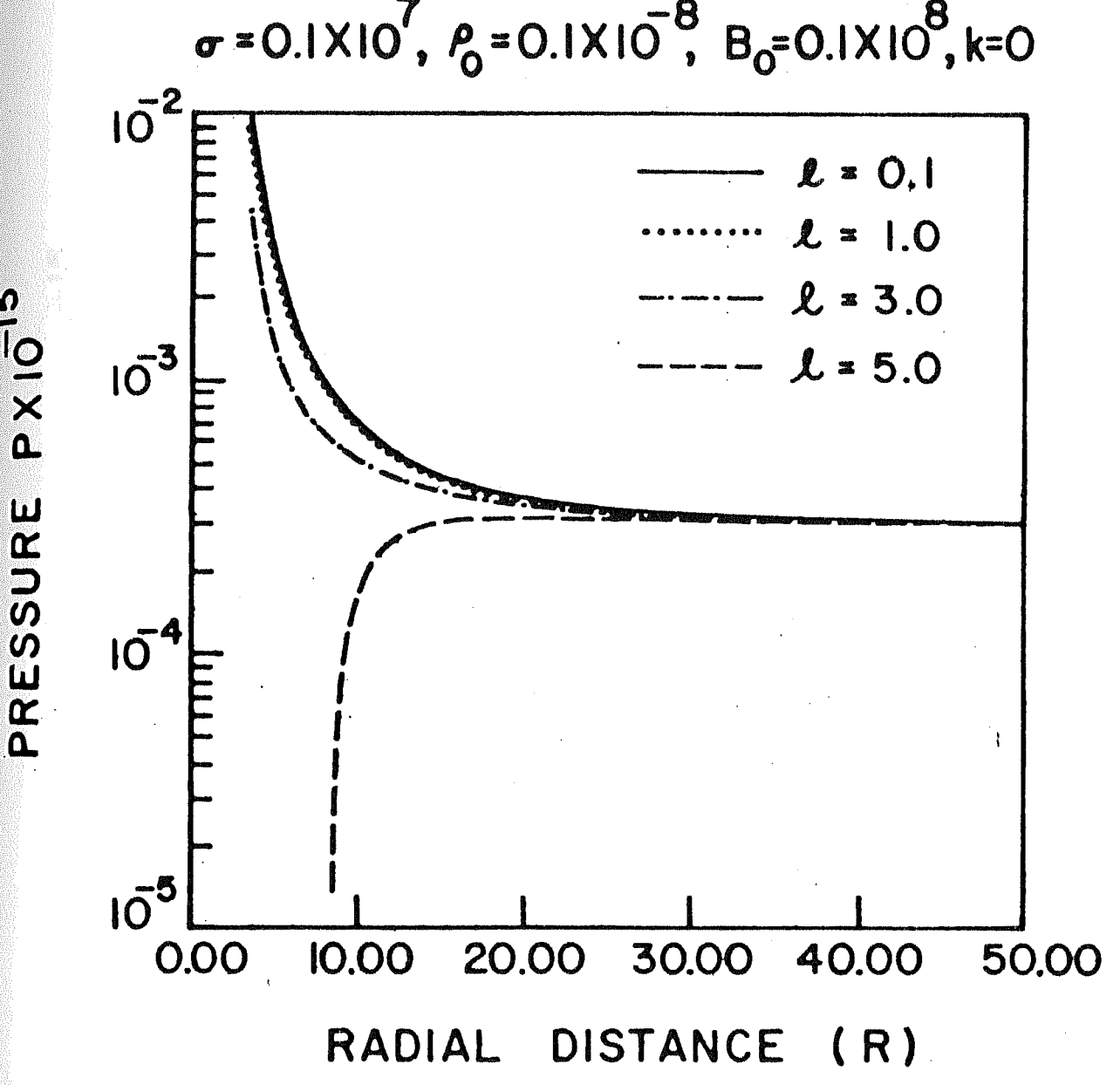
σ = 0.1X10^7, ρ0 = 0.1X10^-8, B0 = 0.1X10^8, k=0
PRESSURE P X 10^-15
10^-2
10^-3
10^-4
10^-5
ℓ = 0.1
ℓ = 1.0
ℓ = 3.0
ℓ = 5.0
0.00
10.00
20.00
30.00
40.00
50.00
RADIAL DISTANCE (R)

Fig. 5.4

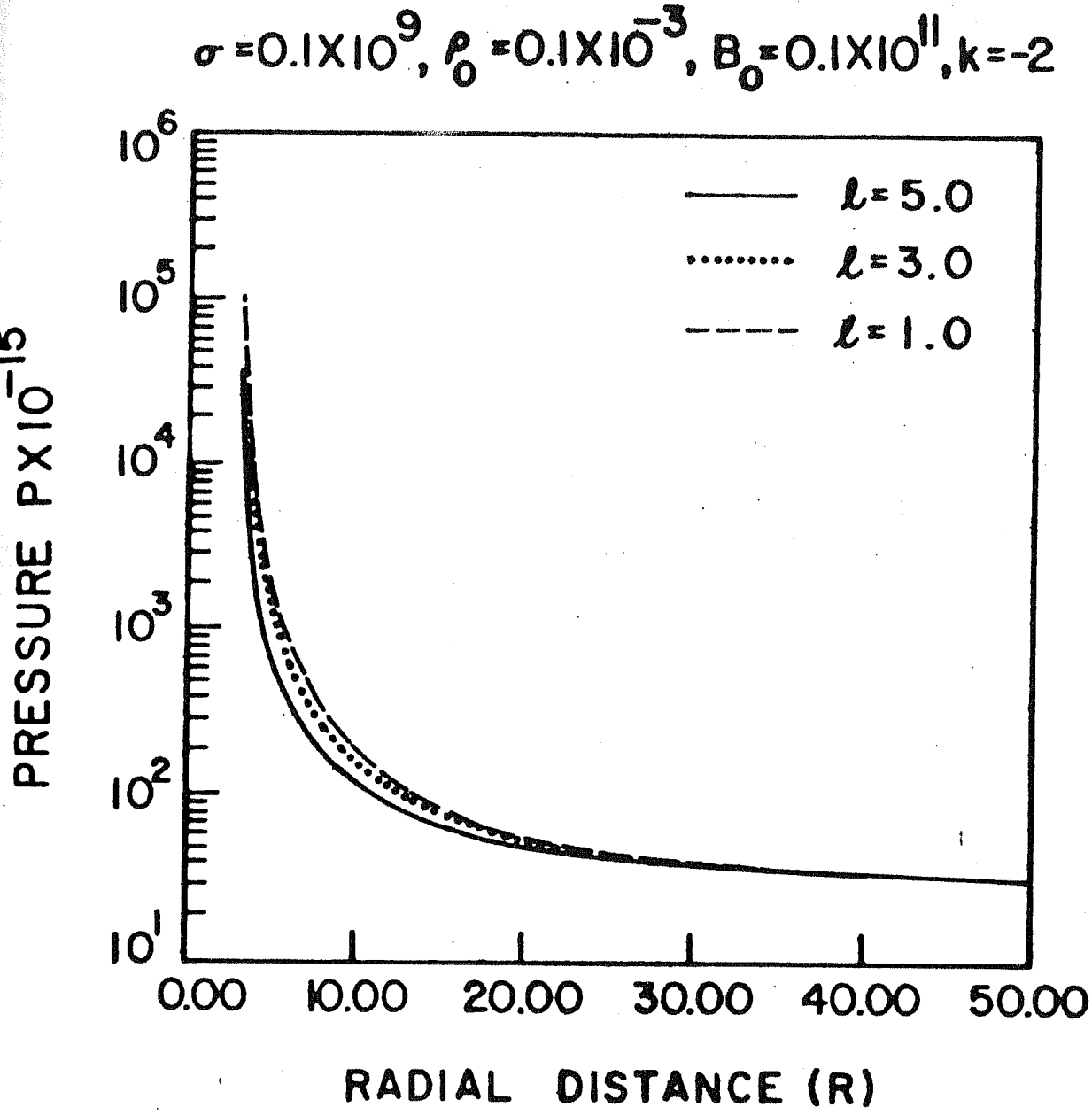
σ =0.1X10^9, ρ0 =0.1X10^-3, B0=0.1X10^11, k=-2
ℓ=5.0
ℓ=3.0
ℓ=1.0
PRESSURE PX10^-15
10^6
10^5
10^4
10^3
10^2
10^1
0.00
10.00
20.00
30.00
40.00
50.00
RADIAL DISTANCE (R)

Fig. 5.5

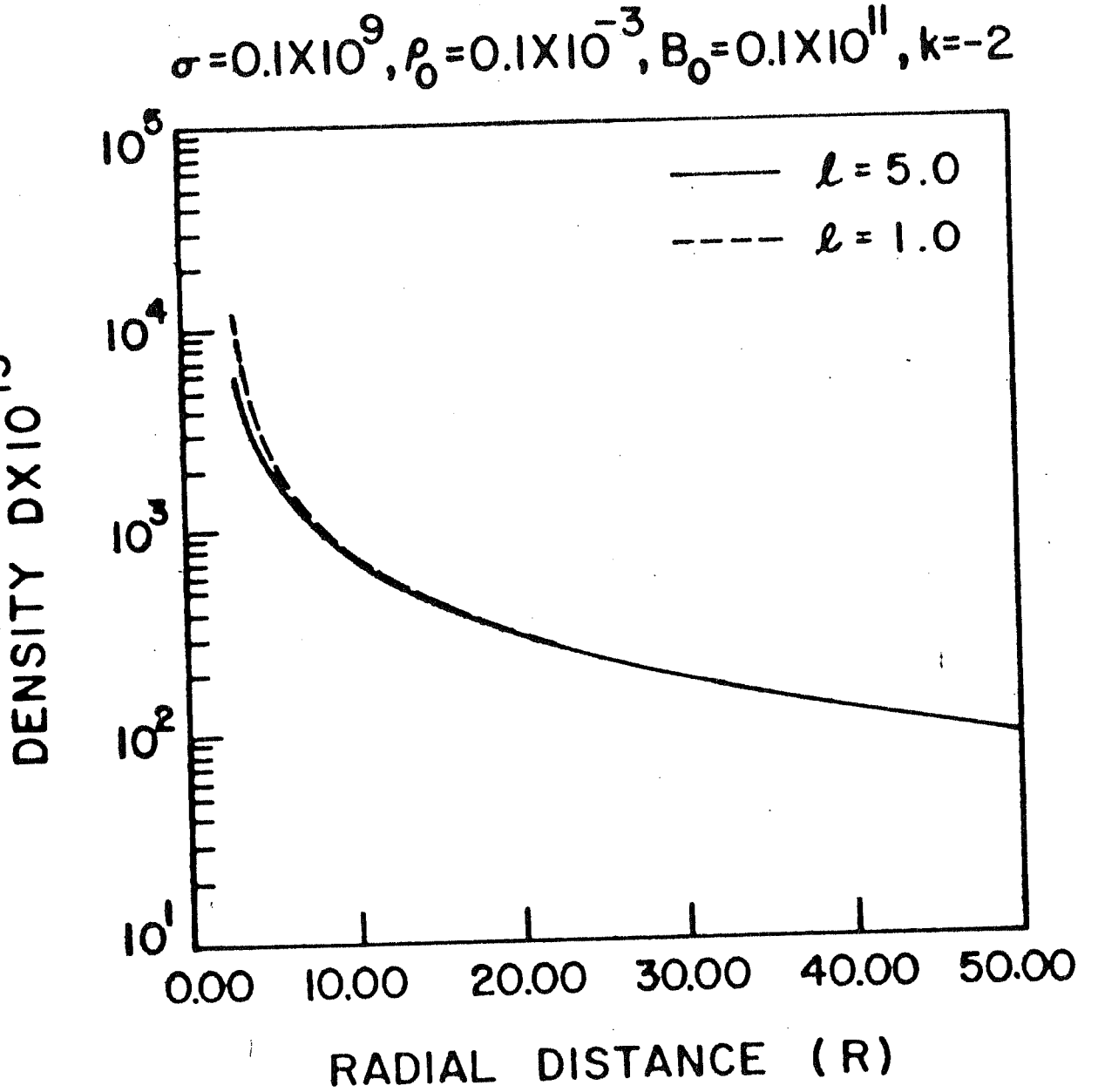
σ=0.1X10^9, ρ0=0.1X10^-3, B0=0.1X10^11, k=-2
ℓ = 5.0
ℓ = 1.0
DENSITY DX10^-15
10^5
10^4
10^3
10^2
10^1
0.00
10.00
20.00
30.00
40.00
50.00
RADIAL DISTANCE (R)

Fig. 5.6

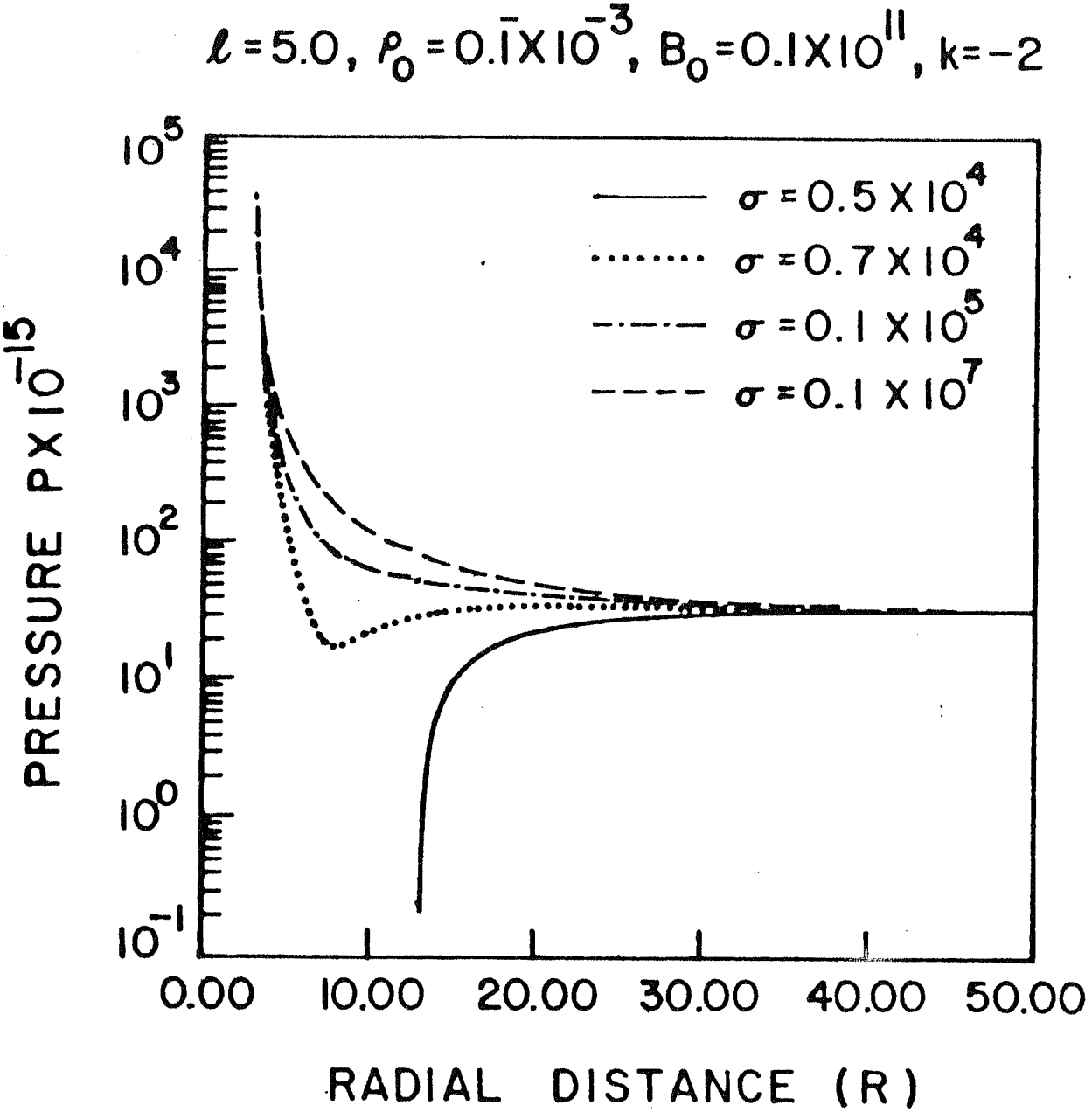
$\ell = 5.0,\ \rho_0 = 0.1 \times 10^{-3},\ B_0 = 0.1 \times 10^{11},\ k = -2$
$\sigma = 0.5 \times 10^4$
$\sigma = 0.7 \times 10^4$
$\sigma = 0.1 \times 10^5$
$\sigma = 0.1 \times 10^7$
PRESSURE $P \times 10^{-15}$
10^5
10^4
10^3
10^2
10^1
10^0
10^{-1}
0.00
10.00
20.00
30.00
40.00
50.00
RADIAL DISTANCE (R)

Fig. 5.7

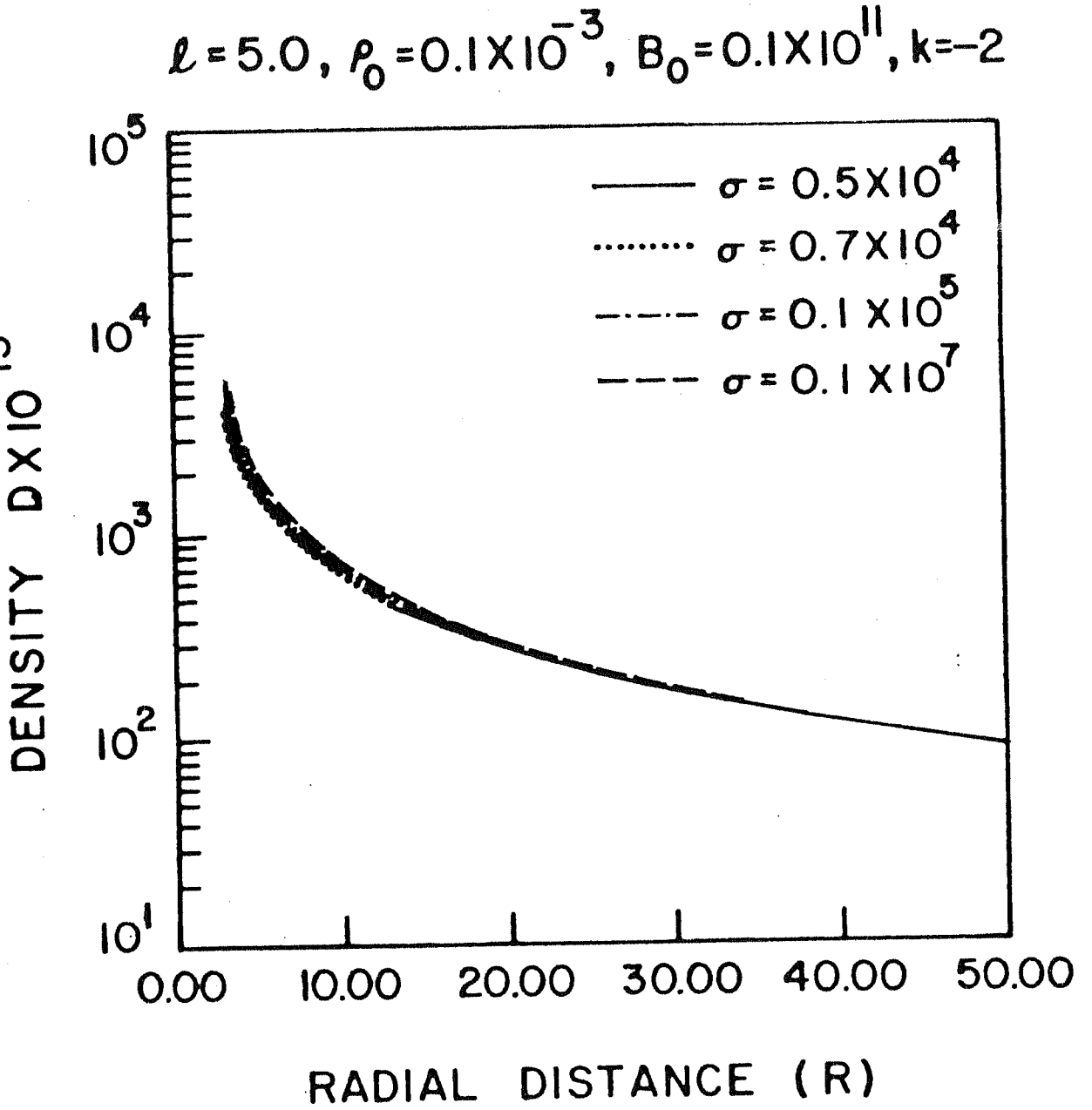
$\ell = 5.0$, $\rho_0 = 0.1 \times 10^{-3}$, $B_0 = 0.1 \times 10^{11}$, k=-2
$\sigma = 0.5 \times 10^4$
$\sigma = 0.7 \times 10^4$
$\sigma = 0.1 \times 10^5$
$\sigma = 0.1 \times 10^7$
DENSITY $D \times 10^{-15}$
10^5
10^4
10^3
10^2
10^1
0.00
10.00
20.00
30.00
40.00
50.00
RADIAL DISTANCE (R)

Fig. 5.8

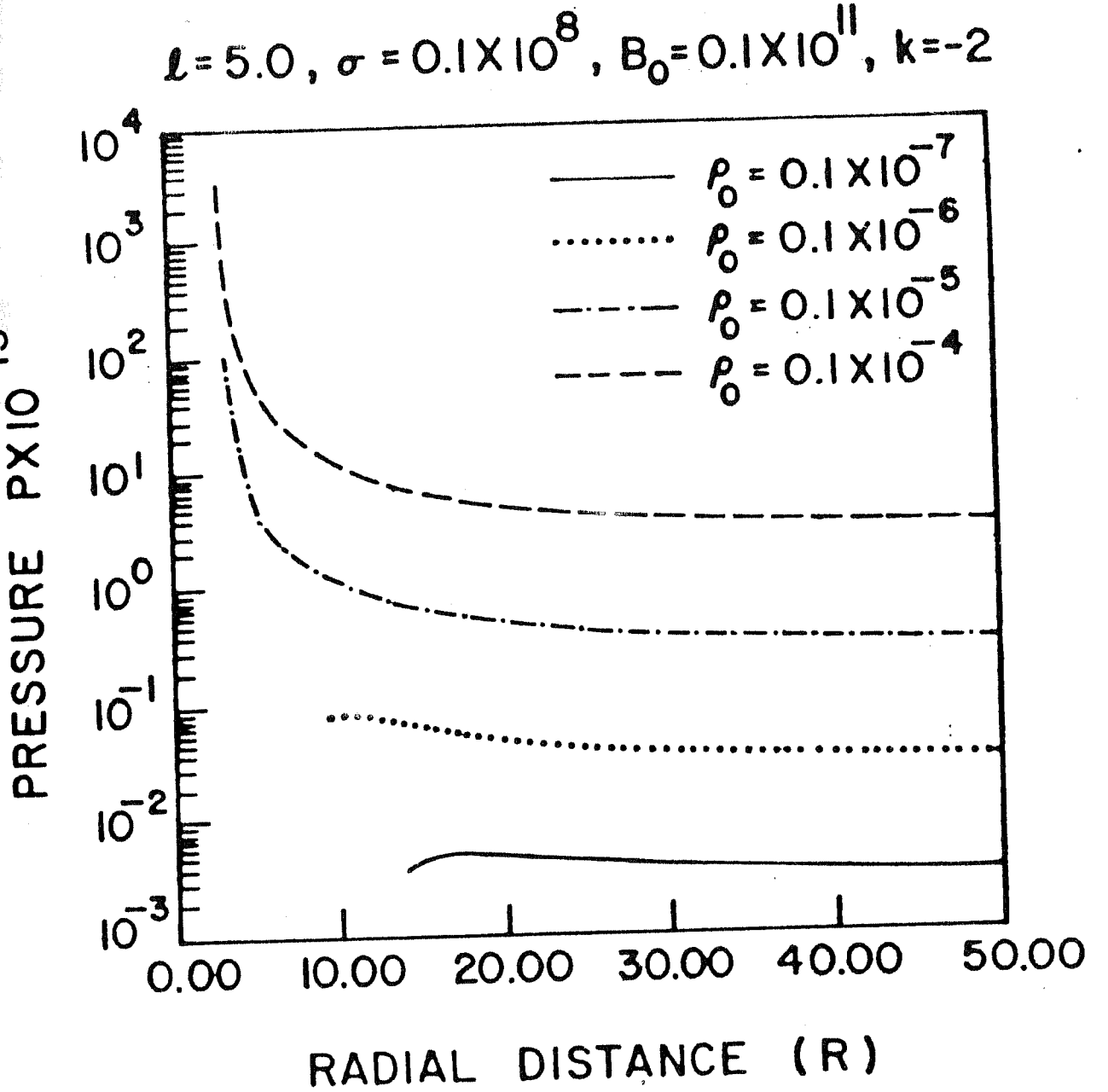
$\ell = 5.0$, $\sigma = 0.1 \times 10^{8}$, $B_0 = 0.1 \times 10^{11}$, $k = -2$
$\rho_0 = 0.1 \times 10^{-7}$
$\rho_0 = 0.1 \times 10^{-6}$
$\rho_0 = 0.1 \times 10^{-5}$
$\rho_0 = 0.1 \times 10^{-4}$
PRESSURE $P \times 10^{-15}$
10^{4}
10^{3}
10^{2}
10^{1}
10^{0}
10^{-1}
10^{-2}
10^{-3}
0.00
10.00
20.00
30.00
40.00
50.00
RADIAL DISTANCE (R)

Fig. 5·9

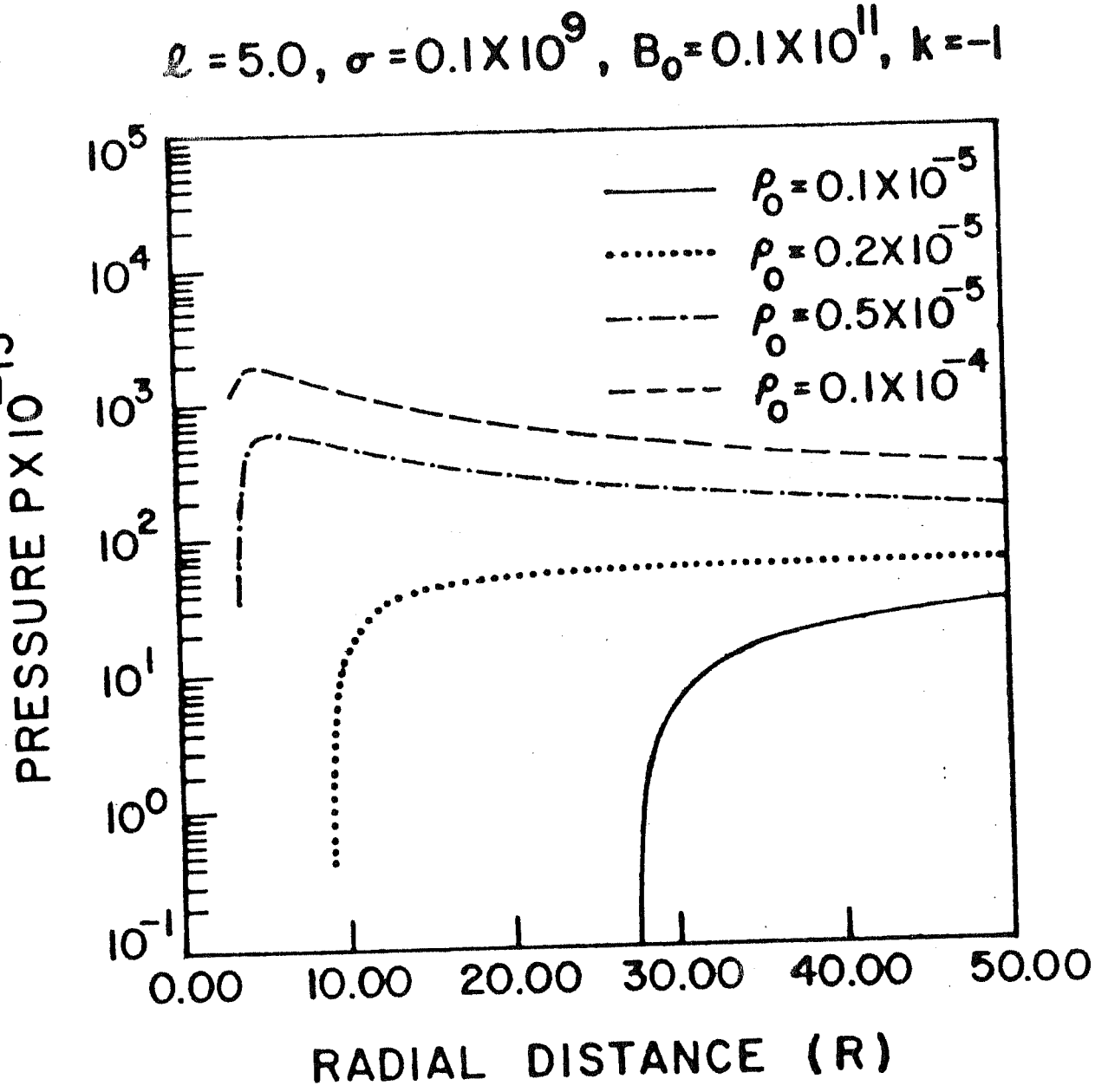
$\ell = 5.0, \sigma = 0.1 \times 10^{9}, B_0 = 0.1 \times 10^{11}, k = -1$
$\rho_0 = 0.1 \times 10^{-5}$
$\rho_0 = 0.2 \times 10^{-5}$
$\rho_0 = 0.5 \times 10^{-5}$
$\rho_0 = 0.1 \times 10^{-4}$
PRESSURE P X 10^{-15}
10^{5}
10^{4}
10^{3}
10^{2}
10^{1}
10^{0}
10^{-1}
0.00
10.00
20.00
30.00
40.00
50.00
RADIAL DISTANCE (R)

Fig. 5.10

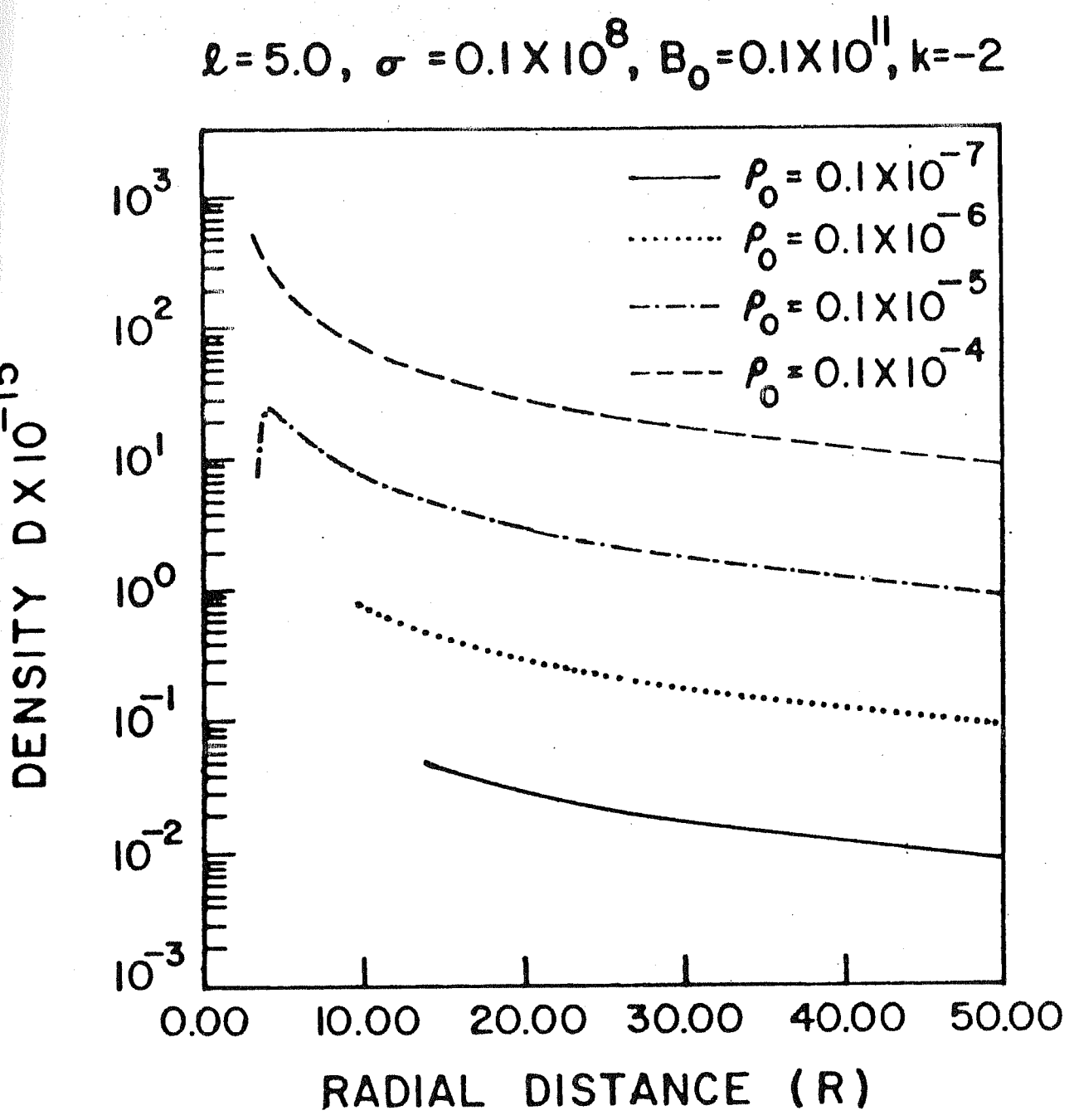
$\ell = 5.0$, $\sigma = 0.1 \times 10^{8}$, $B_0 = 0.1 \times 10^{11}$, $k = -2$
$\rho_0 = 0.1 \times 10^{-7}$
$\rho_0 = 0.1 \times 10^{-6}$
$\rho_0 = 0.1 \times 10^{-5}$
$\rho_0 = 0.1 \times 10^{-4}$
DENSITY $D \times 10^{-15}$
10^{3}
10^{2}
10^{1}
10^{0}
10^{-1}
10^{-2}
10^{-3}
0.00
10.00
20.00
30.00
40.00
50.00
RADIAL DISTANCE (R)

Fig. 5-11

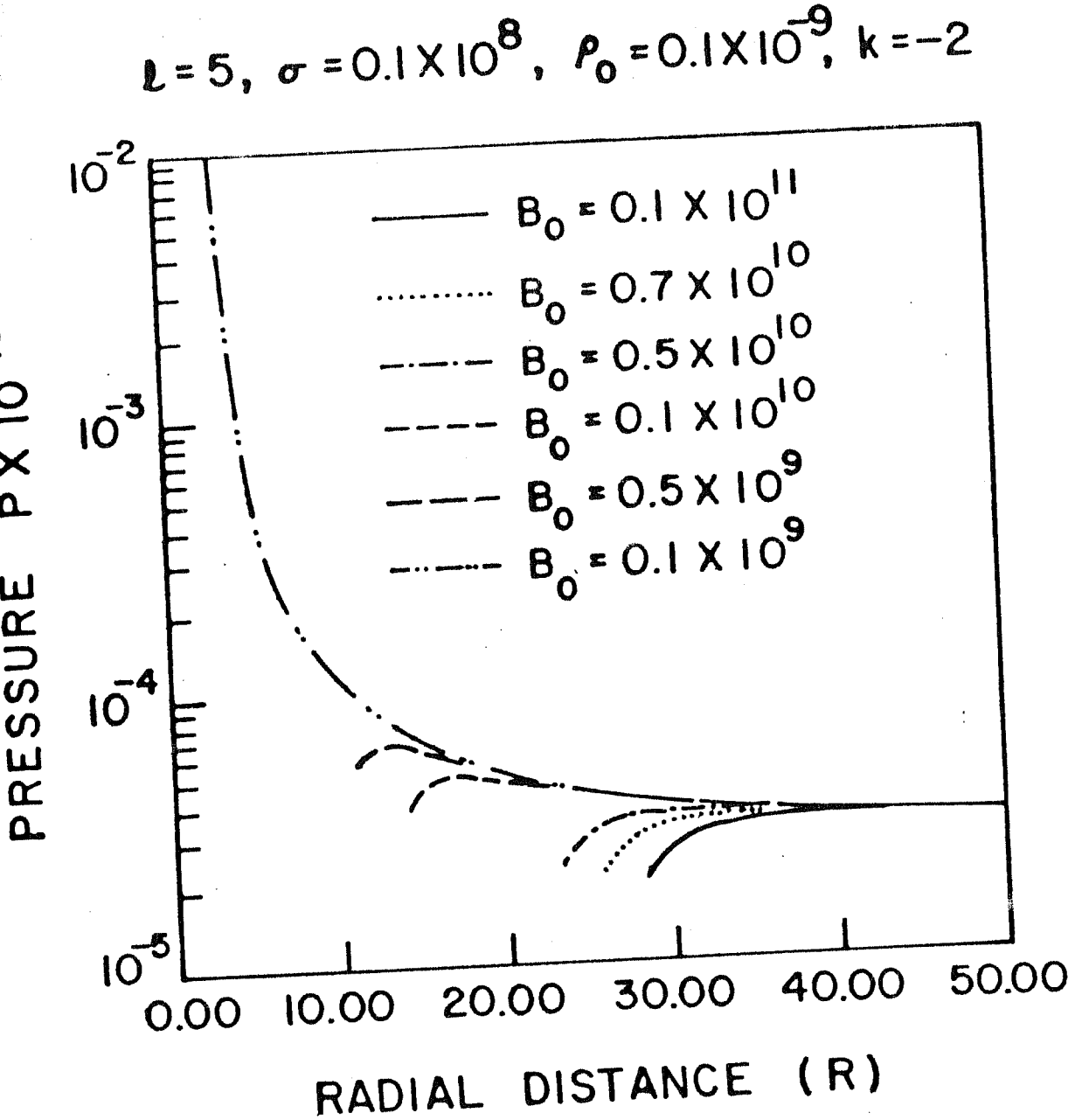
$\ell = 5,\ \sigma = 0.1 \times 10^{8},\ \rho_0 = 0.1 \times 10^{-9},\ k = -2$
$B_0 = 0.1 \times 10^{11}$
$B_0 = 0.7 \times 10^{10}$
$B_0 = 0.5 \times 10^{10}$
$B_0 = 0.1 \times 10^{10}$
$B_0 = 0.5 \times 10^{9}$
$B_0 = 0.1 \times 10^{9}$
PRESSURE $P \times 10^{-15}$
10^{-2}
10^{-3}
10^{-4}
10^{-5}
0.00
10.00
20.00
30.00
40.00
50.00
RADIAL DISTANCE (R)

Fig. 5.12

CHAPTER VI

PLASMA DISKS AROUND A SLOWLY ROTATING COMPACT OBJECT

6.1. Introduction

In the earlier chapters we discussed the equilibrium configurations of plasma disks around a nonrotating compact object. The importance of considering electromagnetic field in the discussions of disk dynamics was clearly brought out from the fact that, it is possible to have disk configuration, very near to the object in the presence of electromagnetic fields and it affects the structure of the disk, especially in regions close to the object where magnetic pressure can become comparable with the gas

pressure. However, such a study would not be complete without taking into effect the rotation of the compact object. The compact object may possess rotation as an end product of the collapse of a rotating star or it can acquire it by the transfer of torque from the disk around it. In this chapter we discuss the structure and dynamics of a plasma disk around a slowly rotating compact object ($\frac{a}{m} < 0.5$).

6.2. Structure of the Disk

For the present case we consider the plasma to be having only azimuthal component of velocity nonzero. The toroidal component of magnetic field B is taken to be zero, and the plasma is of infinite conductivity. Under the conditions of stationarity and axisymmetry, the general equations that we have developed for fluid flow around slowly rotating compact objects (equations (3.1.28) to (3.1.41)) reduces to the following form.

Momentum Equation:

$$\left(p+\frac{P}{c^2}\right) u^{t^2}\left[\frac{mc^2}{r^2}\left(1-\frac{2m}{r}\right)-\frac{2amc}{r^2}\left(1-\frac{2m}{r}\right)\sin^2\theta\, v^\varphi - (r-2m)\sin^2\theta\, v^{\varphi^2}\right] + \left(1-\frac{2m}{r}\right)\frac{\partial P}{\partial r} = F^{\mu}_{\nu}\frac{J^{\nu}}{c}. \tag{6.2.1}$$

$$\left(p+\frac{P}{c^2}\right) u^{t^2}\left[-\sin\theta\cos\theta\, v^{\varphi^2}+\frac{4am}{r^3}\sin\theta\cos\theta\, v^{\varphi}\right]$$

$$+\frac{1}{r^2}\frac{\partial P}{\partial \theta} = F^{\theta k}\bar{J}^{k} \qquad (6.2.2)$$

Maxwell's Equation:

$$J^{\phi} = \frac{1}{r^4 \sin\theta}\frac{\partial}{\partial \theta}\left(\frac{B_r}{\sin\theta}\right) - \frac{1}{r^2 \sin^2\theta}\frac{\partial}{\partial r}\left[\left(1-\frac{2m}{r}\right)B_\theta\right]$$

$$- \frac{2am}{r^2}\left[\frac{\partial}{\partial r}\left(\frac{E_r}{r}\right) + \frac{1}{r^3 \sin\theta}\left(1-\frac{2m}{r}\right)^{-1}\frac{\partial}{r\theta}\left(\sin\theta E_\theta\right)\right] \qquad (6.2.3)$$

$$\bar{J}^{t} = -\frac{1}{r^2}\left[\frac{\partial}{\partial r}\left(r^2 E_r\right) + \frac{1}{\sin\theta}\left(1-\frac{2m}{r}\right)^{-1}\frac{\partial}{r\theta}\left(\sin\theta E_\theta\right)\right]$$

$$- \frac{2am}{r^2}\left[\frac{1}{r^3 \sin\theta}\left(1-\frac{2m}{r}\right)^{-1}\frac{\partial}{r\theta}\left(\sin\theta B_r\right) - \frac{\partial}{\partial r}\left(\frac{B_\theta}{r}\right)\right] \qquad (6.2.4)$$

$$\frac{\partial B_r}{\partial r} + \frac{\partial B_\theta}{\partial \theta} = 0 \qquad (6.2.5)$$

$$\frac{\partial E_r}{\partial \theta} - \frac{\partial E_\theta}{\partial r} = 0 \qquad (6.2.6)$$

The continuity equation is identically satisfied. As we have taken B_ϕ to be zero the r and θ components of current also turns out to be zero

$$J^{r} = 0 \quad ; \quad \bar{J}^{\theta} = 0 \qquad (6.2.7)$$

Ohm's law gives the force free condition

$$F^{i}_{k} u^{k} = 0 \qquad (6.2.8)$$

from which we get two relations between the magnetic and electric field components as given by

$$E_r = \frac{V^{\phi}}{c} B_\theta \quad \text{and} \quad E_\theta = -\frac{V^{\phi}}{c} B_r . \qquad (6.2.9)$$

Now if we assume the azimuthal velocity to be given by the expression

$$V^{\phi} = \frac{L}{r^2 \sin^2\theta}\left(1 - \frac{2mb}{r}\right) \qquad (6.2.10)$$

with

$$b = 1 + \frac{ac}{L} \qquad (6.2.11)$$

which is a generalisation of the earlier considered relativistic Keplerian including the effect of slow rotation of the central object.

Using equations (6.2.9) and (6.2.5) in equation (6.2.7) we can solve for the magnetic field components as given by

$$B_\theta = A' r^{k-1}\left(1 - \frac{3mb}{r}\right)\left(1 - \frac{2mb}{r}\right)^{\frac{-k-1}{2}} \sin^{k}\theta \qquad (6.2.12)$$

$$B_r = -A r^{k}\left(1 - \frac{2mb}{r}\right)^{-k/2} \sin^{k-1}\theta \cos\theta \qquad (6.2.13)$$

where A and K are arbitrary constants.

In terms of the components in the LNRF the electromagnetic field components can be written as

$$B(r) = -A\, r^{k-2}\left(1-\frac{2mb}{r}\right)^{-k/2} \sin^{k-2}\theta\cos\theta \tag{6.2.14}$$

$$B(\theta) = A\, r^{k-2}\left(1-\frac{2m}{r}\right)^{\frac{1}{2}}\left(1-\frac{3mb}{r}\right)\left(1-\frac{2mb}{r}\right)^{\frac{-k}{2}-1}\sin^{k-1}\theta \tag{6.2.15}$$

$$E(r) = \frac{V^{(\phi)}}{c}\, B(\theta) \tag{6.2.16}$$

$$E(\theta) = -\frac{V^{(\phi)}}{c}\, B(r) \tag{6.2.17}$$

with $V^{(\phi)}$ given by

$$V^{(\phi)} = \frac{L}{r\sin\theta}\left(1-\frac{2m}{r}\right)^{\frac{1}{2}}\left[1-\frac{2m}{r}\frac{\omega}{L}\left(1-\frac{2m}{r}\right)^{-1}\left(1+\sin^2\theta\right)\right] \tag{6.2.18}$$

The current components J^{ϕ} and J^{t} are given by

$$J^{(\phi)} = \frac{1}{r}\frac{\partial}{\partial\theta}\left(B(r)\right) - \frac{1}{r}\frac{\partial}{\partial r}\left[r\left(1-\frac{2m}{r}\right)^{\frac{1}{2}}B(\theta)\right] + \frac{6am}{r^3}\sin\theta\, E(r) \tag{6.2.19}$$

$$J^{(t)} = -\frac{1}{r^2}\left(1-\frac{2m}{r}\right)^{\frac{1}{2}}\left[\frac{\partial}{\partial r}\left(r^2 E(r)\right) + \frac{r}{\sin\theta}\left(1-\frac{2m}{r}\right)^{-\frac{1}{2}}\frac{\partial}{\partial\theta}\left(\sin\theta\, E_\theta\right)\right] \tag{6.2.20}$$

which on simplification reduces to

$$\bar{J}^{(\phi)} = A r^{k-3}\left(1-\frac{2mb}{r}\right)^{-k/2}\sin^{k-1}\theta\left[1-(k-2)\frac{\cos^2\theta}{\sin^2\theta}\right]$$

$$-\left(1-\frac{2m}{r}\right)^{\frac{1}{2}}\frac{B(\theta)}{r}\left\{(k-2)+\frac{m}{r}\left(1-\frac{2m}{r}\right)^{-1}+\frac{3mb}{r}\left(1-\frac{3mb}{r}\right)^{-1}\right.$$

$$\left.-(k+2)\frac{mb}{r}\left(1-\frac{2mb}{r}\right)^{-1}\right\}$$

$$-\frac{B(\theta)}{r}\left(1-\frac{2m}{r}\right)^{\frac{1}{2}}\left\{1-\frac{m}{r}-\frac{6am}{r^2}\left(1-\frac{2m}{r}\right)^{\frac{1}{2}}\sin\theta\,\frac{v^{(\phi)}}{c}\right\}$$

(6.2.21)

and

$$\bar{J}^{(t)} = -\frac{B(\theta)}{r}\frac{L}{cr\sin\theta}\left[1-\frac{m}{r}-\frac{6m^2}{r^2}\frac{ar}{L}\left(1-\frac{2m}{r}\right)^{-1}\left(1+\sin^2\theta\right)\right]$$

$$-\frac{B(\theta)}{r}\frac{4LM}{cr}\frac{ar}{L}\left(1-\frac{2m}{r}\right)^{-1}\cos\theta$$

$$-\frac{v^{(\phi)}}{c}\left(1-\frac{2m}{r}\right)^{\frac{1}{2}}\frac{B(\theta)}{r}\left\{(k-2)+\frac{m}{r}\left(1-\frac{2m}{r}\right)^{-1}\right.$$

$$\left.+\frac{3mb}{r}\left(1-\frac{3mb}{r}\right)^{-1}-(k+2)\frac{mb}{r}\left(1-\frac{2mb}{r}\right)^{-1}\right\}$$

$$+\frac{v^{(\phi)}}{c}\frac{1}{r}A r^{k-2}\left(1-\frac{2mb}{r}\right)^{-k/2}\sin^{k-1}\theta\left[1-(k-2)\frac{\cos^2\theta}{\sin^2\theta}\right]$$

(6.2.22)

We are left with the two momentum equations (6.2.1) and (6.2.2) which in terms of the LNRF components can be written as

$$(\rho c^2+p)\left(1-\frac{2m}{r}\right)^{-1}\left(1-\frac{v^{(\phi)2}}{c^2}\right)^{-1}\left[\frac{m}{r^2}-\frac{6am}{r^3}\left(1-\frac{2m}{r}\right)^{\frac{1}{2}}\frac{v^{(\phi)}}{c}\right.$$

$$\left.-\frac{1}{r}\left(1-\frac{2m}{r}\right)\left(\frac{v^{(\phi)}}{c}\right)^2\right]+\frac{\partial p}{\partial r}=$$

$$= \left(1-\frac{2m}{r}\right)^{-\frac{1}{2}} B(\theta)\left[\bar{J}^{(\phi)} - \frac{v^{(\phi)}}{c}\bar{J}^{(t)}\right]$$

(6.2.23)

$$-(\rho c^2+p)\cot\theta\left(1-\frac{v^{(\phi)2}}{c^2}\right)^{-1}\left(\frac{v^{(\phi)}}{c}\right)^2 + \frac{\partial p}{\partial\theta} = -\lambda B(\theta)\left[\bar{J}^{(\phi)} - \frac{v^{(\phi)}}{c}\bar{J}^{(t)}\right]$$

(6.2.24)

where we have used the relation

$$u^{t2} = \left(1-\frac{2m}{r}\right)^{-1}\left(1-\frac{v^2}{c^2}\right)^{-1}$$

(6.2.25)

with

$$v^2 = v^{(r)2} + v^{(\theta)2} + v^{(\phi)2}$$

which is a consequence of the orthonormality relation.

As a special case we will now consider a disk confined to the equatorial plane ($\theta = \pi/2$) of the compact object, wherein equation (6.2.24) is identically satisfied and we are left with only one ordinary differential equation describing the radial dependence of pressure given by

$$\frac{dp}{dr} = -(\rho c^2+p)\left(1-\frac{2m}{r}\right)^{-1}\left[1-\frac{v^{(\phi)2}}{c^2}\right]^{-1} \times$$

$$\left\{\frac{m}{r^2} - \frac{6am}{r^3}\left(1-\frac{2m}{r}\right)^{\frac{1}{2}}\frac{v^{(\phi)}}{c} - \frac{1}{r}\left(1-\frac{2m}{r}\right)\left(\frac{v^{(\phi)}}{c}\right)^2\right\}$$

$$+\left(1-\frac{2m}{r}\right)^{-\frac{1}{2}} B(\theta)\left[\bar{J}^{(\phi)} - \frac{v^{(\phi)}}{c}\bar{J}^{(t)}\right]$$

(6.2.26)

but having two unknown ρ and P. Hence for a complete solution one needs an equation of state, relation between ρ and P. (i) If the fluid is incompressible with the constant

density $\rho = \rho_0$, equation (6.2.6) can be written as a differential equation for the variable ($\rho_0 c^2 + P$) and can be integratged numerically once appropriate boundary conditions are given.For this case,we get

$$\frac{d}{dr}(\rho_0 c^2 + P) = -(\rho_0 c^2 + P)\left(1 - \frac{2m}{r}\right)^{-1} \times$$

$$\left[\frac{m}{r^2} - \frac{G a m}{r^3}\left(1 - \frac{2m}{r}\right)^{\frac{1}{2}} \frac{v^{(\phi)}}{c} - \frac{1}{r}\left(1 - \frac{2m}{r}\right)\left(\frac{v^{(\phi)}}{c}\right)^2\right]$$

$$+ \left(1 - \frac{2m}{r}\right)^{-1/2} B(\Theta)\left[\bar{J}^{(\phi)} - \frac{v^{(\phi)}}{c}\bar{J}^{(t)}\right] \qquad (6.2.27)$$

with $\bar{J}^{(\phi)} - \frac{v^{(\phi)}}{c}\bar{J}^{(t)}$ given by

$$\bar{J}^{(\phi)} - \frac{v^{(\phi)}}{c}\bar{J}^{(t)} = A r^{k-3}\left(1 - \frac{2mb}{r}\right)^{-k/2}\left(1 - \frac{v^{(\phi)^2}}{c^2}\right)^{-1}$$

$$- \left(1 - \frac{2m}{r}\right)^{\frac{1}{2}} \frac{B(\Theta)}{r}\left\{(k-2) + \frac{m}{r}\left(1 - \frac{2m}{r}\right)^{-1} + \frac{3mb}{r}\left(1 - \frac{3mb}{r}\right)^{-1}\right.$$

$$\left. - (k+2)\frac{mb}{r}\left(1 - \frac{2mb}{r}\right)^{-1}\right\}\left(1 - \frac{v^{(\phi)^2}}{c^2}\right)$$

$$- \frac{B(\Theta)}{r}\left(1 - \frac{2m}{r}\right)^{\frac{1}{2}}\left[1 - \frac{m}{r} - \frac{G a m}{r^2}\left(1 - \frac{2m}{r}\right)^{\frac{1}{2}} \frac{v^{(\phi)}}{c}\right]$$

$$+ \frac{B(\Theta)}{r}\frac{L}{cr}\frac{v^{(\phi)}}{c}\left[1 - \frac{m}{r} - 12\frac{m^2}{r^2}\frac{a e}{L}\left(1 - \frac{2m}{r}\right)^{-1}\right] \qquad (6.2.28)$$

The corresponding pressure profiles are as given in Figures (6.1) to (6.8).

(ii) We now consider the case where the total pressure P is given by the equation of state

$$P = C_1 \rho^{\gamma} - B^2/8\pi \tag{6.2.29}$$

where C_1 is a constant and γ is the adiabatic index heat. The constant C_1 is determined from the expression for sound velocity given by

$$V_s^2 = \gamma C_1 \rho^{\gamma-1} \tag{6.2.30}$$

for given values of V_s, and ρ_o, the density at the outer boundary of the disk. In this case we get the equation

$$\frac{dP}{dr} = \left\{ -\left[\rho c^2 + C_1 \rho^{\gamma} - \frac{B(\theta)^2}{8\pi}\right]\left(1-\frac{2m}{r}\right)^{-1}\left(1-\frac{v(\phi)^2}{c^2}\right)^{-1} \times \left[\frac{w}{r^2} - \frac{GMw}{r^3}\left(1-\frac{2m}{r}\right)^{\frac{1}{2}}\frac{v(\phi)}{c} - \frac{1}{r}\left(1-\frac{2m}{r}\right)\left(\frac{v(\phi)}{c}\right)^2\right] + \frac{d}{dr}\left(\frac{B(\theta)^2}{8\pi}\right) + \left(1-\frac{2m}{r}\right)^{-\frac{1}{2}} B(\theta)\left[J^{(\phi)} - \frac{v^{(\phi)}}{c} J^{(t)}\right]\right\} \times \frac{1}{C_1 \gamma \rho^{\gamma-1}} \tag{6.2.31}$$

with $J^{(\phi)} - \frac{v^{(\phi)}}{c} J^{(t)}$ given by (6.2.28)

6.3. Structure of Magnetic Field

To get the structure of magnetic field inside the disk, we match the inside solution given by equations. (6.2.14) and (6.2.15) with the vacuum solution at the boundary as described in Section 5.3. The structure of magnetic field lines is given in figures (6.15) to (6.17). Fig. (6.15) shows the field lines for $\alpha = 0$ (static central object) and for $\alpha = 0.5$ (disk corotating with respect to the central object) whereas Figure (6.16) shows the same for α

= 0 and α = -0.5 (disk counter rotating with respect to the central object) with $\alpha = a/m$. In the case of corotating disk, the field lines are pulled in as compared to that of a disk around a static object, and in the case of counter-rotating disk they are pushed out. Fig. (6.17) shows the field lines for co- and counter-rotating disks.

6.4. Results and Discussion

Case 1: Constant Density

As the rotation parameter a enters the final equation for p linearly, one can distinguish the case of corotating and counterrotating disks with respect to the central source. Figures (6.1) and (6.2) show the pressure profiles in the case of an incompressible thin disk for α = 0, + 0.2 and -0.2 for two different densities. Whereas (6.1) corresponds to the case $\rho_o = 10^{-5}$, (6.2) correspnds to the case where density is 10^{-8}. One finds that when the density is higher the pressure profiles are not sensitive to the fact whether the disk is corotating or not. On the other hand if the density is smaller the impact of the parameter becomes clearer as one moves inwards with the effect being pronounced in the innermost regions. The case of corotating disk needs to have higher pressure in the inner regions as compared to its counterrotating partner. In fact as was found in the nonrotating case here also there exists a critical combination of the surface magnetic field B_o and the density ρ_o which gives physically reasonable

pressure profiles.Figures (6.3) and (6.4) show the pressure profiles for two distinct magnetic fields but ρ_o being the same. Figure (6.5) gives the pressure profile for the same values of α and ρ_o,but for different magnetic fields,and it is clear that for the density 10^{-5},the magnetic field should not be more than $\sim 10^9$.

Figures (6.6) and (6.7) show the behaviour of pressure for the case of high magnetic field $\sim 10^{10}$ but with different α values for both corotation and counter rotation. It is interesting to note that whereas in the case of corotation ($\alpha > 0$) the pressure increases towards the inner edge,in the other case ($\alpha < 0$) the pressure decreases indicating the fact that the pressure gradient force in the inside region acts differently for corotating and counterrotating disks.

Case 2:With Equation of State

The profiles for pressure and density as depicted in Figures (6.8) and (6.9) for $B_o = 10^{-9}$, $\rho_o = 10^{-7}$ again show the distinction for the case $\alpha = 0, 0.2$ and 0.4.

As V_s is taken as a free parameter, Fig. (6.10) indicates the difference in pressure profiles as a function of V_s. One observes that as the pressure gradient varies smoothly for varying values of V_s with the pressure in the inner region would have to be large for lower values of V_s. Fig. (6.11) shows the profiles for the same α but with varying values of the adiabatic index γ .Fig. (6.12) shows the variation with respect to the angular momentum

parameter ℓ (for $\alpha > 0$). It is to be noted that for low value of ℓ ($\ell \sim 0.1$) the trend in the profile is substantially different from those for higher values.The corresponding case of counterrotaitng disk ($\ell > 0$, $\alpha < 0$) is shown in figure 6.13.

Figure (6.14) depicts the behaviour for different initial values of the density for the same surface magnetic field B_o . It is evident that to have a monotonically increasing pressure towards the inner edge of the disk,the density at the outer boundary should be higher than a critical value for a given magnetic field strength.

Figure Captions

Fig. 6.1 : Pressure profiles for $\rho_0 = 1\times10^{-5}$, $\alpha = 0, 0.2, -0.2$

Fig. 6.2 : Pressure profiles for $\rho_0 = 1\times10^{-8}$, $\alpha = 0, 0.2, -0.2$

Fig. 6.3 : Pressure profiles for $\beta_0 = 1\times10^{9}$, $\alpha = 0, 0.4, -0.4$

Fig. 6.4 : Pressure profiles for $\beta_0 = 1\times10^{10}$, $\alpha = 0, 0.4, -0.4$

Fig. 6.5 : Pressure profiles for $\alpha = -0.2$, different β_0

Fig. 6.6 : Pressure profiles for $B_0 = 1\times10^{10}$, different α ($\alpha < 0$)

Fig. 6.7 : Pressure profiles for $\beta_0 = 1\times10^{10}$, different α ($\alpha > 0$)

Fig. 6.8 : Density profile for different values of α

Fig. 6.9 : Pressure profiles for different values of α

Fig. 6.10 : Pressure profiles for different values of V_s^i

Fig. 6.11 : Pressure profiles for different values of r

Fig. 6.12 : Pressure profiles for different values of $\ell\ (\alpha>0)$

Fig. 6.13 : Pressure profiles for different values of $\ell\ (\alpha<0)$

Fig. 6.14 : Pressure profiles for different values of ρ_0

Fig. 6.15 : Structure of magnetic field line for corotating disk .

Fig. 6.16 : Structure of magnetic field line for counter-rotating disk

Fig. 6.17 : Structure of magnetic field line for co- and counter-rotating disk

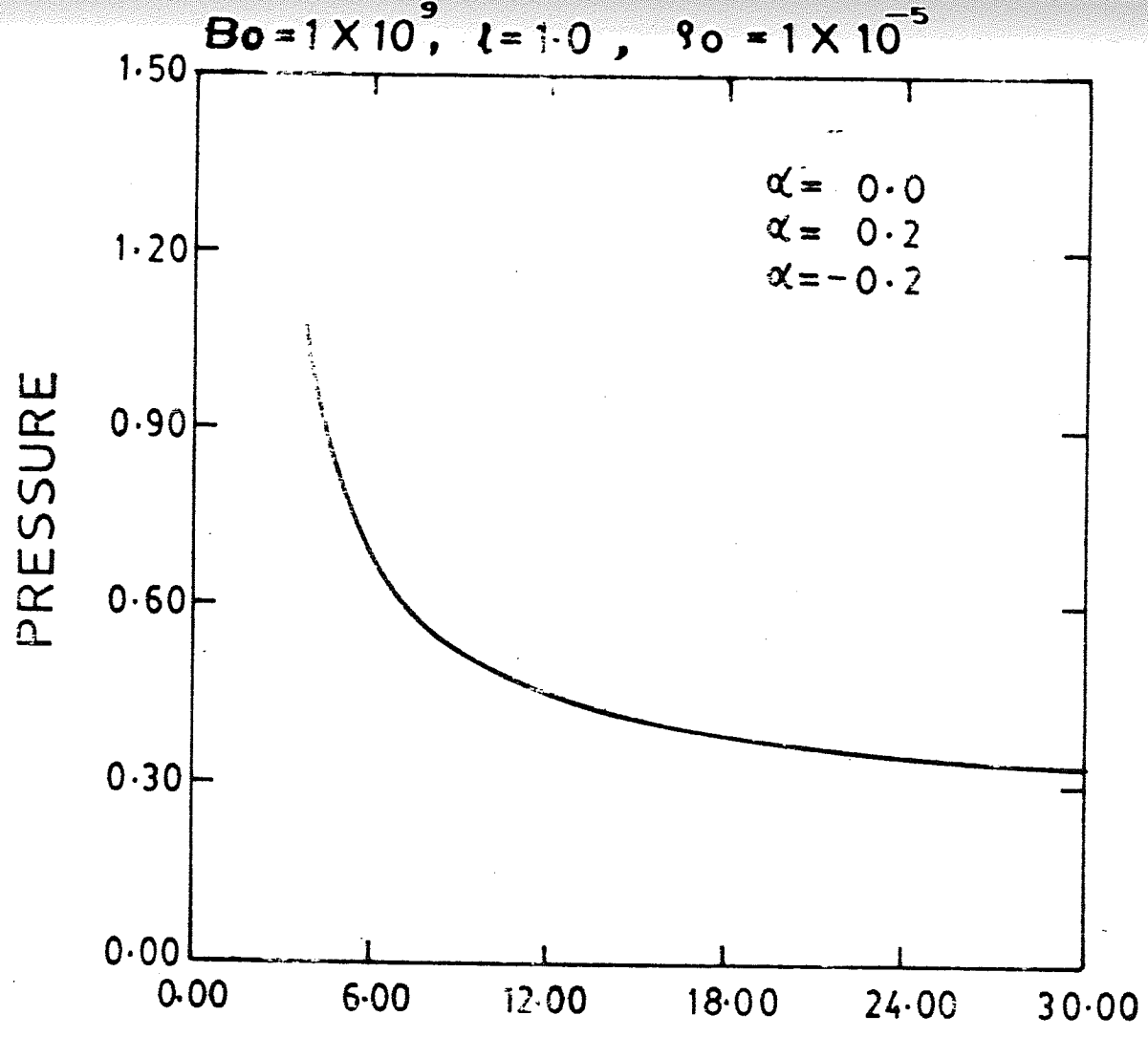
Bo = 1 X 10^9, ℓ = 1·0, ϑo = 1 X 10^-5
α = 0·0
α = 0·2
α = -0·2
PRESSURE
1·50
1·20
0·90
0·60
0·30
0·00
0·00
6·00
12·00
18·00
24·00
30·00
RADIAL DISTANCE (R)

FIG.-6·1

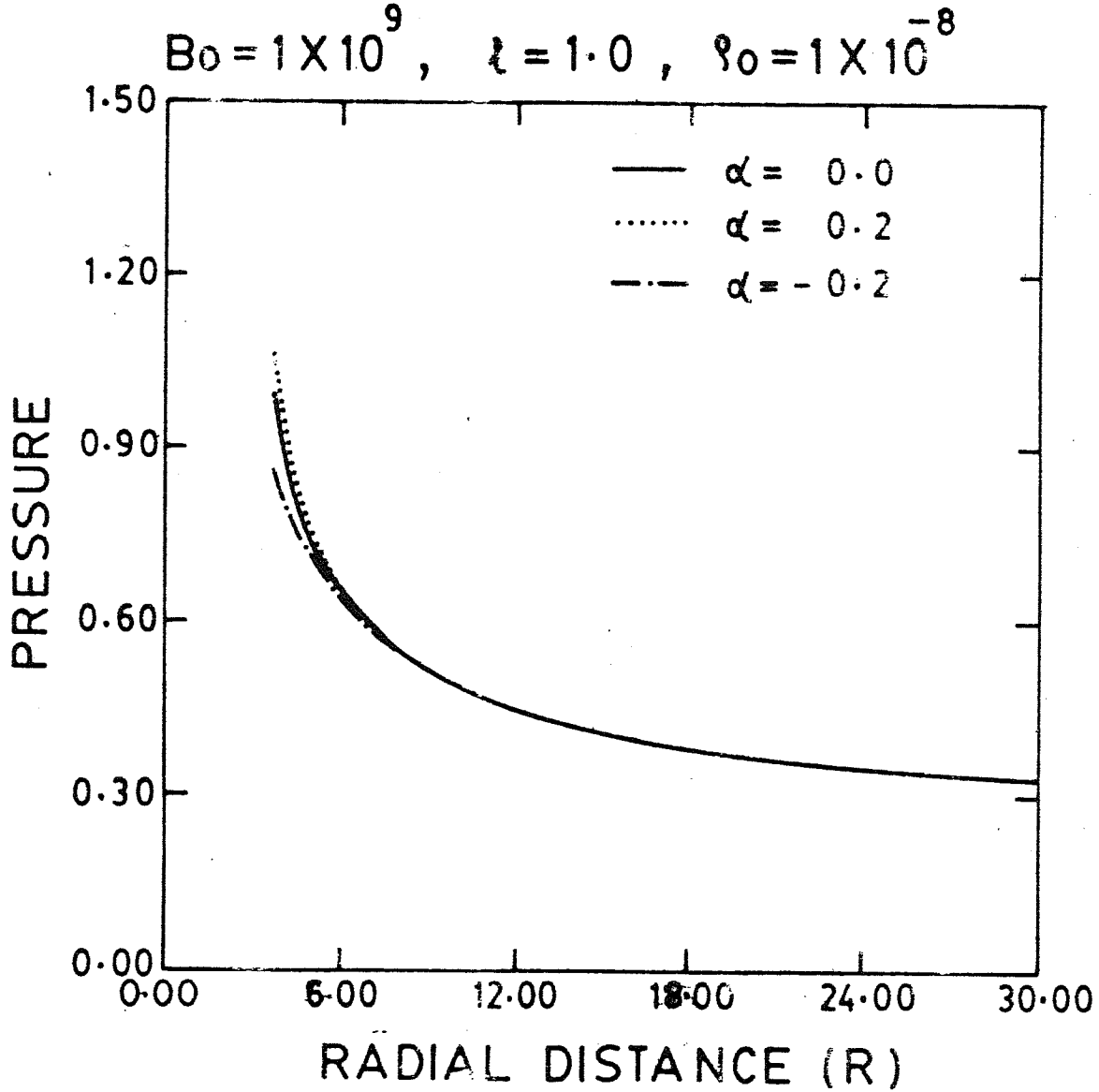
$B_o = 1 \times 10^{9}$, $\ell = 1 \cdot 0$, $\rho_o = 1 \times 10^{-8}$
1·50
1·20
0·90
0·60
0·30
0·00
PRESSURE
α = 0·0
α = 0·2
α = - 0·2
0·00
6·00
12·00
18·00
24·00
30·00
RADIAL DISTANCE (R)

FIG.-6·2

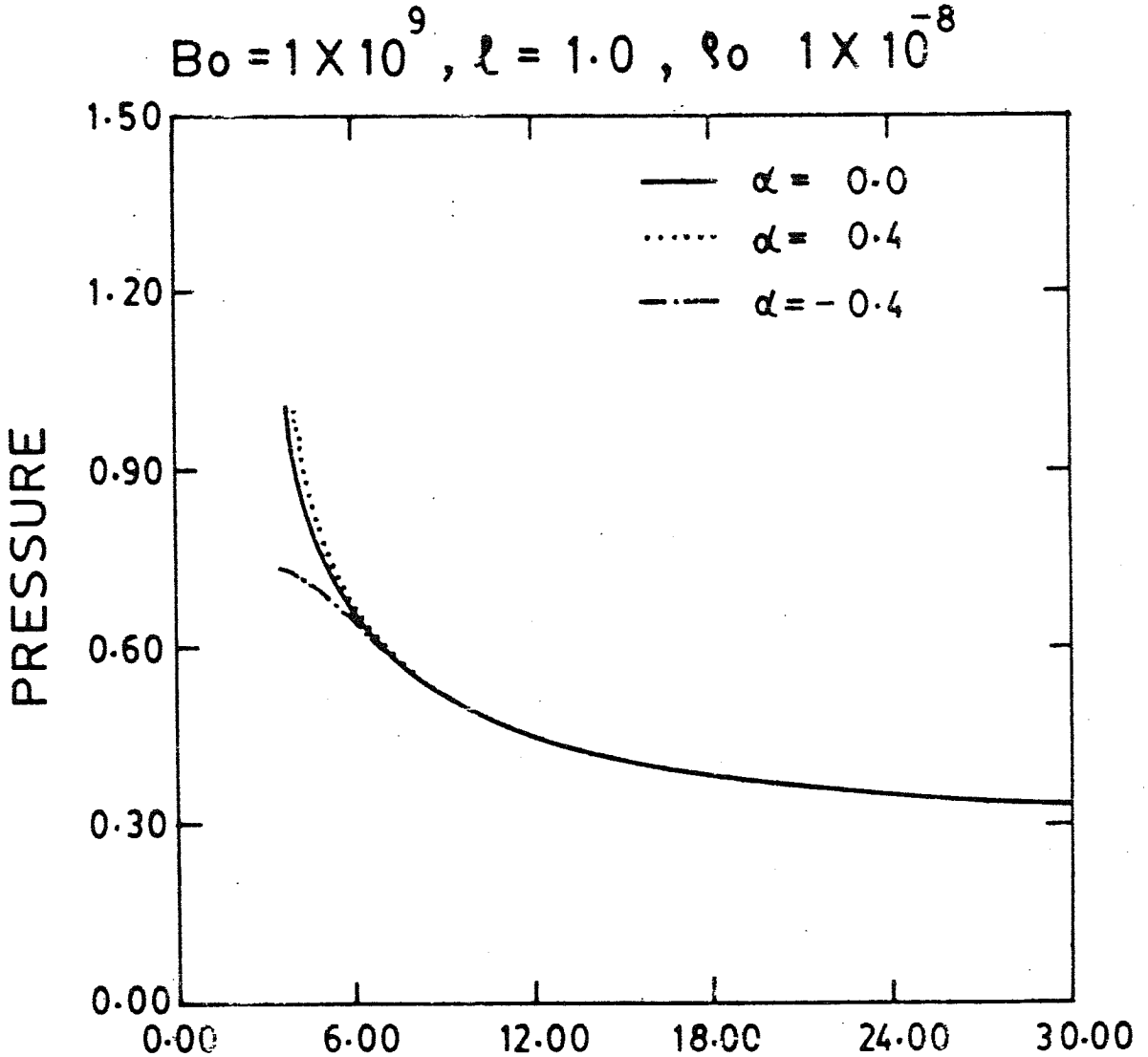
Bo = 1 X 10^9 , ℓ = 1·0 , ℘o 1 X 10^-8
1·50
1·20
0·90
0·60
0·30
0·00
PRESSURE
α = 0·0
α = 0·4
α = - 0·4
0·00
6·00
12·00
18·00
24·00
30·00
RADIAL DISTANCE (R)

FIG.-6·3

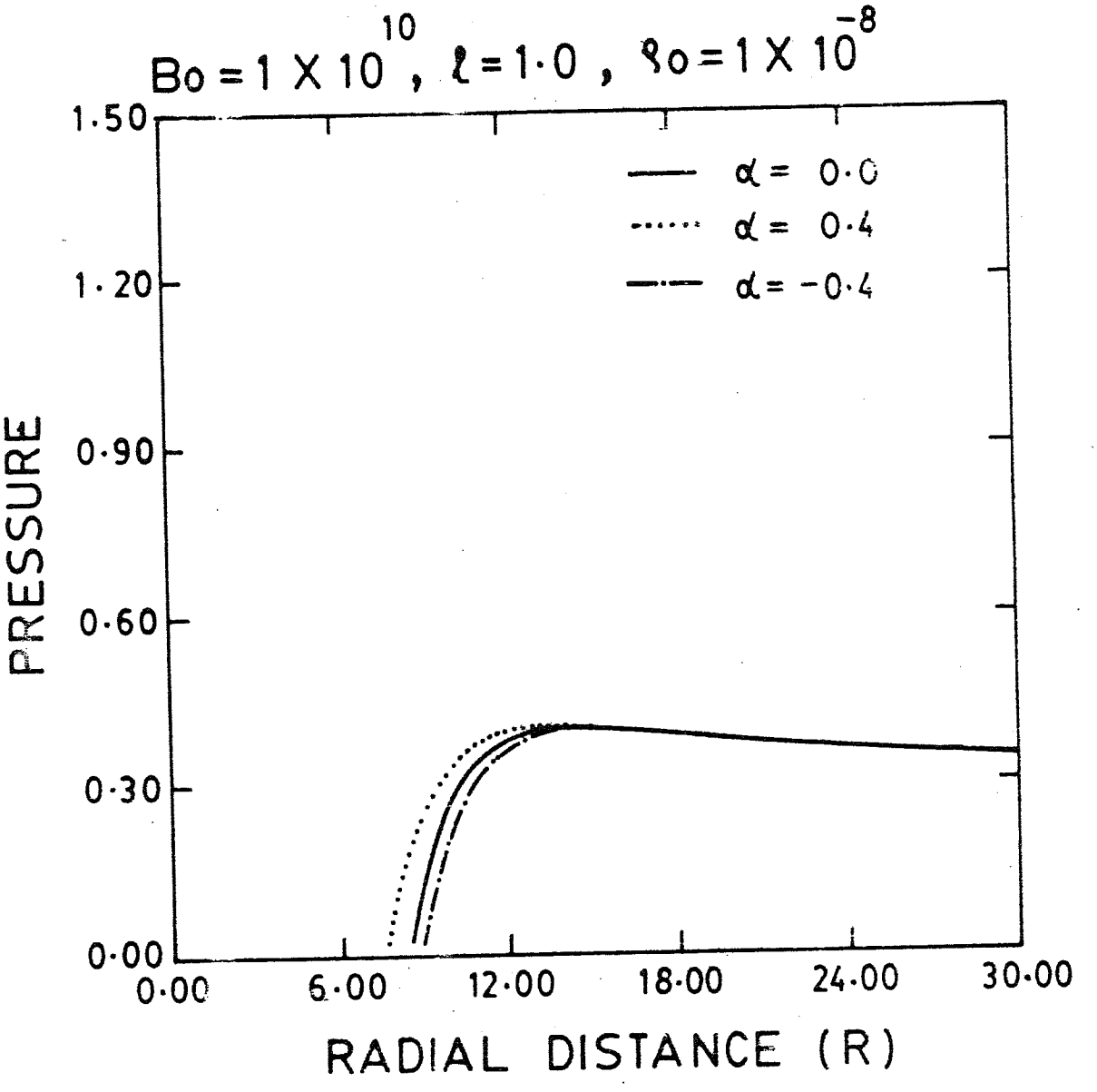
Bo = 1 X 10^10 , ℓ = 1·0 , ρo = 1 X 10^-8
α = 0·0
α = 0·4
α = -0·4
PRESSURE
1·50
1·20
0·90
0·60
0·30
0·00
0·00
6·00
12·00
18·00
24·00
30·00
RADIAL DISTANCE (R)

FIG. - 6·4

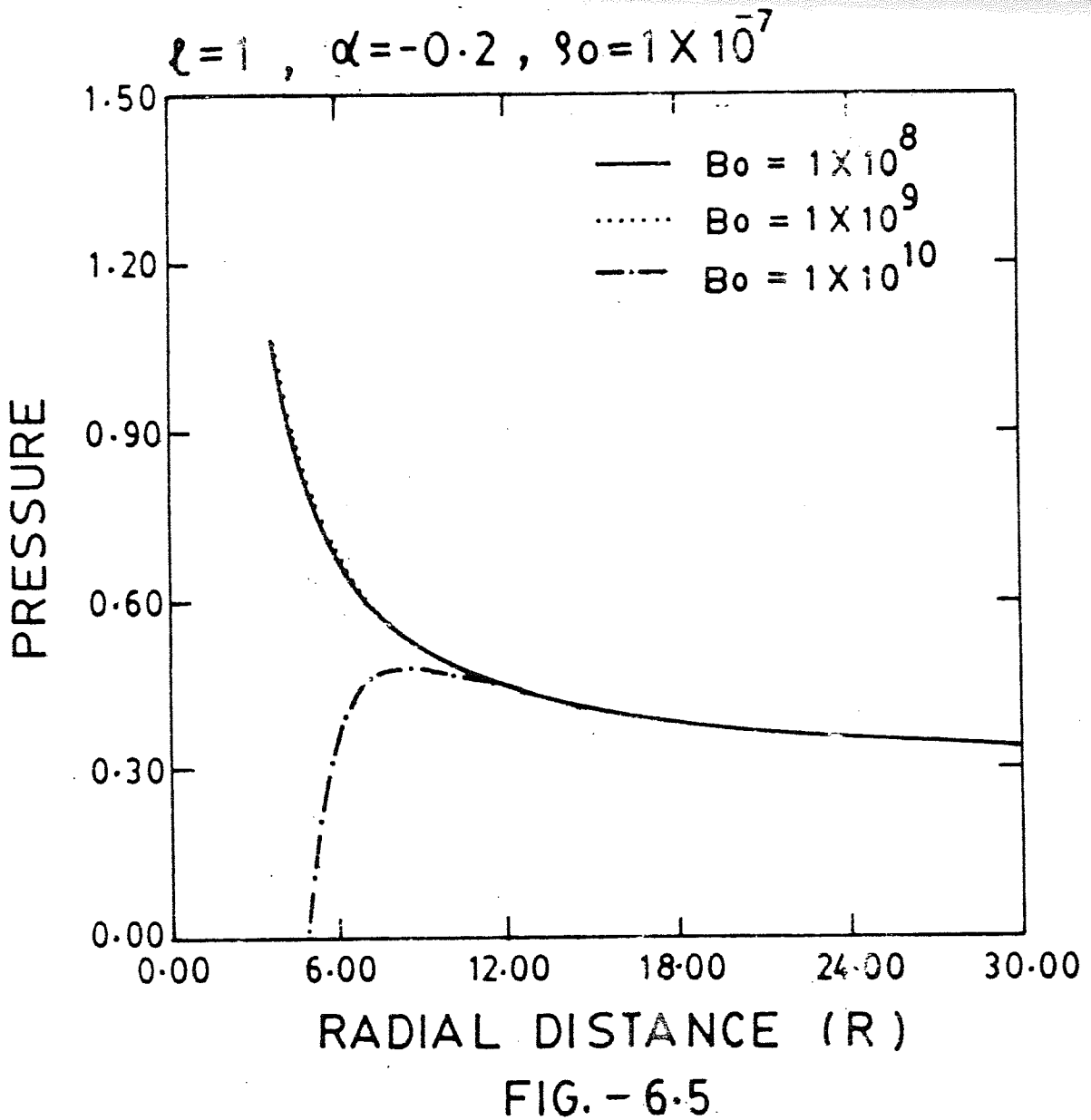
ℓ = 1 , α = -0·2 , ρo = 1 X 10⁻⁷
Bo = 1 X 10⁸
Bo = 1 X 10⁹
Bo = 1 X 10¹⁰
PRESSURE
1·50
1·20
0·90
0·60
0·30
0·00
0·00
6·00
12·00
18·00
24·00
30·00
RADIAL DISTANCE (R)

FIG. - 6·5

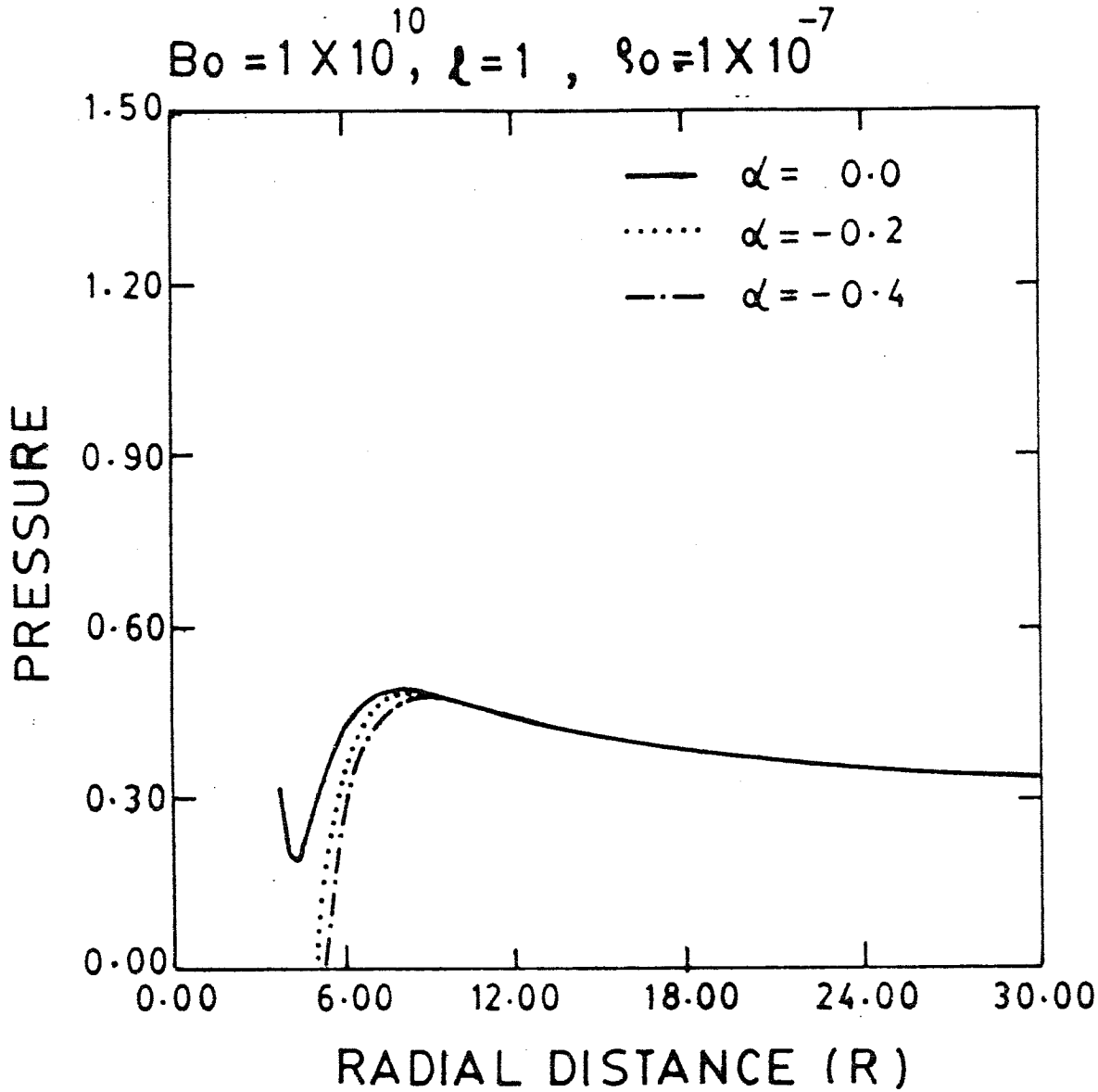
$B_o = 1 \times 10^{10}$, $\ell = 1$, $\rho_o = 1 \times 10^{-7}$
1.50
1.20
0.90
0.60
0.30
0.00
PRESSURE
α = 0·0
α = −0·2
α = −0·4
0.00
6·00
12·00
18·00
24·00
30·00
RADIAL DISTANCE (R)

FIG. – 6·6

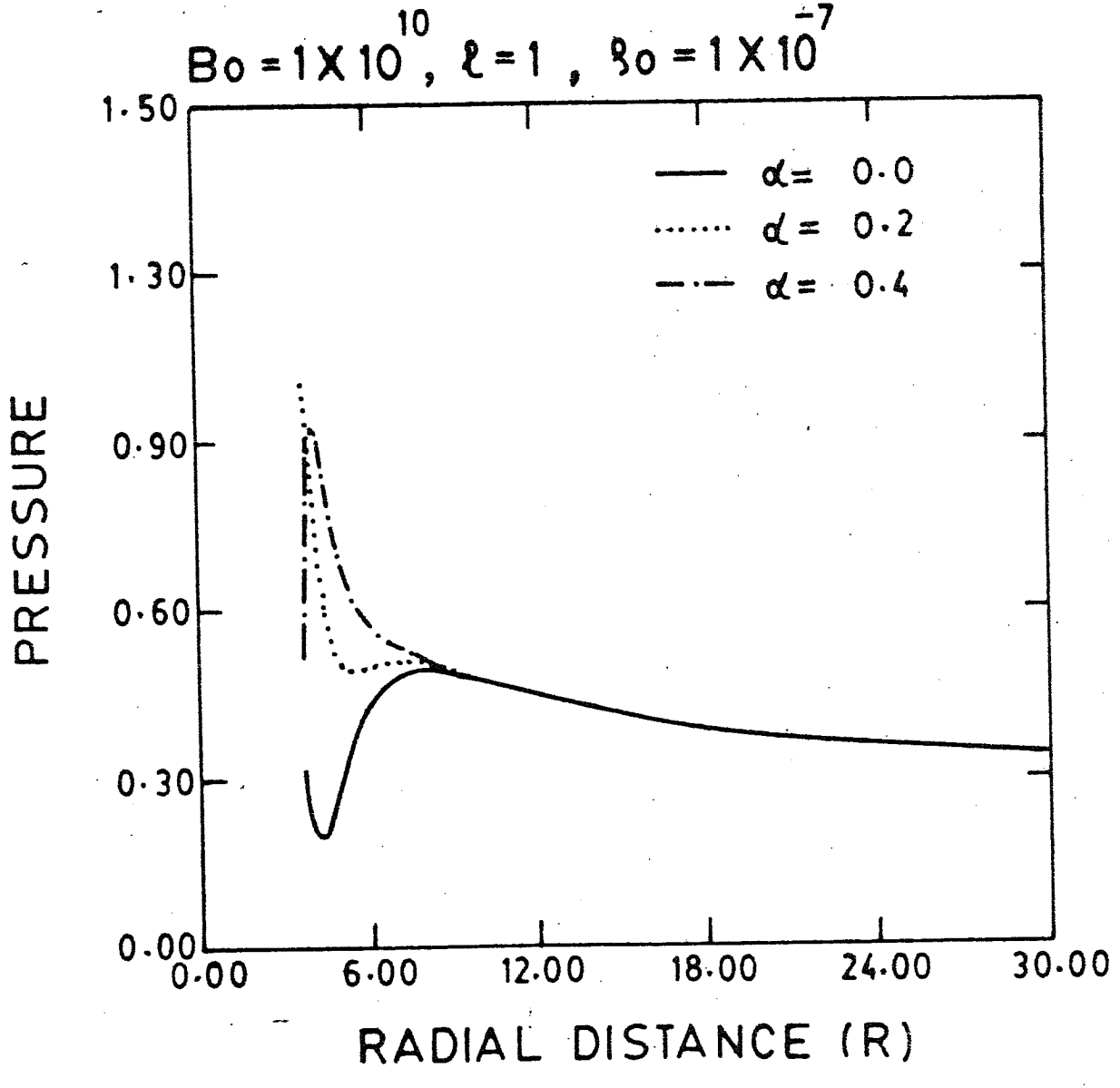
Bo = 1 X 10^10 , ℓ = 1 , ℘o = 1 X 10^-7
1·50
1·30
0·90
0·60
0·30
0·00
PRESSURE
α = 0·0
α = 0·2
α = 0·4
0·00
6·00
12·00
18·00
24·00
30·00
RADIAL DISTANCE (R)

FIG.- 6·7

$B_o = 1 \times 10^{9}$, $\ell = 1$, $\rho_o = 1 \times 10^{-7}$, $r = 4/3$ $V_s = 0.5$

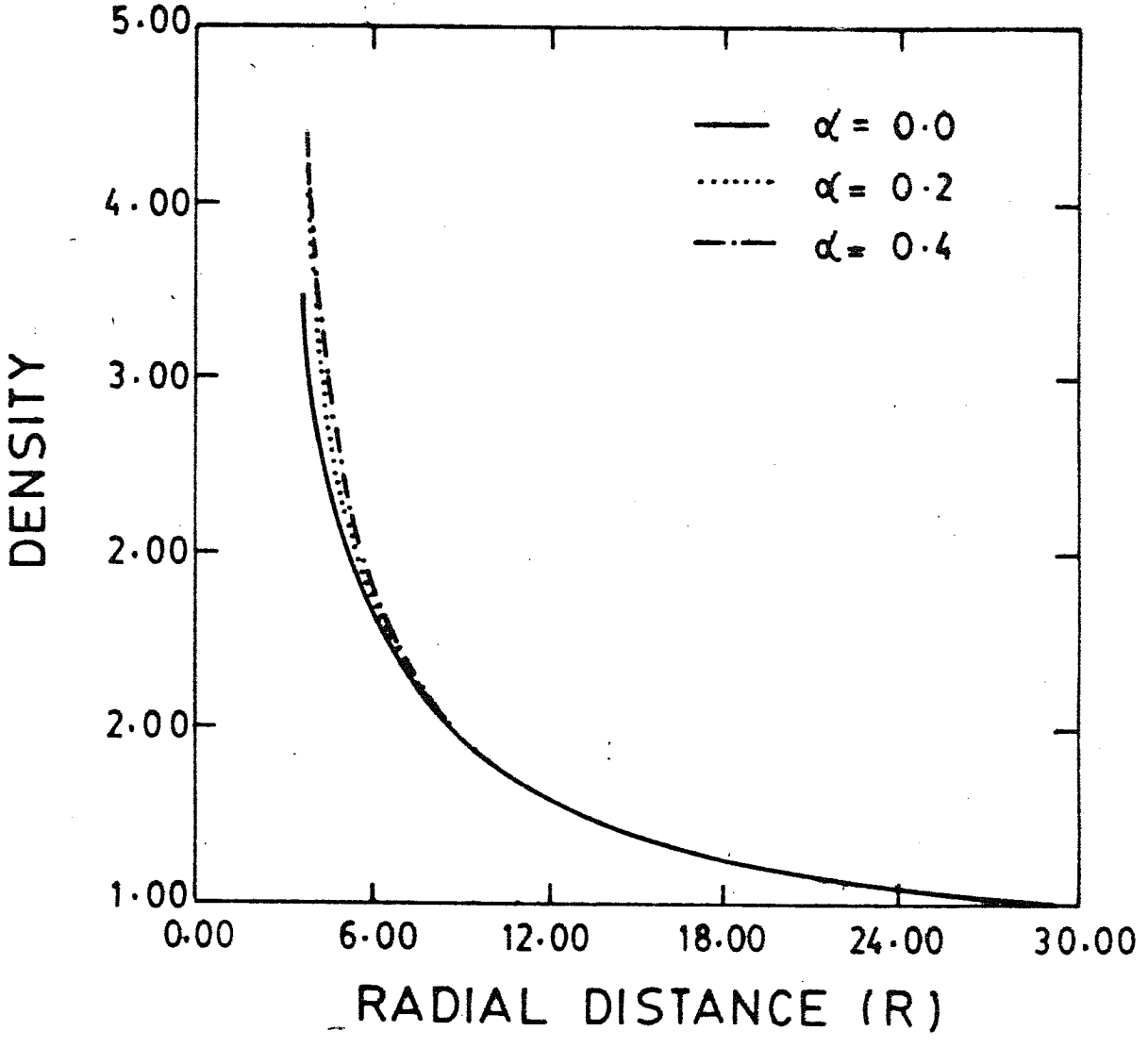

FIG. - 6.8

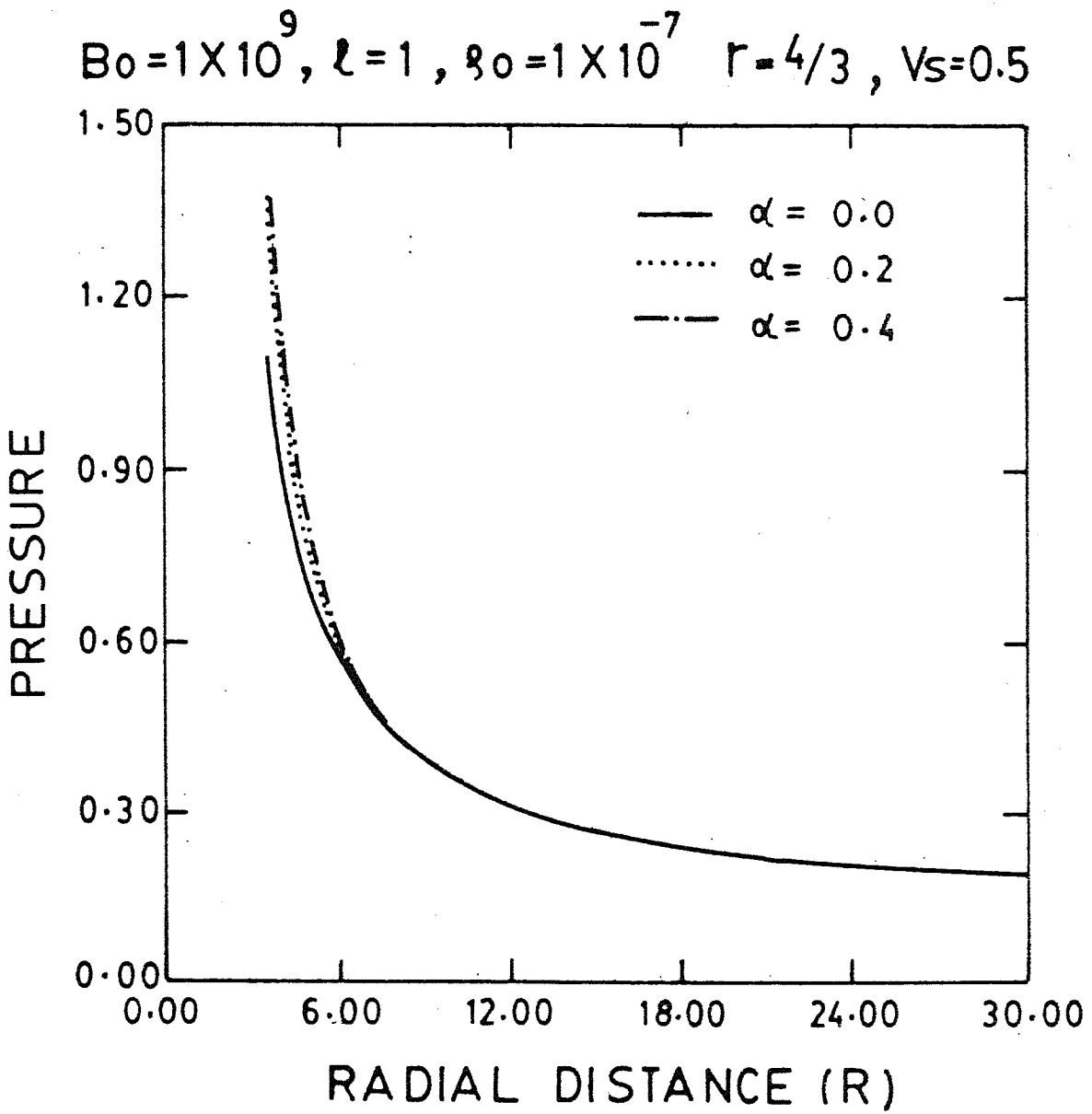
Bo=1X10^9, ℓ=1, ρo=1X10^-7 Γ=4/3, Vs=0.5
1·50
1·20
0·90
0·60
0·30
0·00
PRESSURE
α = 0·0
α = 0·2
α = 0·4
0·00
6·00
12·00
18·00
24·00
30·00
RADIAL DISTANCE (R)

FIG.-6·9

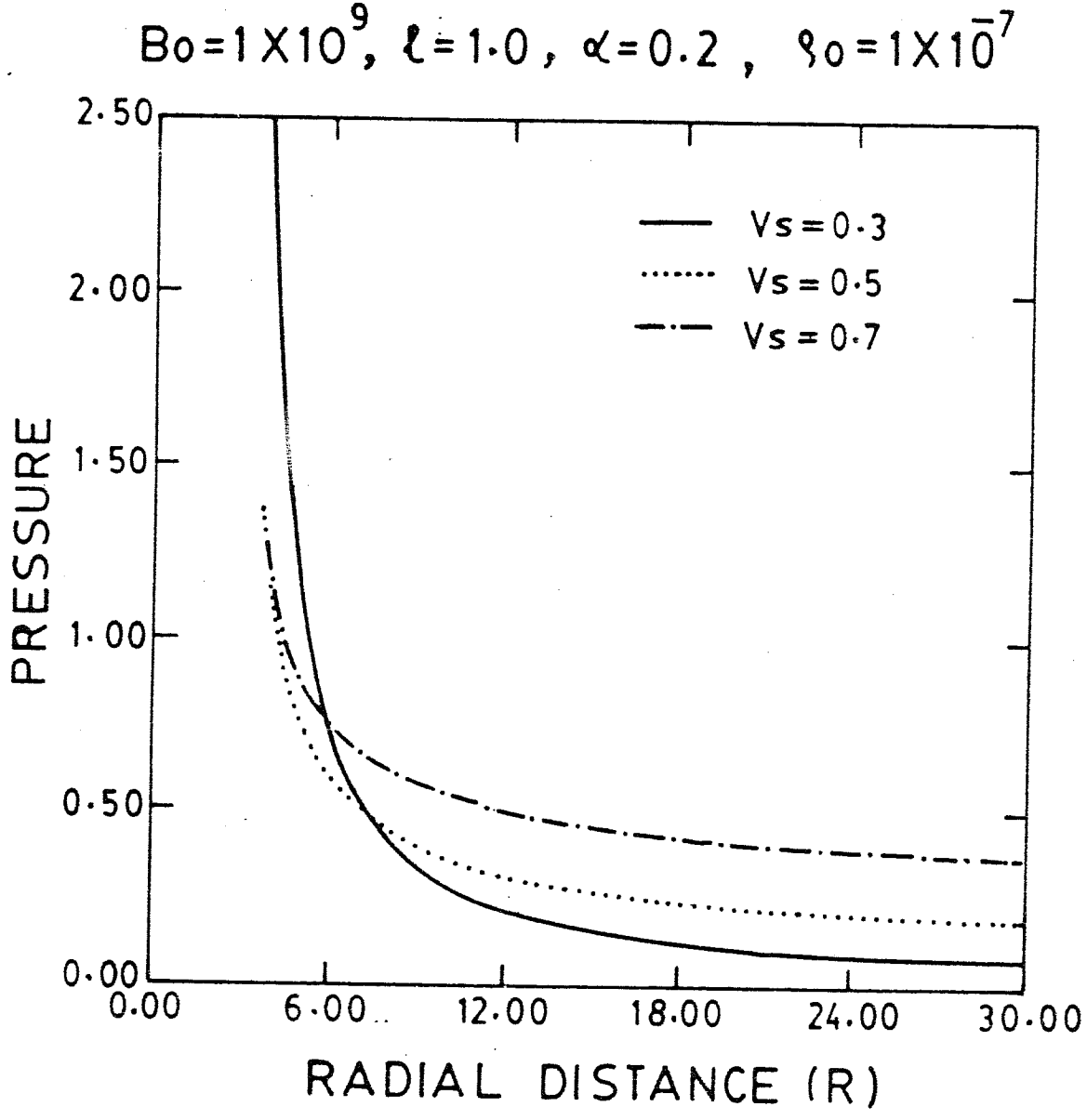
Bo=1X10^9, ℓ=1·0, α=0.2, ρo=1X10^-7
2·50
2·00
1·50
1·00
0·50
0·00
PRESSURE
Vs=0·3
Vs=0·5
Vs=0·7
0.00
6·00
12.00
18.00
24.00
30.00
RADIAL DISTANCE (R)

FIG.-6.10

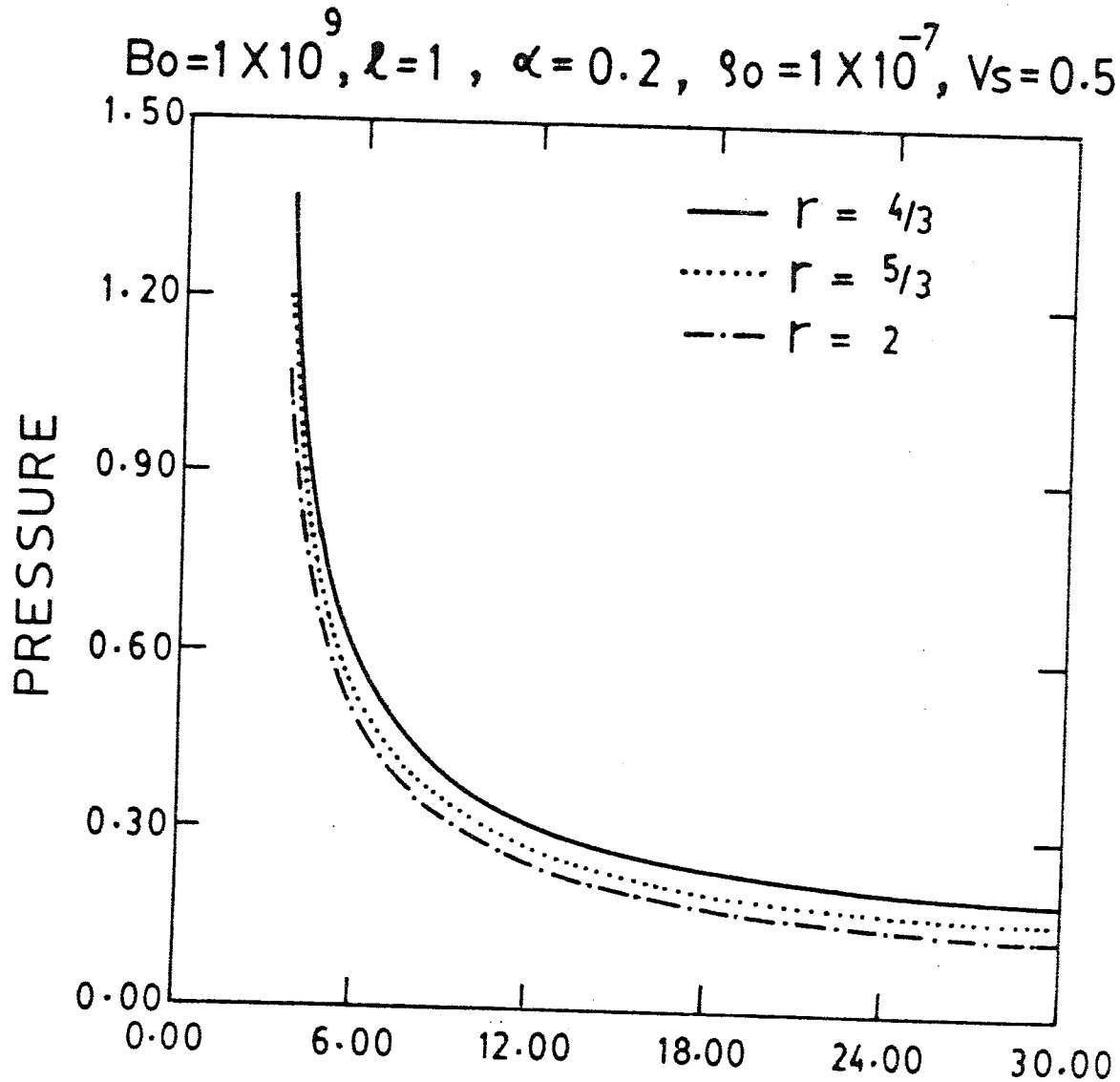
Bo=1X10^9, ℓ=1, α=0.2, ρo=1X10^-7, Vs=0.5
1.50
1.20
0.90
0.60
0.30
0.00
PRESSURE
r = 4/3
r = 5/3
r = 2
0.00
6.00
12.00
18.00
24.00
30.00
RADIAL DISTANCE (R)

FIG.-6.11

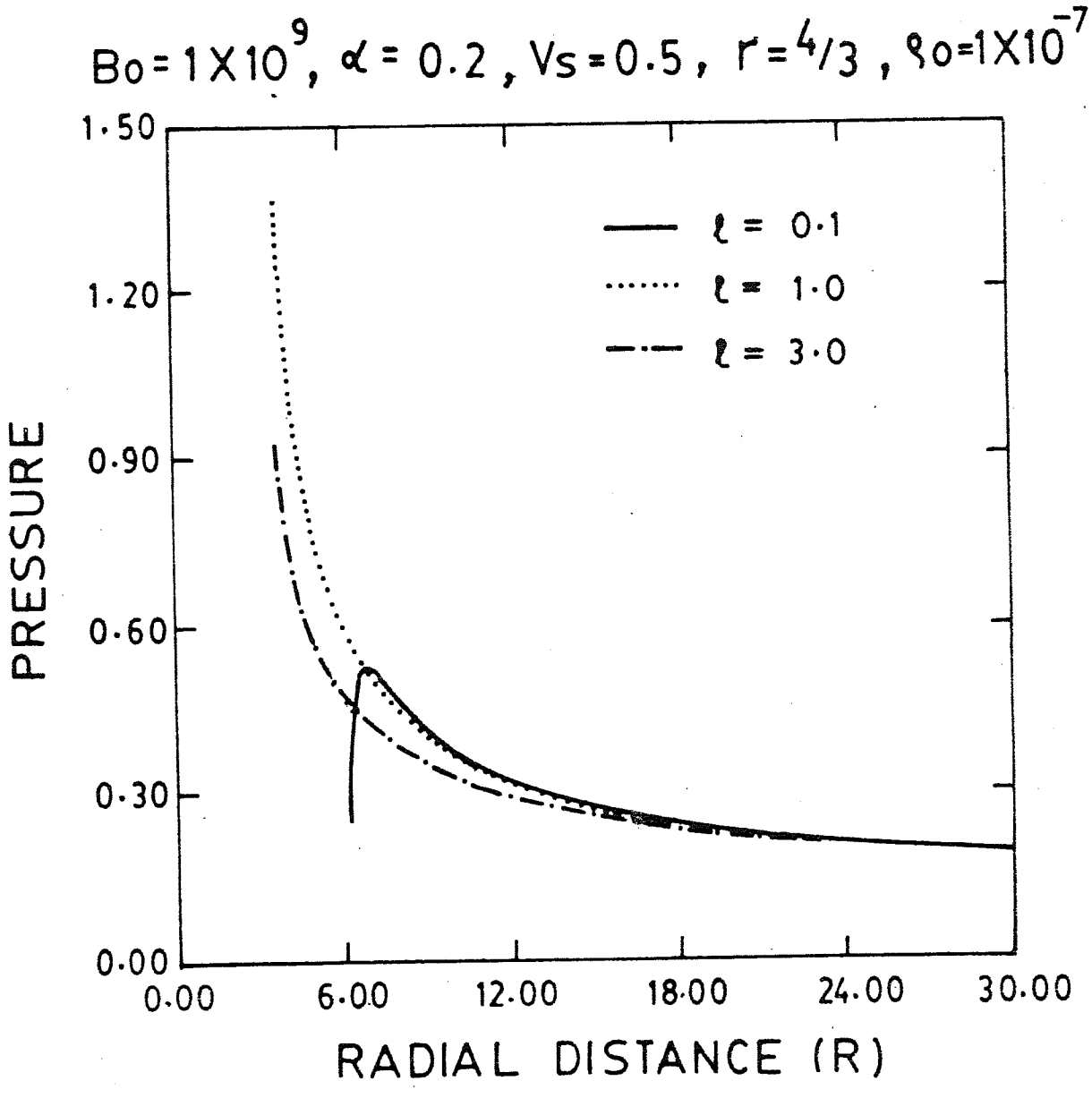
Bo = 1X10^9, α = 0.2, Vs = 0.5, r = 4/3, ρo = 1X10^-7
1·50
1·20
0·90
0·60
0·30
0·00
PRESSURE
ℓ = 0·1
ℓ = 1·0
ℓ = 3·0
0.00
6·00
12·00
18·00
24·00
30.00
RADIAL DISTANCE (R)

FIG.– 6·12

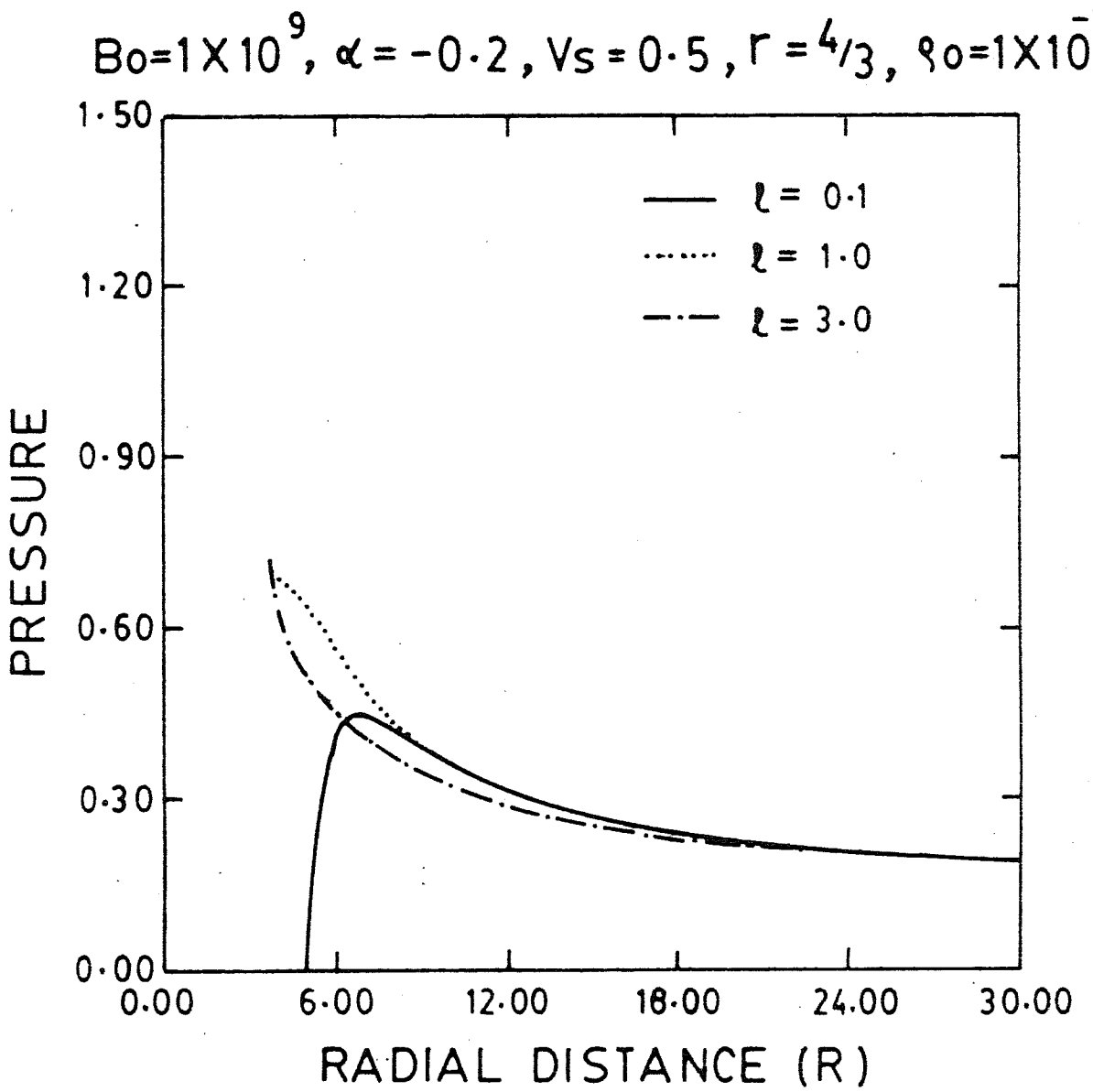
Bo=1X10^9, α=-0·2, Vs=0·5, Γ=4/3, ρo=1X10^-7
1·50
1·20
0·90
0·60
0·30
0·00
PRESSURE
ℓ= 0·1
ℓ= 1·0
ℓ= 3·0
0.00
6·00
12·00
18·00
24.00
30.00
RADIAL DISTANCE (R)

FIG.-6·13

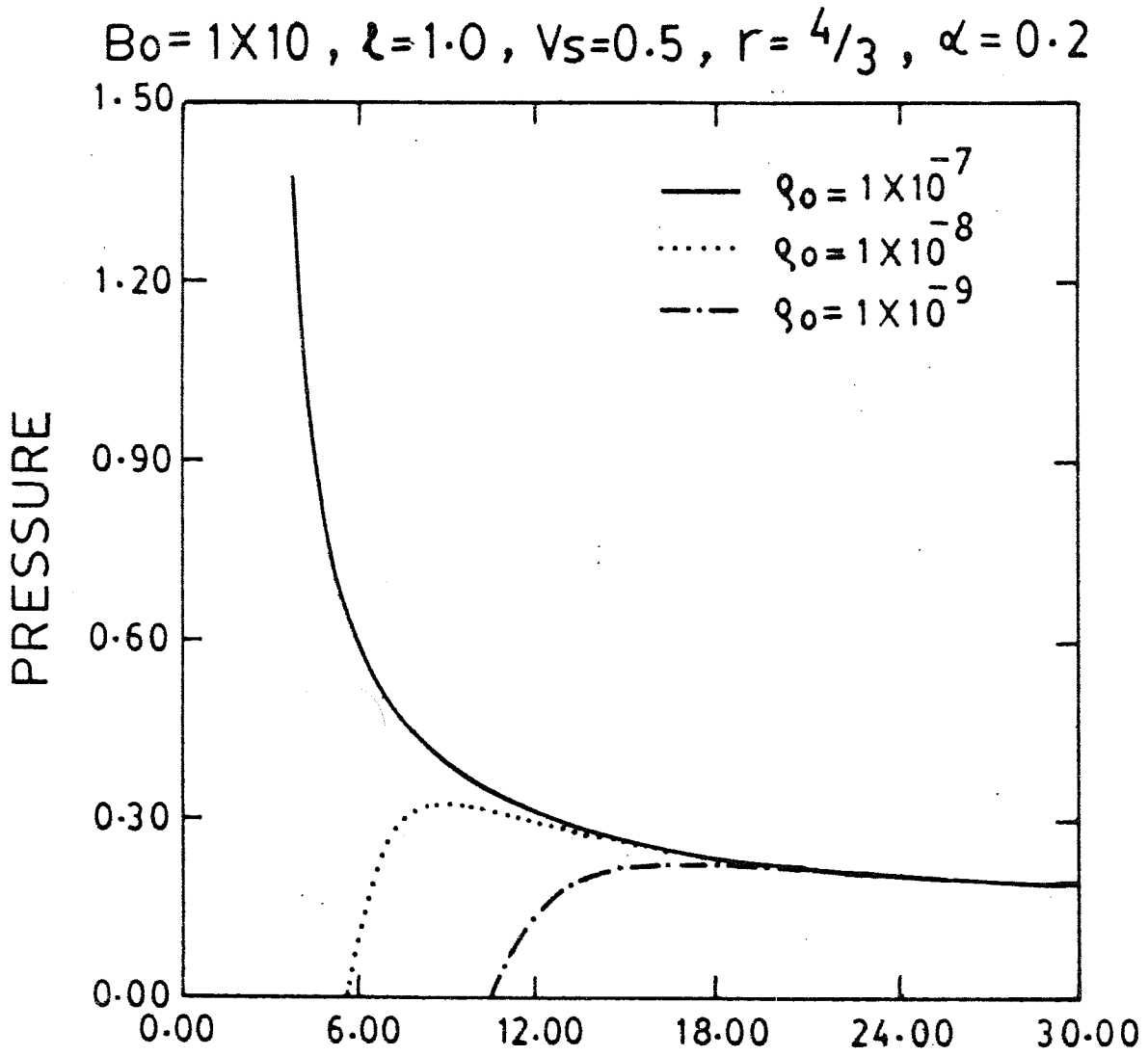
Bo = 1X10 , ℓ=1·0 , Vs=0.5 , r= 4/3 , α = 0·2
1·50
1·20
0·90
0·60
0·30
0·00
PRESSURE
ρo = 1X10⁻⁷
ρo = 1X10⁻⁸
ρo = 1X10⁻⁹
0·00
6·00
12·00
18·00
24·00
30·00
RADIAL DISTANCE (R)

FIG.- 6·14

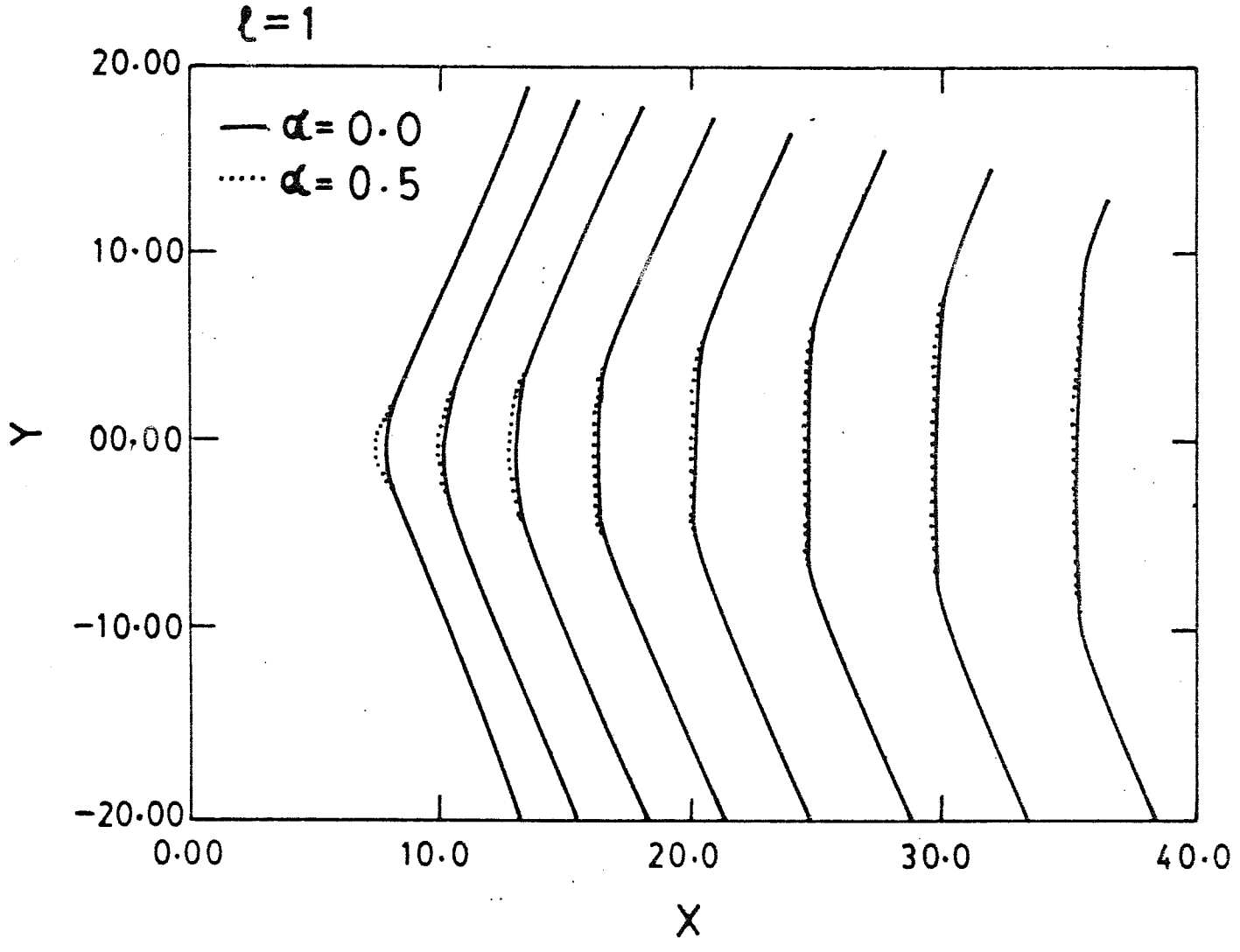

FIG.-6.15

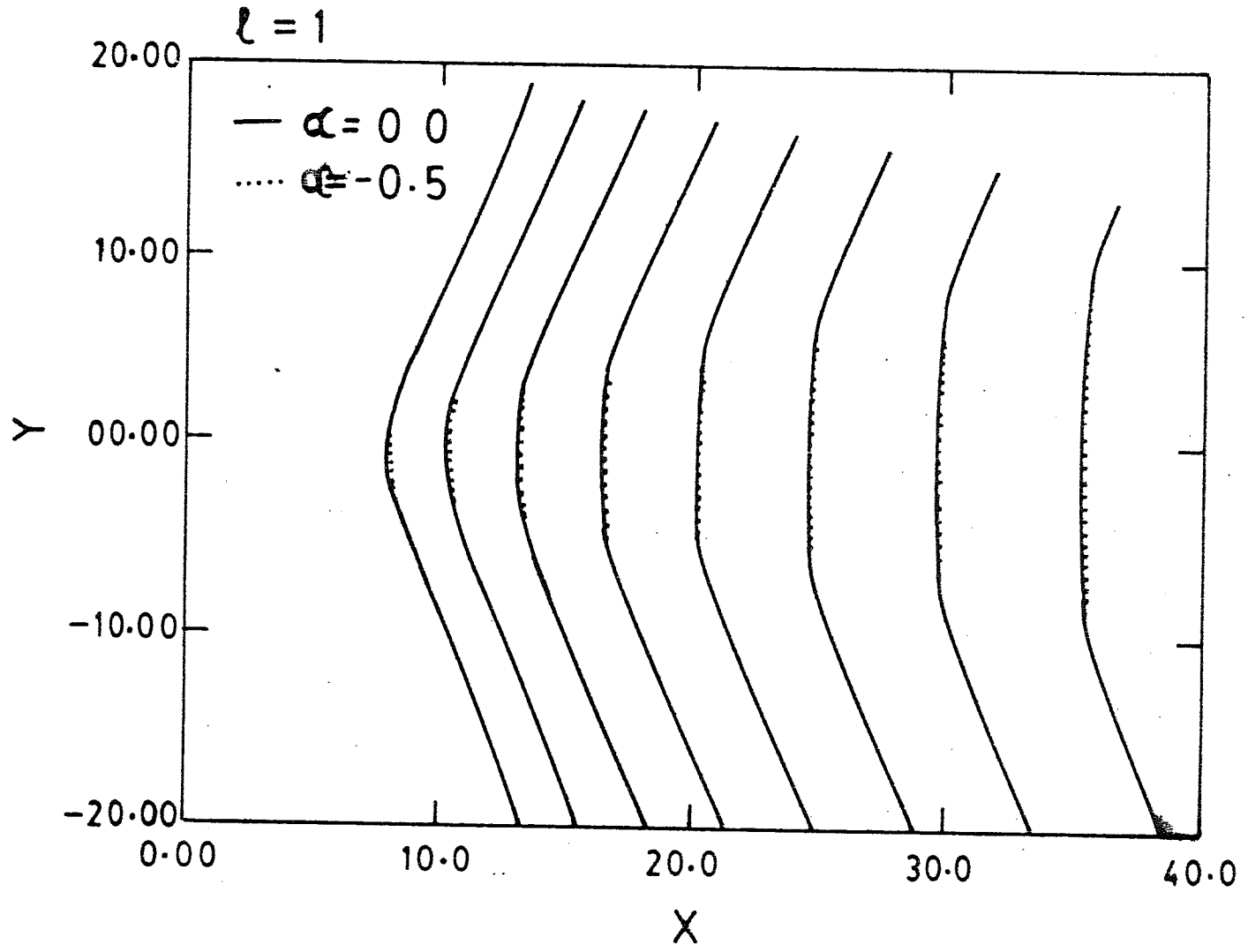

FIG.-6·16

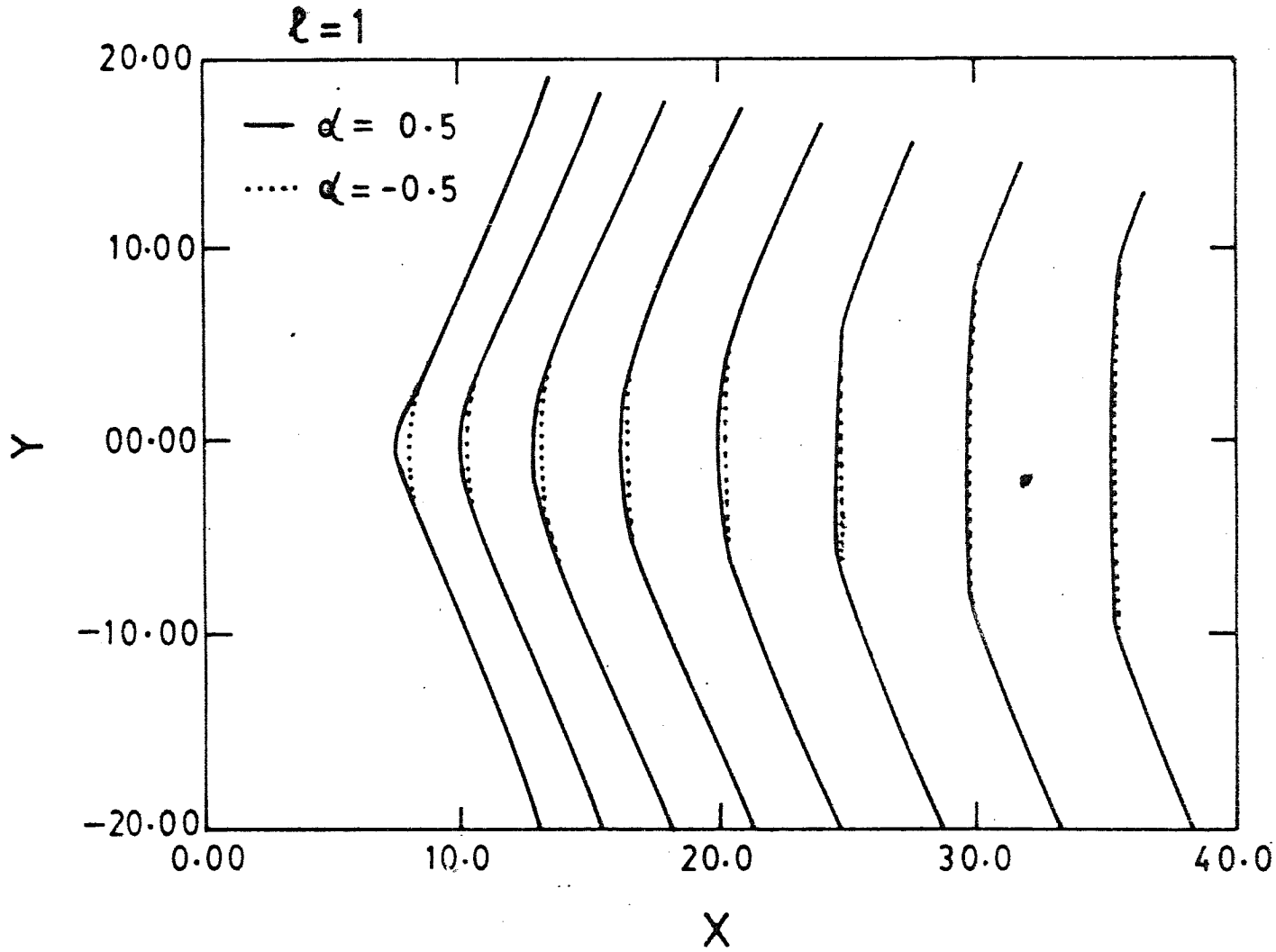

FIG.- 6·17

CHAPTER VII

CONCLUSIONS

Starting with a general formalism for the equilibrium configurations of magnetofluid disks in curved spacetime (neglecting self-gravity) we have studied the possible structures for varying physical parameters like, B_o the surface magnetic field of the compact object, ρ_o the outer density of the disk and $V^{(\phi)}$ the azimuthal velocity and found possible correlations among the class of parameters for physically plausible pressure and density distributions. We have established that the presence of magnetic field clearly helps in getting the inner regions of the disk much closer to the surface of the compact object [particularly for highly collapsed objects ($r \sim 3m$)] than it is possible

in the absence of magnetic field.Also,large magnetic fields produce enough magnetic bouyancy at the inner regions of the disk, where the disk structure may get disrupted and requires a more detailed study to understand the characteristics of flow at this transitional region. A limited discussion of the case of disks around slowly rotating objects has revealed the possible difference between corotating and counterrotating disks.

It is our opinion that these results clearly indicate the necessity to go in for more detailed studies concerning the stability analysis of such disklike configurations under radial and axisymmetric perturbation and further to look for equilibrium configuration of thick disks with possible meridional component of velocity being nonzero.

These studies though preliminary are indicative enough for detailed consideration for model building in the case of astrophysical sources like X-ray binaries and QPO phenomena.

In this study we have confined to the structure of the disk in the equatorial plane of the central object.A more general study will have to take into account the structure of an extended disk, which will require obtaining self-consistent solutions for the set of partial differential equations using appropriate numerical integration procedure. Further the effect of inclusion of the toroidal component of magnetic field B_ϕ particularly its possible role on the formation of jets needs a detailed analysis.

References

1. Abramowicz M., Jaroszynski M. and Shikora M. (1978) Ast. Astrophys. 63,221.

2. Abramowicz M., Calvani M. and Nohili L. (1980) Astrophys. J. 242,772.

3. Aly J.J. (1980) Astro. Astrophys. 86,192.

4. Bhaskaran P. and Prasanna A.R. (1989a) Astrophys. and Space Science (in press).

5. Bhaskaran P. and Prasanna A.R. (1989b) J. Ap. Astrn. (in press).

6. Bicak I. and Dvorak L. (1977) Czech. J. Phys. B27,127.

7. Bisnovatyi-Kogan G.S. and Ruzmaikin A.A. (1974), Astrophys. and Sp. Sciences 28,45.

8. Bisnovatyi-Kogan G.S. and Ruzmaikin (1976),Astrophys. and Sp. Sciences 42,401.

9. Blandford R.D. (1976),MNRAS 176,465.

10. Blandford R.D. and Znajek R.L. (1977),MNRAS 179,433.

11. Bondi H. (1952),MNRAS 112,195.

12. Bornet G. (1980) Physics Reports 60,151.

13. Carter B. (1973) "Les Houches Lectures - Blackholes", ed. B. DeWitt and C. DeWitt (New York:Gordon and Breach).

14. Chakraborty D.K. and Prasanna A.R. (1981) J. Ap. Astr. 2,421.

15. Chakraborty D.K. and Prasanna A.R. (1982) J. Ap. Astr. 3,193.

16. Chitre D.M. and Vishveshwara C.V. (1975) Phys. Rev. D12,1538.

17. Dhurandhar S.V. and Dadhich N. (1984) Phys. Rev. D29, 2712.

18. Eardly D.M. and Lightman A.P. (1975) Astrophys. J. 200, 187.

19. Fishbone L.G. and Moncrief V. (1976) Astrophys. J. 207, 962.

20. Frank J.,King A.R. and Raina D.T. (1985) "Accretion in Binary Systems" p. 56 (Cambridge University Press).

21. Ghosh P., Lamb F.K. and Pethick C.J. (1977) Astrophys. J. 217,578.

22. Ghosh P. and Lamb F.K. (1979) Astrophys. J. 232,259.

23. Ghosh P. and Lamb F.K. (1979) Astrophys. J. 234,296.

24. Ginzburg V.L. and Ozernoi I.M. (1965) Sov. Phys. JETP

20,689.

25. Hanawa T. (1989) Astrophys. J. 341,948.

26. Hayakawa S. and Matsuoka M. (1964) Prog. Theo. Phys. Sup. 30,204.

27. Hayakawa S. (1985) Physics Reports 121 317.

28. Hoyle F. and Lyttleton R.A. (1939) Proc. Cam. Phil. Soc. 35,405.

29. Ichimaru S. (1976) Astrophys. J. 208,701.

30. Jaroszynski M., Abramowicz M. and Paczynski B. (1980) Acta Astron. 30,1.

31. Kaburaki O. (1986) MNRAS 220,321.

32. Kaburaki O. (1987) MNRAS 229,165.

33. Kaburaki O. and Itoh M. (1987) Astron. Astrophys. 172, 191.

34. King A.R., Lasota J.P. and Kundt W. (1975) Phys. Rev. D12,3037.

35. Kozlovski Jaroszynski M. and Abramowicz M. (1978) Astron. Astrophys. 63,209.

36. Kundt W. and Robnik M. (1980) Astron. Astrophys. 91, 305.

37. Kuwahara F. (1978)Prog. Theo. Phys. 80,449.

38. Lightman A.P. (1974) Astrophys. J. 194,419.

39. Lightman A.P. (1974) Astrophys. J. 194,429.

40. Lightman A.P. and Eardly D.M. (1974) Ap. J. (Letters) 187,L1.

41. Luminet J.P. (1979) Astron. Astrophys. 75,228.

42. Lynden-Bell D. (1969) Nature 223,690.

43. Mitsuda K.,Inoue H.,Koyama K.,Makishima K. Matuoka H., Oyawura Y.,Shibazaki N.,Suzuki K. and Tanaka Y. (1984) Publ. Astron. Soc. Japan 36,741.

44. Novikov I.D. and Zeldovich Y.B. (1966),Nuovo Cim. Sup. 4,810.

45. Novikov I.D. and Thorne K.S. (1973) "Les Houches Lectures Blackholes", ed. B. DeWitt and C. DeWitt (New York Gordon and Breach).

46. Paczynski B. (1978) 'Evolution of Binary X-Ray Sources',(Preprint).

47. Paczynski B. (1987) Nature 327,303.

48. Paczynski B. and Witta P.J. (1980) Astron. Astrophys. 88,23.

49. Page D.N. and Thorne K.S. (1974) Astrophys. J. 191,499.

50. Petterson J.A. (1974) Phys. Rev. D10,3166.

51. Petterson J.A. (1975) Phys. Rev. D12,2218.

52. Prasanna A.R. and Varma R.K. (1977) Pramana 8,229.

53. Prasanna A.R. and Vishveshwara C.V. (1978) Pramana 11, 359.

54. Prasanna A.R. (1980) Rivista del Nuovo Cimento 3,(11) 1.

55. Prasanna A.R. (1982) 'Gravitation and Relativistic Astrophysics', Proceedings of Ahmedabad Symposium,World Scientific,New York.

56. Prasanna A.R. and Dadhich N. (1982) Nuovo Cimento 72B, 42.

57. Prasanna A.R. (1983) Astron. Astrophys. 126,111.

58. Prasanna A.R. and Raval V.M. (1983) Astrophys. and Space Science 93,25.

59. Prasanna A.R. and Bhaskaran P. (1989) Astrophys. Space Science 153,201.

60. Prendergast K.H. and Burbidge G.R. (1968), Ap. J. Letters 151,L83.

61. Pringle J.E. and Rees M.J. (1972),Astron. Astrophys. 21,1.

62. Rees M.J., Begelman M.C., Blandford R.D. and Phinney

E.S. (1982) Nature 295,17.

63. Rohrlich F. (1965) "Classical Charged Particles", Addison Wesley.

64. Ruffini R. (1973), "Les Houches Lectures,Blackholes", ed. B. DeWitt and C. DeWitt (New York Gordon and Breach).

65. Shakura N.I. (1972) Astron. Zh. 49,652.

66. Shakura N.I. (1972) Astron. Zh. 49,921.

67. Shakura N.I. and Sunyaev R.A. (1973) Astro. and Astrophys. 24,337.

68. Shapiro S.L. and Teukolsky S.A. (1983) 'Black Holes, White Dwarfs and Neutron Stars',Wiley-Interscience.

69. Shklovsky I.S. (1967) Astrophys. J. 148,L1.

70. Shikora M. (1981) MNRAS 196,257.

71. White N.E., Charles P.A. and Thorstensen (1980) MNRAS 193,731.

72. Znajek R. (1976) Nature 262,270.

List of Publications

1. Prasanna A.R. and Bhaskaran P. (1989) Astrophysics and Space Science 153, 201.

2. Bhaskaran P. and Prasanna A.R. (1989) Astrophysics and Space Science (in press).

3. Bhaskaran P. and Prasanna A.R. (1989) J. Astrophys. and Astron. (in press).

4. Bhaskaran P., Tripathy S.C. and Prasanna A.R. (1989) (to be submitted).